



Review

Gel-state MOFs for environmental decontamination: Synthesis, application and optimization

Xiao Wang^a, Yan Wang^a, Lu Chen^b, Xiaofeng Xie^a, Jing Sun^{a,*}^a The State Key Lab of High Performance Ceramics and Superfine Microstructure, Shanghai Institute of Ceramics, Chinese Academy of Sciences, 585 Heshuo Road, Shanghai, China^b Research Institute of Interdisciplinary Science & School of Materials Science and Engineering, Dongguan University of Technology, Dongguan 523808, China

A B S T R A C T

In the past two decades, gel-state metal organic frameworks (gel-state MOFs, also noted as MOGs), which was formed by the assembly of discrete MOF nano-colloids, have drawn much attention in environmental purification due to the mild reaction conditions, hierarchical porous structure, open active sites and well-defined shapes. Despite the many reviews summarizing the application of MOFs in air and water purification, the ones addressing MOGs for environmental decontamination are rare. This review provides an overview of the synthesis and characterization of MOGs for the detection, adsorption and catalytic degradation of toxic gases, metal ions and organic pollutants in waste water, as well as methods applied to optimize their performance. The possibilities and challenges in the scaling-up synthesis and industrial applications of MOGs are also included. This review is intended to summarize the recent trends in the development of MOGs, highlight the key issues to be solved and promote their practical application in environmental decontamination.

1. Introduction

The disorderly release of anthropogenic pollutants into air and water, including industrial exhausts like solvent volatilization, fuel combustion and traffic exhausts as well as chemical warfare agents, has caused worldwide concern [1,2]. Toxic wastes including air pollutants like NO_x, SO₂, NH₃, O₃, H₂S and typical volatile organic compounds (aldehydes, ketones, aromatic hydrocarbons, etc., noted as VOCs) [3–7], and water contaminants such as heavy metal ions, organic dyes, oil, pesticides/herbicides, microorganisms and antibiotics. [8,9], not only cause environmental problems, but also seriously endanger human health. The sensing, capture and degradation of environmental pollutants in air and drinking water, is of great importance for environmental protection and avoiding health issues.

Metal organic frameworks (MOFs) are a kind of newly emerged porous material constructed with metal nodes and organic ligands. Since it was firstly reported in 1897 by Hoffman et al. [10], over 20,000 kinds of MOFs have been developed based on the coordination of a vast number of metal centers and ligands for applications like energy storage [11], solvent/ gas separation [12,13], drug delivery [14], cancer therapy [15,16] and environmental decontamination [17–19]. Due to the large specific surface area, permanent porous structure, exposed active sites and abundant surface functional groups, MOFs have shown great potential in the sensing [20–23], adsorption [24,25], separation [26,27]

and degradation [28–34] of low-concentration air/ water pollutants.

Despite the achievements in the synthesis and application of MOFs in environmental decontamination, problems still exist. Firstly, the harsh synthesis conditions, which usually require high temperature, high pressure, toxic solvents and long reaction time [35–37], as well as the powder state of crystalline MOFs, severely limited their industrial application [38]. Besides, the micropores of MOFs, especially the ones with a caged shape, would be an obstacle for the migration of target molecules, which makes the active sites unavailable for the adsorption, detection and catalytic transformation of target molecules [39,40].

In response to the shortcomings, gel-state MOFs (MOGs, including MOF aerogels and xerogels), which was formed by the self-assembly of MOF colloids, have drawn much attention in recent years. By extracting solvents from MOF gels, a “non-fluid colloidal network or polymer network that is expanded throughout its whole structure by a fluid”, as defined by IUPAC, gel-state MOFs could be easily fabricated. Depending on the methods and parameters applied during solvent extraction, gel-state MOFs in the form of xerogel, aerogel and powders were obtained (Fig. 1a). Unlike crystalline MOFs, which present mainly micropores, gel-state MOFs exhibit hierarchical porous structure and abundant open metal sites (OMSs) due to the stacking of MOF colloids, which provides channels for the rapid migration and effective adsorption of guest molecules [41]. On the basis of these advantages, MOGs and their composites have been developed for the adsorption (Fig. 1b) [40,42],

* Corresponding author.

E-mail address: jingsun@mail.sic.ac.cn (J. Sun).<https://doi.org/10.1016/j.cej.2024.156241>

Received 17 April 2024; Received in revised form 26 September 2024; Accepted 26 September 2024

Available online 27 September 2024

1385-8947/© 2024 Elsevier B.V. All rights are reserved, including those for text and data mining, AI training, and similar technologies.

sensing (Fig. 1c) [43], catalytic degradation of environmental pollutants (Fig. 1d) [41], as well as the capturing and catalytic transformation of CO₂ (Fig. 1e) [44,45].

Herein, we aim to summarize the state-of-the-art work on the synthesis, characterization and modification of MOGs, MOG composites and their derivatives, as well as their performance in the capture, separation, detection, storage and catalytic decomposition of typical environmental pollutants. Besides, the capture and catalytic transformation of greenhouse gas CO₂ into high-value products will also be discussed. Finally, we present the problems need to be resolved before the industrial application of MOGs and propose an outlook for future research.

2. Sol-gel synthesis of gel state MOFs

As a commonly applied synthesis method of MOGs, the sol-gel process shows advantages in simple operation and easy to scale-up. During a typical sol-gel synthesis, metal precursors and organic linkers are dissolved in a solvent, in which a series of reactions leads to the nucleation, sol-gel transition and self-assembly of MOF gels [47,50]. By drying the wet MOF gels under suitable conditions, gel-state MOFs including aerogels, xerogels or powders could be obtained. The precisely control over the nucleation and sol-gel transition to avoid the continuous growth of colloids into crystalline MOFs is the key to a successful synthesis, while the choose of drying parameters determines the macro-structure of MOGs (Table 1).

2.1. Nucleation of colloid nanoparticles and sol-gel transition

The formation of MOGs could be understood through the classical crystallization theory (Fig. 2) [47]. Firstly, controllable metal ion dissociation and ligand deprotonation happen at suitable reaction temperatures, which releases free metal and ligand ions into the solution. Once supersaturation is reached, the nucleation happens and MOF colloids are formed. Unlike the sol-gel synthesis of crystalline MOFs, in which a controllable crystal growth happens after the nucleation, the colloid nanoparticles formed stop growing and combine together through weak interactions under suitable aging conditions. Therefore, the seek for rightful synthesis parameters like solvent applied, metal precursors, type of ligands, as well as the reaction temperature and aging

times to balance the rates and degree of the aggregation, crystal growth and precipitation of the MOF colloids, is necessary for the formation of MOF gels. As there is no clear demarcation line between nucleation /gelation and the influences of reaction parameters on these two processes may interfere with each other. Therefore, the nucleation and gelation of colloid particles are discussed together.

2.1.1. The choose of solvents

The type of solvents applied is one of the key parameters for synthesizing gel-state MOFs. For one reason, solvents may coordinate with metal ions, which alters the concentration of free metal precursors and interferes with the coordination between metal ions and deprotonate ligands, and therefore influence the nucleation process. For another, the solvation effect on the surface of colloid nanocrystals would affect their self-assembly and gelation processes. Chaudhari et al. [51] studied the influences of both polar-protic and polar-aprotic solvents (ACN, DMF, DMSO, EtOH and MeOH) on the formation of HKUST-1 [Cu₃(BTC)₂]. Among these solvents, the product obtained in DMSO showed a typical gel-like morphology, while products obtained in ACN, DMF, EtOH and MeOH are all smaller bundles of microscopic fibers. The S and O atoms in DMSO, as soft and hard electron donor atoms, respectively, not only trigger the sol-gel transition by facilitating switchable connections for weak bond making-breaking process, but also extend the structural connectivity by forming hydrogen bonds with BTC (Fig. 3a-c). Unlike DMSO, other solvent could only form monodentate interaction, which is not sufficient for triggering microstructural reintegration and sol-gel conversion. Benefited from the strong bidentate interaction between Cu (II) and DMSO and the close packing of small colloids, gel-state HKUST-1 formed in DMSO exhibit the best mechanical stability. However, reduction in the conductivity was also observed due to the "cage effect" of small colloid particles.

Mallick et al. [53] applied DMF, DMSO, DMA, quinoline, DEF and DMF/H₂O mixtures as the solvent for the synthesis of Ca-5TIA-MOF. Kamlet-Taft parameters [70], α , β and π^* (Table 2), are applied to evaluate the potential of various solvents in the formation of gel-state Ca-5TIA-MOFs. Among the parameters, α , the hydrogen bond donor ability, represents the ability of a solvent in building 3-D networks through hydrogen bonding, while β , the hydrogen acceptor ability, is associate with the thermal stability of the gel. The polarizability (π^*)

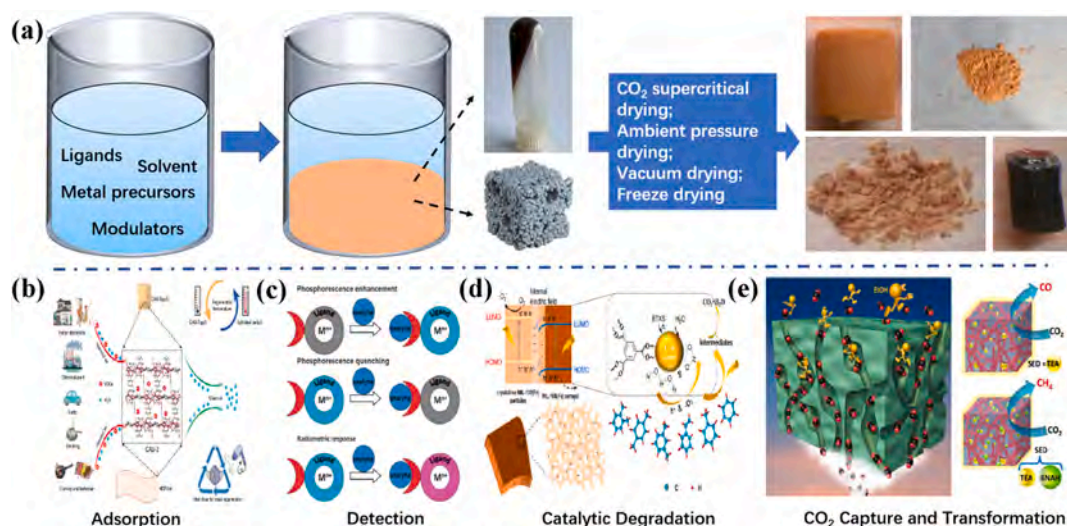


Fig. 1. (a) The schematic illustration of the sol-gel synthesis of gel-state MOFs [46,47]. The application of gel-state MOF in the (b) adsorption [40], (c) detection [48], (d) catalytic degradation [41] of environmental decontamination and (e) CO₂ transformation [44,49]. Reproduced with permission [40]. Copyright 2020 American Chemical Society. Reproduced with permission [41]. Copyright 2021 Elsevier. Reproduced with permission [46]. Copyright 2009 The Royal Society of Chemistry. Reproduced with permission [47]. Copyright 2022 The Royal Society of Chemistry. Reproduced with permission [48]. Copyright 2013 The Royal Society of Chemistry. Reproduced with permission [44]. Copyright 2022 John Wiley & Sons. Reproduced with permission [49]. Copyright 2010 The Royal Society of Chemistry.

Table 1
Summary of sol–gel synthesis of gel-state MOFs.

Gel-state MOFs	Type of solvents	Ligands	Modulators	Aging temperature/time	Solvent extraction methods	Ref.
HKUST-1	Polar-protic solvents: ethanol (EtOH), methanol (MeOH) Polar-aprotic solvents: acetonitrile (ACN), N, N-Dimethylformamide (DMF), dimethyl sulfoxide (DMSO)	Trimesic acid (H ₃ BTC)	Trimethylamine (TEA)	/	Dry at room temperature	[51]
HKUST-1	Ethanol	H ₃ BTC	/	Room temperature (RT)/ 2 min	Heating at 200 °C	[52]
Ca-5TIA-MOGs	DMF, DMSO, dimethylacetamide (DMA), quinoline, N, N-diethylformamide (DEF), DMF/H ₂ O	5TIA (5-(1,2,4-triazoleyl) isophthalic acid) > 0.1 M	/	30 °C, 60 °C, 90 °C, 120 °C / 2 days	Heating at different temperature for 2 days	[53]
DCBTF ₆ -Al ³⁺	EtOH, MeOH, n-propanol (n-PrOH), n-butanol (n-BuOH)	O-DCBTF ₆	/	80 °C/ 1 h	/	[54]
UiO-66 (Zr) UiO-67 (Zr) MOF-801 (Zr) NU-1000 (Zr)	DMF (-H ₂ O)	(P-phthalic acid) H ₂ BDC 4,4-biphenyldicarboxylic acid Fumaric acid (H ₂ FDC)	HCl, glacial acetic acid	100 °C/ 2 h	Supercritical CO ₂ extraction and a two-stage evacuation step	[55]
Cr ³⁺ /Fe ³⁺ MOG	Alcohols, DMF, DMF-EtOH, DMF-H ₂ O	1,3,6,8-tetrakis(p-benzoic acid)pyrene 5- <i>tert</i> -butylisophthalic acid (H ₂ BuDC), H ₂ FDC, 1,4-naphthalenedicarboxylic acid (H ₂ NDC), azoxybenzene-3,30,5,50 tetracarboxylic acid (H ₄ AOBTC), benzene-1,3,5-trisbenzoic acid (H ₃ BTB), 5-aminoisophthalic acid (H ₂ ADC), 5-(pyridin-4-yl)isophthalic acid (H ₂ (4-Py)DC), 5-(pyridin-3-yl)isophthalic acid (H ₃ (3-Py)DC)	HCl, benzoic acid	100 °C/ 48 h Varied with parameters like Fe/BTC ratio	Subcritical CO ₂ extraction	[56]
Al-MOGs	H ₂ O-TEA	4-[2,2':6',2'-terpyridine]-4'-ylbenzoic acid (Hcpty)	/	RT/5 min	Vacuum freeze-drying	[57]
MIL-100(Fe) MOF/MOX	DMF	H ₃ BTC	/	150 °C/ 16 h	Vacuum drying	[41]
MOG-Rh	DMF-H ₂ O/ methanol/ ethanol (volume percentages should be higher than 5 %, 5 % and 25 %, respectively)	4,4',4''-[1,3,5-benzenetriyltris(carbonylimino)] trisbenzoic acid (H ₃ btctb)	/	85 °C/ 50 h in a closed container	Subcritical CO ₂ drying	[58]
Al-ATA	DMF	2-aminoterephthalic acid (H ₂ ATA) -3-[4-(2,4-dioxopentan-3-yl) phenyl] pentane-2,4-dione (PDA)	/	80 °C/ 24–120 h	Freeze drying	[59]
Cd/Cu/Co/Zn-MOGs	H ₂ O	N, N', N''-bis-(4-carboxylate) trimesicamide	/	RT	/	[60]
Fe-MOGs	Ethanol	Propanedioic acid (H ₂ PA), succinic acid (H ₂ SA), glutaric acid (H ₂ GA), fumaric acid (H ₂ FA)	/	RT/ ~1 min	Supercritical CO ₂ drying	[61]
2D Zn-BDC-MOG	DMF	H ₂ BDC	TEA	RT	Vacuum drying	[62]
ZIF-8/71 (Zn) MOG	DMF	2-methylimidazole, 4,5-dichloroimidazole	TEA	RT	Drying at RT	[63]
Fe-MOG	Tetrahydrofuran	Bis(3-pyridyl)terephthalate	/	25 °C/ 5 h	Drying under reduced pressure	[64]
Ag-MOG	H ₂ O	4,4'-Bipyridine (4,4'-bpy)	/	150 °C/ 120 h	/	[65]
Cu/Cd-MOGs	MeOH/ EtOH/ n-BuOH/ n-hexanol/ n-heptanol/ iso-propanol/ t-butanol	Pyridine-3,5-bis(benzimidazole-2-yl) (noted as (L))	/	RT	Vacuum drying	[66]
Cu-MOG	MeOH/ EtOH	2,6-Bis(2-benzimidazolyl) pyridine	TEA	60 °C/ 0.5 h	Freeze drying	[67]
Al-carboxylate MOGs	Ethanol, DMF-ethanol	H ₃ BTC, H ₂ BDC, H ₂ FDC, H ₂ NDC, H ₃ BTB, H ₂ BDC-NH ₂ , H ₂ ADC	/	80 °C/ 30 min	Liquid CO ₂ extraction followed by aging at 308 K	[68]
Fe/Al-BTC MOG	ethanol	H ₃ BTC	/	120 °C/ 24 h	Supercritical drying	[69]

factor, which measures the solvent polarity, is essential for the solvation and gelation of MOF colloids. According to the results by Mallick et al., solvents with lower α would benefit the gelation of MOGs, while water with a α as high as 1.17 prefers the formation of crystalline Ca-5TIA-MOF (Fig. 3d and e). Therefore, considering the Kamlet-Taft parameters of the solvents, DMSO with low α (0) but high β (0.76) and π^* (1.00), is one of the ideal solvents for the formation of gel-state Ca-5TIA-MOF with high mechanical stability. Similar phenomenon was also observed by Qi et al. [52] during the formation of HKUST-1 gel, the introduction of water would not only reduce the solubility of ligand in the solvent, but also interrupt the anion-ligand coordination as a strong hydrogen-bond

donor/ acceptor. Both effects result in nanocrystals with larger size and are unfavorable for gel formation. Wei et al. [54] also observed that the gelation of DCBTF₆-Al³⁺ could be achieved in several alcohols including EtOH, MeOH, n-PrOH, and n-BuOH, while the addition of water would prevent gel formation.

However, the role of water is not always negative during gel formation. Bueken et al. [55] synthesized gel state Zr⁴⁺-MOFs, including UiO-66, UiO-67, MOF-808 and NU-1000 in DMF. When ZrCl₄ is applied as the metal precursor, a slight amount of water seems to be essential for gel formation. The authors attributed the positive role of water to the hydrolysis of ZrCl₄ to ZrOC₁₂·8H₂O, a direct precursor for Zr₆-clusters.

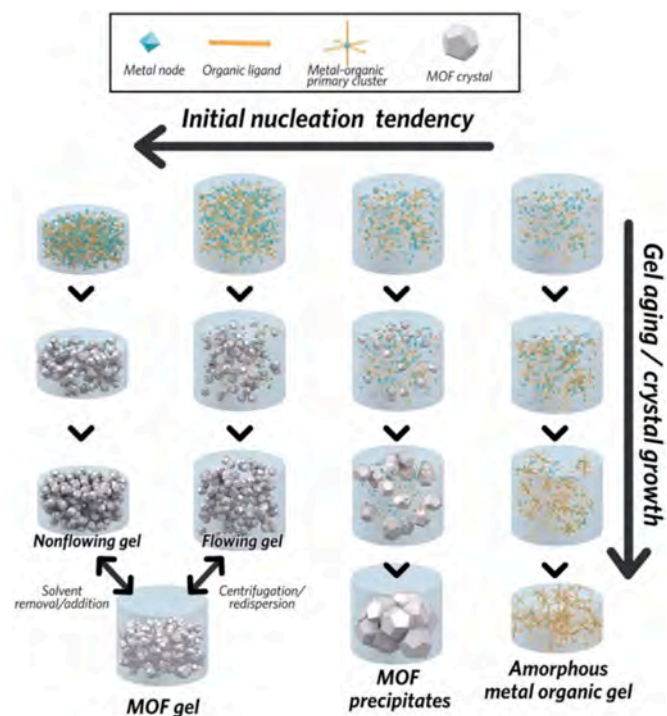


Fig. 2. The formation of gel-state MOFs, Crystalline MOFs and metal-organic gel. Reproduced with permission [47]. Copyright 2022 The Royal Society of Chemistry.

The high concentration of metal precursor and ligands, as well as the addition of water, result in the rapid and excessive nucleation of MOF colloids, which is the origin for gelation (Fig. 3f). Pair distribution function (PDF, Fig. 3g) analysis from X-ray total scattering results confirmed the formation of UiO-66 nanocrystals with short-range ordering. Further STEM results revealed that the monolith was formed by the combination of colloid particles of ~ 10 nm (Fig. 3e). Similarly, Xiang et al. [56] found that no gelation happens in anhydrous systems like absolute ethanol with FeCl_3 and H_3BTC precursors. Small amount of water as hydrogen bond donor could assist the gelation by stabilizing the gel network through H-bonding, or participate in the formation of oxo-bridged clusters [71]. Guo et al. [57] found water as a desired component in mixed solvents to favor the gelation of Al-MOGs due to its priority in forming hydrogen bonds.

Based on the above analysis, polar-aprotic solvents with lower hydrogen bond donor ability (DMSO, DMF, etc.) enable the dissolution of ligand and the anion-ligand self-assembly, which is more favorable for the formation of most gel-state MOFs. The wisely introduction of water would enable the dissolution and hydrolysis of metal ions and help with the gelation process by providing hydrogen bonds, which therefore benefit the formation of specific MOGs like Zr-/Fe-/Al- MOGs. In addition, the choice of solvents and pH value which benefit the solventization and deprotonation of metal ions and linkers is also the key to the successive gelation. They could increase the concentration of free metal ions and deprotonated linkers and lead to a burst nucleation, which therefore enable the formation of small and closely packed colloid particles [72].

2.1.2. Type and concentration of metal salts and ligands

In addition to the solvents applied, the type and concentration of metal precursors are also key factors to be considered during gelation. Bueken et al. [55] reported the importance of metal source selection in the formation of gel-state Zr-MOFs. Under comparable synthesis parameters, the usage of $\text{ZrOCl}_2 \cdot 8\text{H}_2\text{O}$ were more favorable for synthesizing gel-state Zr-MOF, while ZrCl_4 tended to form crystalline Zr-MOFs.

Besides, increasing the concentration of reactants (metal precursor and ligand) was also found beneficial for obtaining 'non-flowing' gels, even for the circumstances where ZrCl_4 was applied as the metal source. Based on the differences in dissociation rates of different metal precursors, Chen et al. [41] proposed a one-pot method for the controllable synthesis of Fe-MOF/MOX composites by using the mixture of $\text{Fe}(\text{NO}_3)_3 \cdot 9\text{H}_2\text{O}$ and $\text{FeCl}_3 \cdot 6\text{H}_2\text{O}$ as the metal source and DMF as the solvent. Compared with $\text{FeCl}_3 \cdot 6\text{H}_2\text{O}$, the dissociation of $\text{Fe}(\text{NO}_3)_3 \cdot 9\text{H}_2\text{O}$ happened almost immediately after its addition into DMF. Free Fe^{3+} ions were released and coordinated with BTC^{3-} into Fe-complex. Under increased temperature and pressure, these Fe-complex enabled an explosive nucleation process, which consumed Fe precursors and facilitated the gelation of Fe-MOG. The dissociation of $\text{FeCl}_3 \cdot 6\text{H}_2\text{O}$ in DMF was much harder than $\text{Fe}(\text{NO}_3)_3 \cdot 9\text{H}_2\text{O}$, which consequently slowed down the nucleation rate and enabled the controllable growth of crystalline Fe-MOF. By using $\text{FeCl}_3 \cdot 6\text{H}_2\text{O}$ and $\text{Fe}(\text{NO}_3)_3 \cdot 9\text{H}_2\text{O}$ mixtures as the metal precursors, both the gelation and crystallization processes happen, leading to the formation of hierarchically porous MIL-100(Fe) MOF/MOX homojunctions. Different counter-anion may also lead to MOGs with different properties. As reported by Zhu et al. [58], the reaction of dirhodium pivalate ($\text{Rh}_2(\text{Piv})_4$), dirhodium trifluoroacetate ($\text{Rh}_2(\text{TFA})_4$) and $\text{Rh}_2(\text{OAc})_4$ with H_3btctb in 1:1 DMF:MeOH lead to gels with the color of red, dark green and purple, respectively. No gelation happens when $[\text{Rh}^{\text{I}}\text{Cl}(\text{COD})]_2$ and $\text{Rh}^{\text{III}}\text{Cl}_3$ are used. In addition to counter anions, the reactivity of metal ions would also influence the formation of gel-state MOFs. By mixing metal ions with different reactivity, mismatch growth would happen and interrupts the crystallization of MOF chains. By introducing Al, which coordinates with BTC only at an increased temperature of 120°C , into the synthesis system of Fe-BTC MOF, gels with heterogeneous MOFP was obtained [69]. Mahmood et al. separated the formation of FeAl-MOG into two sections: the fast coordination of Fe ions with BTC to form abundant MOF clusters (MOFPs), and the coordination of Al with the leftover BTC linkers under increased reaction temperatures to form Fe/Al bimetallic MOGs.

Aside from metal precursors, the structure and molecular configuration of ligands applied, as well as their ability in coordinating with metal ions, should also be taken into consideration during the gelation of MOGs. Based on the differences in the protonation and coordination ability of H_2ATA and PDA ligands with metal ions, Xu et al. [59] synthesized Al-ATA MOGs with mixed ligands. The ratio of H_2ATA and PDA ligand in the Al-ATA MOGs products is about 1:0.03. Despite the small proportion in the final product, PDA is the key for gelation. Compared with H_2ATA , PDA with the structure of diacetone could strongly chelate with metal ions, which enabled a rapid coordination with free metal ions and thus the fast nucleation and gelation of MOGs. Zhu et al. [58] developed a MOG with Rh^{2+} - Rh^{2+} bonds by using a semi-rigid H_3btctb as the ligand. The amide groups in H_3btctb not only generated larger pores in the MOG product by adjusting the size of ligands, but also provided driving force for gelation by acting as hydrogen bond donor/acceptor groups [60,73].

Ligands have also been found as key factors affecting the microstructure of obtained MOGs. Gao et al. [61] synthesized a series of Fe-MOGs with H_2PA , H_2SA , H_2GA , and H_2FA ligands. Unlike the MOGs obtained with H_2PA , H_2SA and H_2GA , which showed microstructures of fibrous networks, nanosheets was synthesized by H_2FA and Fe^{3+} . As flexible molecules, the C-C bonds can easily spin in H_2GA , making it difficult for Fe-MOG to grow into 2-D or 3-D microstructures. H_2FA , on the other hand, is a rigid planar molecule, which enables the growth in 2-D direction and the formation of nanosheets.

Adjusting the concentration of metal source and ligand, and their concentration ratio, is another common way for regulating the synthesis of gel-state MOFs. Chaudhar et al. [62] proposed a 'high-concentration reactions' (HCR) approach for the gelation of HKUST-1 ($(\text{HNEt}_3)_2[\text{Zn}_3\text{BDC}_4] \cdot \text{solvent}$, in which solvent represents DMF or DMA). The HCR approach applies modulators like TEA (triethylamine base) to promote the deprotonation of H_2BDC or H_3BTC , which triggers

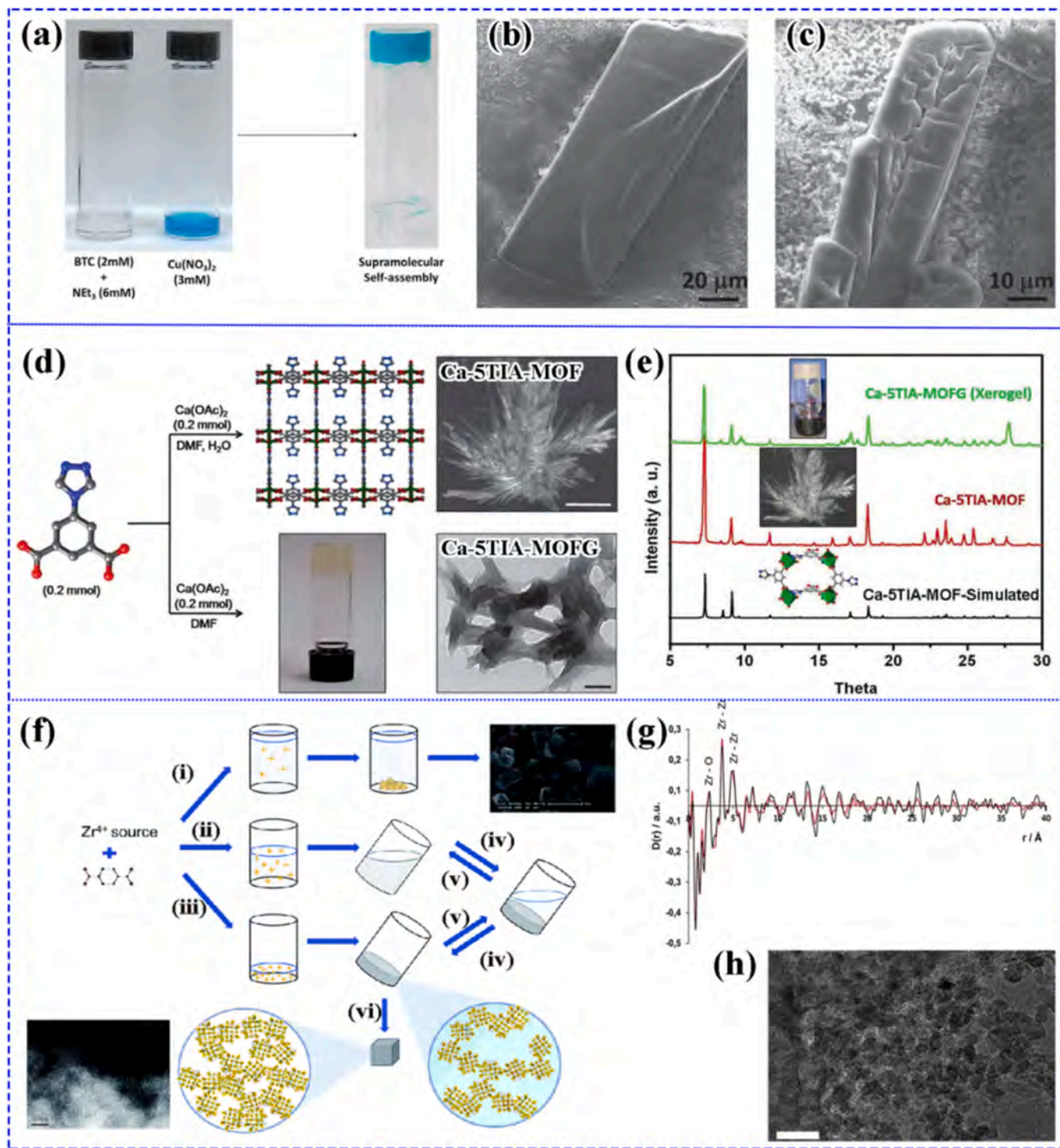


Fig. 3. (a) The synthesis scheme and (b, c) SEM images of HKUST-1 gel obtained in DMSO [51]; (d) The schematic diagram showing the synthesis of Ca-5TIA-MOF (top) and Ca-5TIA-Gel (bottom) and the corresponding SEM (Ca-5TIA-MOF) and TEM (Ca-5TIA-Gel) images [53]; (e) The XRD pattern of Ca-5TIA-MOF and Ca-5TIA-Gel; (f) Schematic overview of the formation of gel-state Zr-MOFs: (i) The formation of crystalline particles in dilute conditions and (ii,iii) formation of gel-state Zr-MOF under high reactant concentration and the existence of water; (iv,v) the reversible transformation between “flowing” and “non-flowing” gels when tuning the nanoparticle concentration; (vi) the extraction of solvent from ‘non-flowing’ gel to form gel-state Zr-MOF monoliths; (g) The pair distribution functions for a crystalline UiO-66 (black) and monolithic xerogel of UiO-66 (red); (h) The TEM image of UiO-66 xerogel particles (scale bar = 50 nm) [55]. Reproduced with permission [51]. Copyright 2015 John Wiley and Sons. Reproduced with permission [53]. Copyright 2012 The Royal Society of Chemistry. Reproduced with permission [55]. Copyright 2017 The Royal Society of Chemistry.

Table 2
Kamlet-Taft parameters of common solvents [53].

Solvent	Kamlet-Taft parameters		
	α	β	π^*
H ₂ O	1.17	0.47	1.09
DMF	0.00	0.69	0.88
DMSO	0.00	0.76	1.00
DMA	0.00	0.76	0.88
Quinoline	0.00	0.64	0.92
[BMIM][PF ₆]	0.63	0.21	1.03
Methanol	0.98	0.66	0.60
Ethanol	0.86	0.75	0.54
Isopropyl alcohol	0.76	0.84	0.48
Acetonitrile	0.19	0.40	0.75
Acetone	0.08	0.43	0.71
Butanol	0.84	0.84	0.47
Tetrahydrofuran (THF)	0.00	0.55	0.58
n-Hexane	0.00	0.00	-0.04
Ethyl ether	0.00	0.47	0.27
1,4-Dioxane	0.00	0.37	0.55
Cyclohexane	0.00	0.00	0.00
Ethyl acetate	0.00	0.45	0.55
CH ₂ Cl ₂	0.13	0.10	0.82
CHCl ₃	0.20	0.10	0.82
Benzene	0.00	0.10	0.59
Toluene	0.00	0.11	0.54
CH ₃ CN	0.19	0.40	0.75

the fast nucleation process and results in a large number of colloids with uniform diameters for the formation of gel-state MOFs. The HCR method was also applied by Tricarico et al. [63] for the synthesis of ZIF-8 and ZIF-67 MOGs. Similar phenomenon has also been reported by Bueken et al. [55] during the synthesis of Zr-based MOGs. At a DMF (solvent): Zr ratio of ~1500, only a microcrystalline precipitate was obtained. When decreasing the DMF (solvent): Zr ratio to 620 and 388, viscous solutions with a gel-like consistency could be obtained. Zr-MOGs was synthesized with the ratio being further reduced to ~200. The above results confirmed the universality of the HCR method.

Li et al. [64] studied the impacts of the molar ratio between metal source (Fe(NO₃)₃) and ligand (3-BPT, bis(3-pyridyl)terephthalate) on the fabrication of Fe(III)-MOG. Although the theoretical coordinating ratio between Fe(III) and 3-BPT was 1:2, the researchers found that gelation could happen at ratios between 1:2 and 1:5. When increasing the amount of Fe(III) to a molar ratio of 1:1, only partial gelation happened, together with the precipitation of an amorphous phase. Excessive Fe(III) disrupted the π - π stacking between ligands, which hindered the nucleation process and destroyed the short-range order of colloid nanocrystals, and therefore hindered the formation of MOGs. The appropriate redundancy of ligands would help with the formation of MOGs by suppressing the growth of the coordination complex. At the molar ratio of 1:3, the obtained Fe(III)-MOG showed the highest thermal stability, while further increasing the concentration of ligand resulted in the growth of disordered nano aggregates and altered the 3-D network micro-morphology of Fe(III)-MOG. Similarly, Zhao et al. [65] reported that when excess 4,4'-bpy linker was applied, the growth of Cu-MOG nuclei was limited while the gelation was encouraged. The excess 4,4'-bpy distributed between adjacent nanocrystals during the formation of Cu-MOGs with a mosaic structure. However, as reported by Wang et al. [74], during the formation of MOG-100-Fe, a slight surplus of metal ions (metal-to-ligand ratio of 3:2) would result in the gelation in 2 min while an excess in the ligand would prevent the formation of gel-state MOFs. No further discussion about the gelation was given in the literature and we suppose that the addition of polyethylene glycol (PEG) might influence the coordination and gelation of Fe-MOG.

Samai et al. [66] comprehensively analyzed the influences of solvents applied, the metal source-linker concentration ratio and the type of counter-anions on the formation of Cu (II) and Cd (II) MOGs. They firstly designed and synthesized pyridine-3,5-bis(benzimidazole-2-yl)

molecule (noted as L) and applied it as the ligand and gelator molecule for its ability in forming hydrogen-bond and π - π interactions, which are essential for the supramolecular self-aggregation. Halide ions including chloride and bromide ions were found to promote the gel formation better than some univalent anions such as NO₃⁻, OAc⁻, ClO₄⁻, and BF₄⁻. Both alcoholic and nonalcoholic solvents like methanol, ethanol, n-butanol, n-hexanol, n-heptanol, isopropanol, t-butanol and tetrahydrofuran (THF) were applied. All the alcoholic solvents could promote the formation of MOGs, while no gelation happens in THF, which could be attributed to its lower tendency to form hydrogen bonds. As a conclusion, the adjustment of reaction parameters to enable the coordination of metal ions with linkers, as well as the ability to form weak interactions including hydrogen-bond and π - π interactions in reaction systems, are the keys for a successful gelation.

2.1.3. The dosage of modulators

Modulator is another key factor influencing the synthesis of gel-state MOFs. A slight amount of modulator may significantly affect the dissolution and coordination of metal salts and linkers by altering the pH value of the reaction system. Some modulators could participate in the synthesis process by coordinating with metal ions to induce "mismatch growth" and hinder the growth of colloid particles into MOF crystals. Some bidentate modulators may work as bridges between colloid particles to form gel-state MOFs. The use of modulators with proper dosage was found as an efficient means in modifying the synthesis of gel-state MOFs. TEA [57,67] has been reported as an important modulator for it could promote the deprotonation of the ligands and enable successful HCR gelation processes. Besides, according to the results by Chaudhari et al. [51], TEA could also modulate the growth of HKUST-1 gel due to its propensity of coordinating with Cu(II), which resulted in a "mismatching molecular effect" [68] (Fig. 4b) and provided the chances for gelation. When coupling with the patterned growth of HKUST-1 NMOFs, the gel of nano-HKUST-1 particles integrated in fibers is obtained (Fig. 4d). In addition to bases, HCOOH has also been applied as the modulator for the synthesis of MOGs with different mesopore sizes. As reported by Tu et al., by varying the amount of HCOOH modulator, the sizes of mesopores in UiO-66 MOGs could be well tuned from 8.2 to 21 nm [75]. They attributed the changes in mesopores to the modulating of particle size in UiO-66 gels and larger particle sizes would result in larger mesopores. Brozek et al. [76] analyzed the impacts of modulators on the sizes of colloid particles and found that monotopic modulators at the surface of colloid particles could work as the capping agent and disturb their growth of into crystalline MOFs. By altering the type of modulators, they revealed that modulators with strong coordination ability to metal nodes (n-butylamine) would lead to small particles while the weak modulators (5-bromo-1-methylimidazole) produces larger ones. The decrease in the particle sizes caused differences in the electronic structure and improve the conductivity of the obtained products due to the quantum effects and higher packing density. In addition to work as capping agents, modulators could also alter the sizes of colloid particles by adjusting the deprotonation of linkers and the nucleation rates. C. A. Mirkin and colleagues [77] examined the impacts of modulators on the sizes of colloid particles during the synthesis of UiO-66 gel. Their results revealed that the addition of strong modulators (dichloroacetate and trifluoroacetic acid) with high pKa value lead to the formation of large particles with improved specific surface area and more micropores. With the addition of these modulators, the deprotonation of H₃BTC slowed down, which limited the burst nucleation and enabled the growth of nuclei into large nanoparticles. Similar results has also been found for HCOOH modulators by Tu and coworkers during the adjustment of particle sizes in UiO-66 xerogel monoliths. [78].

2.1.4. Synthesis temperature and duration

The impacts of reaction temperature vary on the basis of the precursors, solvents, modulators and other reaction parameters applied. Generally, an appropriate temperature range is necessary for initializing

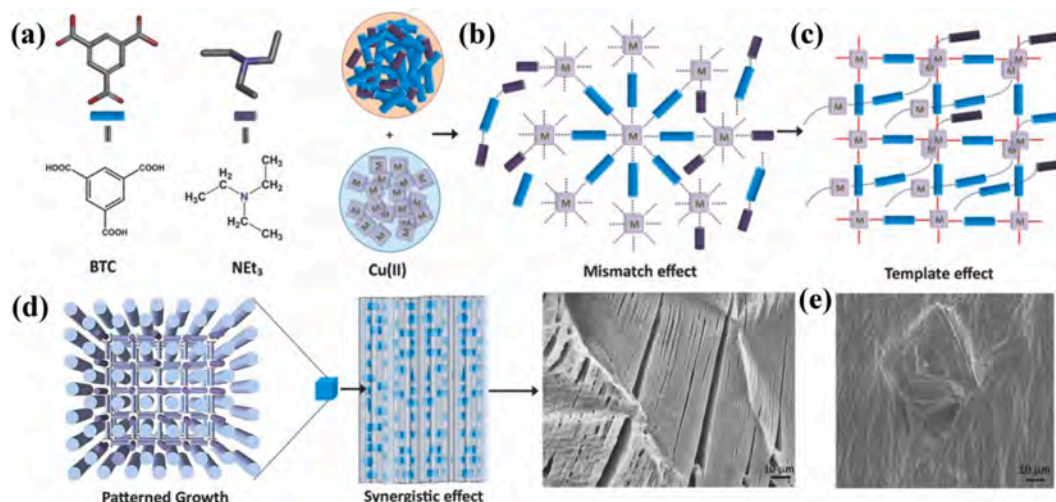


Fig. 4. (a) Building blocks for HKUST-1 gel; (b) mismatch formation of multiple coordinating molecular species and (c) template growth of HKUST-1 NMOF by the coordination between BTC^{3-} and Cu(II) ; (d) synergistic growth of nanoparticles and self-assembled fibrous structure; (e) defective crystal of HKUST-1 in the fiber network. Reproduced with permission [51]. Copyright 2015 John Wiley and Sons.

the nucleation process and higher temperature would increase the nucleation rates, which consumes the number of precursors in the solution and lead to smaller colloid particles. Fischer et al. [79] analyzed the nucleation and crystal growth of MOF-5 ($[\text{Zn}_4\text{O}(\text{bdc})_3]$) at variable conditions using time-resolved static light scattering (TLS). At an appropriate temperature of 105 °C, the nucleation of MOF-5 began and the sizes of nuclei linearly increase with the aging time. Their work confirmed the relationship between the reaction temperature/duration and the sizes of colloid particles.

Aging was found as an effective means in adjusting the sizes and interconnectivity of colloid particles. Furukawa et al. [80] used aging as an effective strategy to tune the hierarchical structure of HRhMOP gels (MOP stands for metal–organic polyhedral/ cages). The as-synthesized gel was aged in DMF at 80 °C for several times. Bidentate linker **bix** (1,4bis(imidazol-1-ylmethyl)benzene) was firstly attached to the surface of HRhMOP to form HRhMOP(**bix**)₁₀(**diz**)₂ (**diz** refers to 1-dodecyl-1H-imidazole, a ligand to increase the solubility of HRhMOP in DMF) through a ligand-exchange process. Under aging condition (80 °C in DMF), the dissociation of **bix** and **diz** linker happens, leaving open Rh sites to coordination with **bix** linkers from adjacent MOPs. The formation of new coordination bonds between MOPs reduced the size of colloid particles from 28.4 nm to 23.6 nm due to densification, increased the packing density of HRhMOP gel and created more micropores inside the gel, which improved the stiffness, but decremented the elasticity and increase brittleness of the gel products. A moderate particle sizes, as well as the connection between colloidal particles, are the key factors influencing the mechanical stability of MOGs. In addition, due to the removal of monodentate linkers in the voids between MOPs and the rearrangement of MOPs inside colloidal particles, the surface area and the pore volume increased from 565 m^2/g and 1.66 cc/g to 758 m^2/g and 1.77 cc/g , respectively. This work not only provide a useful method for adjusting the sizes of colloid particles, but also confirmed their influences on the textural structure, mechanical stability and adsorption capacity for the first time. Similarly, Li et al. [68] found that moderate heating makes the coordination bonding competitive to other weak interactions, which was the key for triggering gelation [81,82].

2.1.5. The controllable synthesis of gel-state MOFs and the prediction of optimal parameters

As discussed above, the reaction parameters, including the type and pH value of solvents, the reaction temperature/duration, the concentration/ ratio of precursors, and the dosage of modulators during the nucleation and gelation processes, have a great impact on the sizes and

packing density of colloid particles, and therefore influence the porous structure, surface area and crystallinity of gel-state MOFs. On the basis of previous reports, some empirical patterns could be found. The high reaction temperature and concentration of precursors, an appropriate solvent and pH which benefits the solvotization and deprotonation of metal ions and linkers, along with the wisely dosage of modulators, would result in smaller and closely packed colloid nanoparticles and gel state MOFs with higher mechanical stability, more open active sites and large specific surface area, which are beneficial for the capture, migration and adsorption of pollutants. In addition, the higher packing density could also improve the conductivity of MOGs, which is favorable for the sensing and catalytic degradation of pollutants.

Despite these laws of experience above, the controllable synthesis of gel-state MOFs is still difficult for the optimal parameters vary with the type of metal nodes and linkers. Predicting the optimal synthesis parameters could be quite complicated and time- and labor-consuming.

In face of these problems, Miyazaki et al. [85] applied a high-throughput screening method to investigate the gelation conditions for ZIF-zni gel (Fig. 5d). The influences of type and concentration of metals (Co and Zn), ligands (imidazole, benzimidazole, 2-nitroimidazole, 5,6-dimethylbenzoimidazole, 2-methylimidazole, 4,5-dichloroimidazole, purine and their mixtures), solvents (ethanol, DMF and deionized water) and bases (sodium hydroxide and potassium hydroxide) are thoroughly studied. According to their results, Zn is more likely to gel than Co. The reaction systems with lower concentration of metal sources and higher concentration of ligands are more inclined to gel. Regarding the solvents, gelation was easier in DMF while the impacts of water and ethanol were blurred depending on the type of ligands. KOH and NaOH were found to have similar effects on gelation, and increasing the concentration of base would benefit the gelation of MOGs. This work provided a useful way for comprehensively estimating the role of gelation factors and shed light on the controllable fabrication of new MOGs. Orthogonal experiments could be applied to further reduce the time and labor consumption. AL-Jarsha et al. [86] have used Taguchi orthogonal array in the synthesis of MOF-5 with adjustable crystallinity and distinguished the optimal parameters for obtaining MOF-5 with the highest degree of crystallinity (DOC). Sub-optimal conditions, according to their results, would result in distorted MOF-5 with lower DOC.

However, when it comes to the controllable synthesis of a series of new MOGs or building universal laws, it still needs tremendous time and labor inputs and is almost impossible with traditional methods, even with the help of orthogonal arrays. In the past few years, machine learning (ML) or computational modeling have shown great potential in

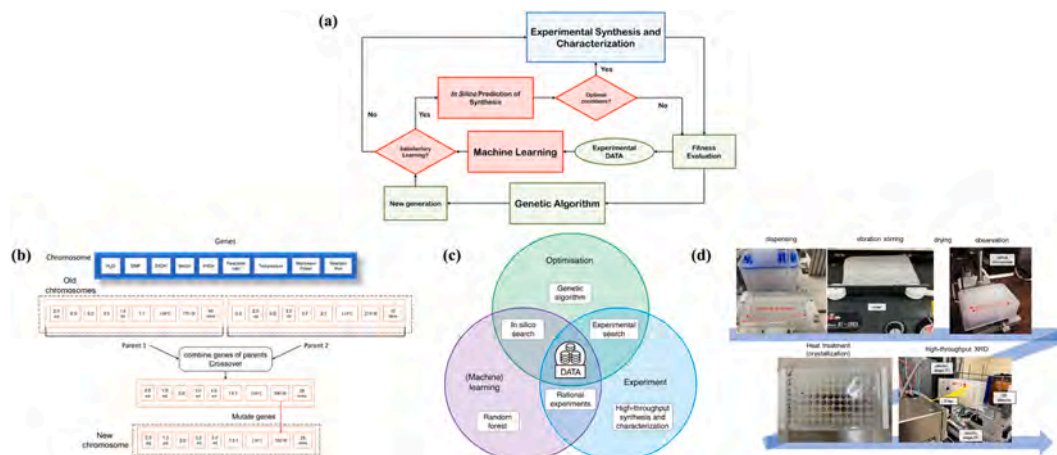


Fig. 5. (a) The flow chart of the synthesis accelerated by machine learning; (b) An illustrative example of the genetic operation; (c) Schematic illustration of the components of synthesis assisted by genetic algorithm and machine learning; (d) The high-throughput screening of Zn-MOGs. Reproduced with permission [83], copyright © 2019, Seyed Mohamad Moosavi et al. Reproduced with permission [84], copyright 2023 The Royal Society of Chemistry.

transforming the way of material discovery and efforts have been devoted for their application in guiding the synthesis of new MOFs. In 2019, Moosavi et al. [83] combined a robotic synthesis platform, genetic algorithms and ML to study all 9 parameters those may influence the synthesis of HKUST-1 (Fig. 5a-c). The robotic platform ensures the precise control over the synthesis variables, lowers the noise in the outcomes and improves reproducibility. The genetic algorithms, in which only the genes of the successful parents could be transferred to the next generation, significantly lowers the complexity of the system. At last, ML will study the importance of various parameters, and guide more rational experiments design. Their work provides a useful methodology for the discovery and controllable synthesis of new MOGs. High-throughput (HT) methods, together with automatic operations, as a labor-, time- and material-saving way for generating and collecting large amounts of data, is the prerequisite for machine learning and computational modeling, while ML and computational model, could in turn rationalize the design of high-throughput experiments. The controllable synthesis of MOGs is still in its infancy and future work, both experimental and computational ones, are needed.

Unlike MOFs, the crystallinity of which could be qualitatively analyzed and work as a criterion for evaluating synthesis products. The criteria for defining if the synthesis was successful for gel state MOFs is still unclear. For example, some researchers confirmed the formation of MOG gels by a ‘test-tube reversion test’, which is simple but rigorous and cannot reflect the in-depth structural and chemical information of the products. In addition, the lack of universal standard for defining MOGs and the sloppy description by many groups when discussing their materials further limit the controllable synthesis of MOGs. These problems should be solved in ahead of the implantation of ML and computational modeling into the prediction of optimal parameters for controllable synthesis of MOGs.

2.2. Solvent extraction of wet MOF gels

The transformation from MOF gels to aerogel, xerogels or powders through suitable solvent extraction (drying) methods are necessary for most application scenarios. Several drying methods like CO₂ supercritical drying, freeze drying and ambient/vacuum drying have been applied to extract solvents from MOF gels without destroying its micromorphology and pore-structures.

Ambient pressure/vacuum drying evaporates the pore liquid in MOF gels at room or higher temperatures [87]. As the evaporation of solvent happens, capillary pressures of nearly a thousand bar is exerted on gel surface, which causes the shrinkage of gel matrix and leads to the

formation of MOF xerogels with lower porosity. Vilela et al. [88] prepared a series of UiO-66-NH₂ xerogels through ambient drying MOF gels with different nanoparticle concentrations with the assistance of silica gel. The removal of 98% ethanol solvent happens in 24h and volume contractions of 89.5% to 98.9% were observed for MOF gels with nanoparticle concentrations of 20 mg/mL to 55 mg/mL, respectively. They further prepared a series of UiO-xerogel samples and found that the samples with lower initial colloid concentrations (10 and 20 mg/ml) have more mesopores with diameters in the range of 5~15 nm and 20~30 nm than the one with an initial concentration of 55 mg/ml, confirming that the adjustment of initial colloid concentration allows for the fine tune of pore structure in xerogel products. Connolly et al. [89] evaluated the importance of drying temperature in monolith formation. A high drying temperature induced the fast removal of pore solvent and destroyed the gel macrostructure due to the large capillary vapor-liquid interface. Therefore, a mild dry condition with appropriate temperature is required for the formation of MOF xerogel/aerogels. They also studied the influences of pore solvents on the drying products by washing the gel in fresh DMF or ethanol. Compared with ethanol (boiling point at 78 °C), DMF has higher boiling point (153 °C) and larger surface tension, which slowed down its evaporation and extended the time of reaction, therefore facilitating the formation of more interactions between primary particles. Besides, the differences in the evaporation rates and surface tension could also influence the capillary force during the extraction of pore solvents, which finally altered the porous structure and properties of the UiO-66 xerogel products. Compared with ethanol, the MOG products obtain with DMF as the washing solvent exhibited higher micropore to mesopore ratio and larger specific surface area.

Supercritical CO₂ drying, which use CO₂ supercritical fluid to replace and extract the solvent from the pores of wet MOF gels, is quite a promising means for the fabrication of MOF aerogels for it could overcome the shortcomings of ambient/vacuum drying like structure shrinkage and long operation time. [46,87,88,91] Fig. 6a gives a typical flow diagram of a supercritical CO₂ drying procedure. The wet MOF gel is placed in a vessel, in which the extraction temperature and pressure are slightly higher than CO₂ critical temperature and CO₂-solvent mixture critical pressure. Supercritical CO₂ passes through the MOF gel and extracts solvent in the pores. Benefited from the liquid-like properties of supercritical CO₂, the capillary force at the liquid-vapor interface is eliminated [92], which preserves the larger pores inside MOGs and enables the formation of aerogels with higher pore volumes and larger specific surface areas [87]. Lohe et al. [46] compared the micro-structure of air-dried gels (xerogel) and MOF aerogels obtained through CO₂ exchange. Compared with the xerogels, aerogels exhibited

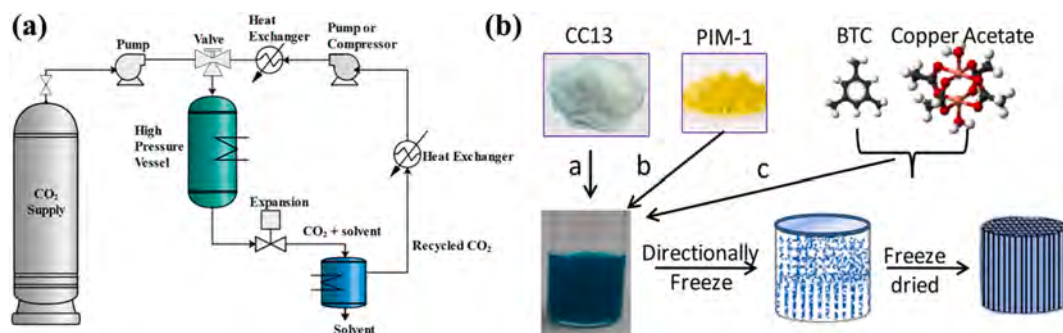


Fig. 6. (a) The flowsheet of a supercritical CO₂ drying cycle and (b) scheme of the frozen-solvent-templating approach for the preparation of aligned porous monoliths. Reproduced with permission [90]. Copyright 2012 The Royal Society of Chemistry. Reproduced with permission [87]. Copyright 2017 MDPI.

a much higher degree of microporosity with almost no shrinkage in the volume. Vilela et al. [88] compared the UiO-66 xerogel/aerogel products obtained under silica gel or supercritical CO₂ drying (Fig. 7). When dried in a desiccator with silica gel, xerogels were obtained in 7–9 days with a volume contraction of ~90%. Supercritical CO₂ drying, as a comparison, provided aerogel product with much smaller volume contraction (~59%), higher mesoporosity and larger pore sizes than the xerogels. As a commonly applied drying method, supercritical CO₂ drying has also been applied in the synthesis of Zr-MOFs (MOF-808, UiO-66 and MOF-801) [91], HKUST-1@silica aerogel [93], MOF(Fe)/

HNTs composite aerogel [94] and other aerogel materials.

Freeze drying, also known as ‘ice templating’ or lyophilization [47,95], is another important solvent extraction method applied in the synthesis of gel-state MOFs. During a typical freeze-drying process, solvents (or frozen templates, including water, DMF and DMSO) in the pores is frozen at a relatively low temperature and removed from the pores through sublimation at a pressure lower than the sublimation pressure. The formation of liquid–vapor interfaces is effectively avoided through freeze-drying and the capillary force is eliminated. Pores inside the gels are therefore preserved and aerogels could be obtained. By

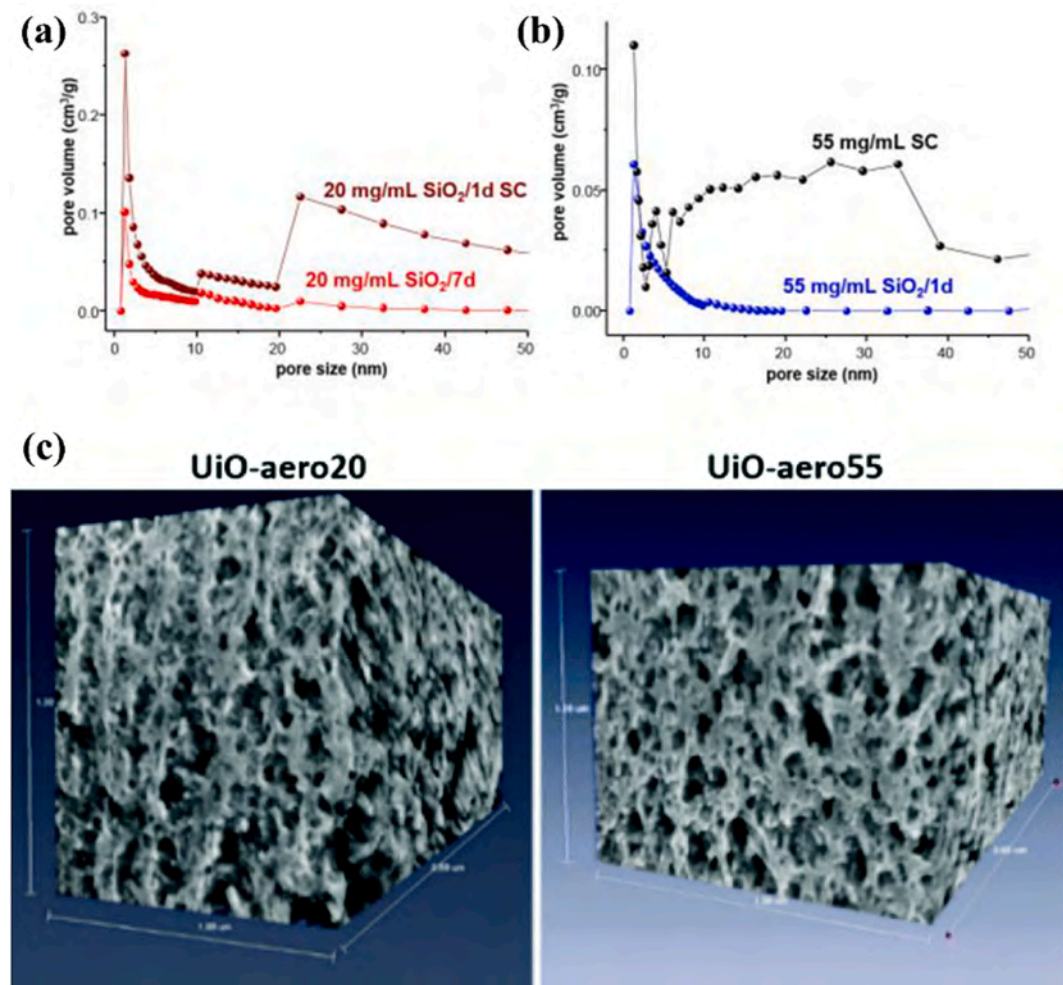


Fig. 7. Pore size distribution of UiO-66 monolith obtained by supercritical CO₂ drying and ambient drying with the assistance of silica gel: monolith obtained from colloid with particle concentration of (a) 20 mg·mL⁻¹ (UiO-aero20) and (b) 55 mg·mL⁻¹ (UiO-aero55); (c) 3D models of porous UiO-aero20 and UiO-aero55 reconstructed with FIB-SEM image stacking. Reproduced with permission [88]. Copyright 2018 The Royal Society of Chemistry.

orientating the growth of ice crystals during the fast-freezing process, aligned porous materials could be obtained. Ahmed et al. [90] applied frozen-solvent-templating approach for the preparation of HKUST-1 (Fig. 6b). The solution of Cu (CH₃COO)₂ and 1,3,5-benzene tricarboxylic acid (BTC) in DMSO was directionally freeze-dried to generate aligned porous monolith. A post-treatment in ethanol at 80~120 °C is then needed for the generation of HKUST-1 monolith. SEM images revealed the existence of aligned porous structure across the monolith. Li et al. [96] further confirmed the universality of the freeze-drying method in the fabrication of gel-state NENU-9, MIL-53 and ZIF-8 with hierarchical pores. No shrinkage in the mesopores happened during the freeze-drying process, resulting in samples with larger mesopore size and surface area (~30.1 nm, 624 m²/g) than samples obtained through simply volatilizing solvent (~11.1 nm, 166.6 m²/g). However, despite the many advantages of freeze-drying, only few hierarchically gel-state MOFs have been obtained by freeze-drying due to the difficulties in choosing suitable solvents. Water is the mostly applied solvent in freeze-drying, but only has poor solubility for commonly applied linkers. Besides, as discussed above, water is not suitable for the gelation to happen. Other solvents, like ethanol, DMF, DMSO etc., often have quite low freezing point or are difficult to be freeze-dried. Therefore, the seeking for a suitable solvent or solvent mixtures, is urgent for the application of freeze-drying method in the solvent extraction of gel-state MOFs.

3. The characterization of gel-state MOFs

The deep understanding of the microstructure, chemical composition and coordination mode of gel-state MOFs are quite challenging due to their amorphous nature. In the purpose of revealing the microstructure, composition and textural structure of gel-state MOFs, advanced and novel characterization methods have been proposed.

3.1. The structures of gel-state MOFs over multiple length scales

XRD, SEM and TEM are the most commonly applied means for microstructure characterization. However, due to the lack of long-range ordering in gel-state MOFs, their XRD pattern usually show broad diffraction peaks, which hinders the structural refinement and the calculation of particle size from the Scherrer equation. In addition, the blurred interface between crystalline and amorphous phase in MOGs also impeded the observation of the micro-morphology of MOGs through SEM or TEM. Spectroscopic methods like Raman spectroscopy [97], infrared spectroscopy have been applied to reveal the coordination of metal centers in MOGs, which may help with determining the microstructure of gel-state MOFs. However, these methods could only give information on the atomic range. The in-depth characterization of colloid particles, as well as the way in which they are assembled, are still a mystery to researchers. In addition, the characterization of gel-state MOFs is sometimes ignored by some groups, which hindered the systematical study over the synthesis mechanism of gel-state MOFs and their performance in environmental decontamination.

In face of this problem, pair distribution function (PDF) analysis, which was obtained from the Fourier transition of total scattering pattern, has been implanted in recent years [98–101]. In 2018, Bennett et al. [102] studied the microstructures of gel-state ZIF-8 via collecting the neutron and X-ray total scattering data and analyzing them through PDF analysis. By combining PDF analysis with advanced electron microscopy and computational methods, they revealed the microstructure of Fe-BTC-MOG on various length scales [98,103]. High-resolution scanning transmission electron microscopy (HR-STEM) graph showed that Fe-BTC-MOG is composed of crystalline nanoparticles (10–50 nm) embedded in an amorphous matrix, which represent the majority of the material. Based on the PDF analysis results, they further compared the ratio of the trimer: tetrahedra peak intensity between crystalline MIL-100(Fe) and Fe-BTC-MOG and found that only 39% of trimers in Fe-

BTC-MOG are in the form of tetrahedra, smaller than that of MIL-100 (Fe) (100% assembled structure). This might pave the way to the quantitatively characterization of the crystallinity of MOG materials. Polymatic algorithm was further applied to build an atomistic structure for Fe-BTC. A MIX model (a 50/50% mixture of trimers and tetrahedra) was found to best reflect the synthesized Fe-BTC material (Fig. 8). They also found that the MIX model could also fit the microstructure of Basolite® F300, a commercial MOFs material. In addition to neutron and X-ray total scattering data, PDF analysis on electron scattering data could also be obtained from STEM (STEM-ePDF). Laulainen et al. [101] combined STEM-ePDF with unsupervised machine learning methods to reveal the short-range order of ZIF-62 in a composite glass within a pixel size of <10 nm. This method showed great potential in revealing the interface properties between crystals and amorphous substrate in gel-state MOFs. As discussed above, the combination between PDF analysis and computational methods has proven to be effective in determining the microstructure of gel-state MOFs. However, the practical application of these methods was still limited, which could be attributed to the high demand for funding and technology. Therefore, the developing of characterization methods which are simple, inexpensive and easily accessible, are still necessary in future research.

3.2. The chemical composition of gel-state MOFs

Unlike crystalline MOFs, in which the linkers and metal centers combine in the stoichiometric, the ratio of linker to metal centers are not fixed in gel-state MOFs due to the self-assembly of colloids, which induces a large number of defects. Revealing the chemical composition of MOGs, not only helps with the analysis of defects and type of open active sites in MOGs, but also enabled the performance prediction of MOGs in environmental decontamination through theoretical methods. Elemental analysis methods, like energy dispersive X-ray spectroscopy (EDS), thermogravimetric analysis (TG), nuclear magnetic resonance spectroscopy (H-NMR) and inductively coupled plasma atomic emission spectroscopy (ICP-AES) and X-ray photoelectron spectroscopy (XPS) could help to clarify the chemical composition of gel-state MOFs. The precisely characterization of the chemical composition of gel-state MOFs provides a much easier way to evaluate the consistency and variability between products of different synthesized batches, and might therefore help with the scaling-up synthesis and industrial applications.

3.3. The textural structure of gel-state MOFs

As a kind of hierarchical porous material with both micro- and mesopores, the sizes and distribution of pores in gel-state MOFs strongly relies on the very nature of MOFs (the coordination and topology structure) and the reaction parameters and could be regarded as a simple standard when evaluating the success of the synthesis process. In addition, the volume of micro-/ mesopores and the specific surface area, could be used to predict the performance of gel-state MOFs in the adsorption of air/water contaminants for they could reflect the amount and exposure degree of active sites to some extent. Therefore, the characterization of the textural structure of gel-state MOFs are quite essential in the field of environmental decontamination. The textural examination is usually carried out through N₂ adsorption-desorption isotherms. By fitting the isotherms using models such as BET, Langmuir, BJH, and HK, the size distribution of pores from micropores to macropores, and the specific surface area can be determined [46,88].

4. The application of gel-state MOFs in environmental decontamination

4.1. Adsorption and separation of environmental pollutants

The migration of pollutants and the interactions between pollutant molecules and adsorption sites, are the two factors influencing the

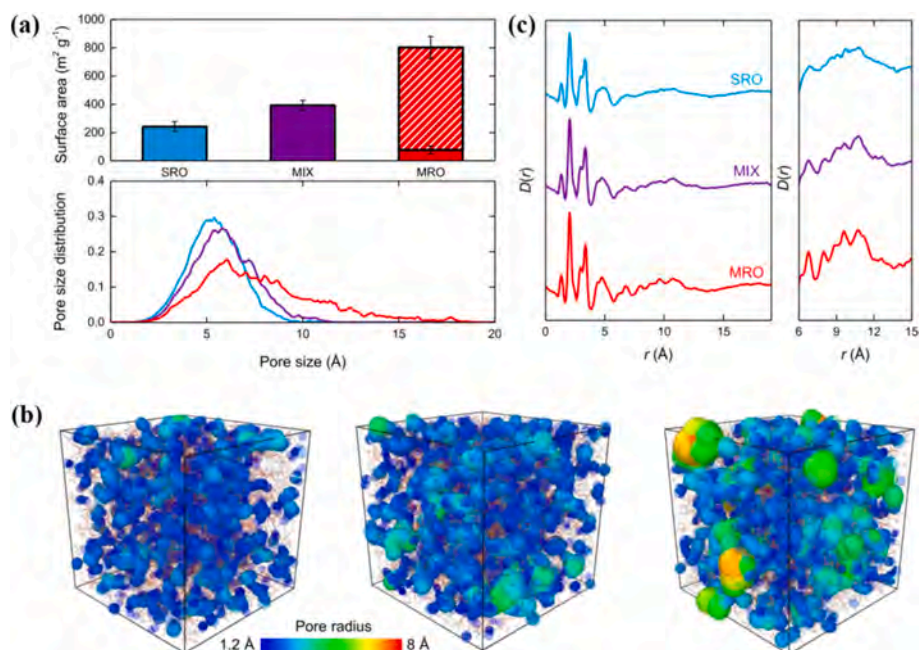


Fig. 8. (a) Top: The surface areas to a nitrogen probe (radius 1.82 Å) for all three amorphous model types of Fe-BTC; Bottom: The average pore size distribution for the SRO (short-range order model, blue), MIX (mixed model, purple) and MRO (medium-range order model, red) models, averaged over five simulations; (b) Visual representation of the pore size distribution for the SRO (left), MIX (centre) and MRO (right) systems from a representative model of ~ 70 Å in length; (c) Calculated PDFs for the SRO (blue), MIX (purple) and MRO (red) models. Reproduced with permission [98] Copyright 2021, Adam F. Sapnik et al.

adsorptive removal of target pollutants [137]. The hierarchical porous structure of gel-state MOFs provides open channels for the rapid migration of pollutants [68], while the open active sites and surface functionalization possibility enable the effective capture and storage of hazardous substances (Table 3). Based on the type and function groups of pollutants, 5 kinds of interactions may exist between MOGs and target pollutants: (1) electrostatic attraction, which usually happen during the adsorption of heavy metal ions, cationic or anionic dyes and microplastics; (2) π - π interactions between the aromatic hydrocarbons and the linkers of MOGs [41,138]; (3) Lewis acid-basic interactions between electron-rich molecules and open metal sites of MOGs [77]; (4) van der Waals interactions and (5) the combination of (1) to (4). The design and modification of MOGs with regard to the properties of target molecules is necessary for performance optimization.

4.1.1. Capture and storage of hazardous gas

As discussed above, the specific surface area, the pore structure, the type, distribution and strength of active sites are the key determinants of gel-state MOFs in the capture and storage of hazardous gas. Li et al. [68] studied the reversible adsorption of non-polar aromatic benzene, linear n-hexane and polar methanol by gel-state MIL-53(Al) (noted as Al(III)-MOG). All the isotherms were close to type IV curves, confirming the hierarchical porous structure of Al(III)-MOG. With abundant open metal sites capturing target molecules through Lewis acid-basic interactions, Al(III)-MOG showed relatively high adsorption capacity for non-polar benzene (1008.25 mg/g), linear n-hexane (432.19 mg/g), and polar methanol (865.67 mg/g).

Water vapor in air may greatly influence the adsorption of VOCs by competing for active sites or affecting the stability of MOGs. Therefore, hydrophobicity and water stability should be taken into consideration when evaluating the performance of MOG adsorbents. In order to exclude the adverse effect of moisture on the adsorption of pollutants, Sellars et al. [42] prepared hydrophobic ZIF-8 and ZIF-67 monolith by using monodentate ligand as the modulator and tested their adsorption ability for toluene and methanol vapors. Unlike the cases of crystalline ZIF-8 and ZIF-67, which exhibited only micropores and presented type III isotherms with a plateau, the vapor adsorption isotherms of ZIF-8/67

MOGs could be described as type II or type IV curves with more toluene adsorption in the $P/P_0 = 0.2$ – 0.9 region, indicating the effective gas adsorption by the mesopores (Fig. 9a, b). ZIF-8 and ZIF-67 monolith samples could adsorb 826.3 and 1030.9 mg/g of toluene, outperforming their crystalline counterparts of 29.8% and 38.6%, respectively.

Zheng et al. [40,104] synthesized hydrophobic CAU-3-NH₂ gel with both micropores and mesopores by applying Al as the metal nodes, terephthalic acid (BDC) and 2-aminoterephthalic acid (NH₂-BDC) as the mixed ligands. In comparison with other reported hydrophobic MOGs, CAU-3 MOG shows a much higher BET-SSA of ~ 2050 m²/g (Fig. 9c). The large surface area and active defects sites formed during the formation of CAU-3 gel enabled much higher adsorption capacity towards VOCs (hexanal, toluene and p-xylene) with trace concentration (2 ppm) and high space velocity (600 L/g·h) than active carbon (AC), a commonly applied adsorbent (Fig. 9d). CAU-3 gel showed higher toluene selectivity (in toluene/water mixtures) than some well-known adsorbents like AC, zeolite 13X, and some representative MOFs including HKUST-1, UiO-66, et al. GCMC simulation results confirmed that hexanal preferentially entered the small tetrahedral cages of CAU-3 and adsorbed onto the sites near the phenyl rings or between methyl groups and phenyl rings at low pressures (1–10 Pa). Under high pressures (up to 100 Pa), the adsorption of hexanal would also happen near the uncoordinated carboxylate oxygen sites in the octahedral cages of CAU-3 (Fig. 9e). In addition, the complete desorption of toluene from CAU-3-NH₂ gel could happen at a relatively low temperature of 328 K, making it a great candidate for commercial applications. Based on these advantages, the author coated CAU-3 MOG on nonwoven fabric (NWF) through dip-coating to fabricate filters and filled them in masks for VOC purification (Fig. 10). [40] Breakthrough curves revealed that the filter based on CAU-3 MOG could better capture hexanal from wet clean air than activated carbon (AC) filters and could be simply regenerated by household hair dryer. These excellent performances made CAU-3 MOG filters promising for personal protection.

4.1.2. Adsorptive removal of water contaminates

Aside from air decontamination, gel-state MOFs like Al-MOGs [69], Fe-MOGs [69,117], Ni-MOGs [139], Zr-MOGs [106,107] etc. have also

Table 3

The applications of MOGs in the adsorption, detection and decomposition of environmental contaminants.

Applications	Materials (metal nodes, ligands)	Synthesis Method	Target pollutants	Adsorption Capacity	Selectivity	Regeneration	Ref
Adsorption of gas/water pollutants	CUA-3 MOG (Al(III), 2,5-dimethylterephthalic)	Solvothermal reaction	hexanal	291 mg/g and 1737 mg/g at P/P ₀ = 0.03 and 0.95, 298 K for hexanal	High Q _{toluene} /Q _{water} value	358 K	[40]
	ZIF-8/67 MOG (Zn(II)/Co(II), 1-methylimidazole, n-butylamine)	Mixed-modulator synthesis	toluene	322 mg/cm ³ at high relative humidities	Selectivity for non-polar molecules	/	[42]
	CAU-3-NH ₂ -MOG (Al(III), 2-aminoterephthalic acid)	Solvothermal reaction	Hexanal	3.86 mmol/g toluene at P/P ₀ = 0.1	High Q _{toluene} /Q _{water} value	358 K/ 350 min	[104]
	N-doped granular carbons	Carbonization of CAU-3-NH ₂ MOG	Toluene	4.5 mmol/g toluene at P/P ₀ = 0.1	/	378 K	[39]
			Toluene	9.0 mmol/g toluene at P/P ₀ = 0.1	/	/	[68]
	Al(III)- MOG (Al(III), 1,4-dicarboxybenzene (bdc))	Room temperature reaction	Congo red and brilliant blue R-250	633.4 mg/g for Congo red and 621.3 mg/g for BBR-250	High selectivity for (D) and (T)	/	[68]
	Fe-Al MOG (Fe(III) and Al(III), 1,3,5-Benzenetricarboxylic acid (btc))	Solvothermal reaction	Rhodamine B and methyl orange	290 mg/g for rhodamine B and 265 mg/g for methyl orange	/	/	[69]
			Nonpolar organic solvents	/	/	Washing by acetone	[59]
	Al-ATA-F with mixed ligands (2-aminoterephthalic acid (H ₂ ATA) and 1,4-Bis-(3'-acetylacetonate)benzene (PDA))	Solvothermal reaction	As(V) ions	232 ± 24 mg/g	/	/	[61]
	Fe-PA/SA/GA/FA-MOG (Fe(III), propanedioic acid/ succinic acid/ glutaric acid/ fumaric acid)	Room temperature reaction	Dyes	/	/	/	[105]
	Ni-BCA MOG (Ni(II), bis-catechol-terminated azobenzene)	Room temperature reaction	Toluene in water	242 mg/g	/	/	[106]
	IPD-mesoMOF-12 (Zn(II), 2-methylimidazole)	Solvothermal reaction	Pb(II) ions	102.03 mg/g	/	Regenerated with 0.1 M ethylenediaminetetraacetic acid (EDTA) solution	[107]
	UiO-66-NH ₂ -CS MOG (Zr(IV), NH ₂ -bdc)	Solvothermal reaction	Chlortetracycline hydrochloride	479.05 mg/g	/	/	[108]
	(Fe-Eu) JLUE-MOGs (Fe(III) and Eu(III), 4,4',4''-s-triazane-2,4,6-triyl-tribenzoate(TATB))	Solvothermal reaction	Hg(II) ions	925.9 mg/g	Selective removal of 99.0 % Hg(II) ions with interferences (Na ⁺ , K ⁺ , Fe ³⁺ , Zn ²⁺ , Mg ²⁺ , Ba ²⁺ , Mn ²⁺ , Ni ²⁺ , Ca ²⁺ , Al ³⁺ , Cu ²⁺) through ion exchange	/	[109]
	ZnS-ZIF-8 MOG (Zn(II), 2-methylimidazole)	Room temperature reaction	Hg(II) ions	91 % removal efficiency	/	/	[110]
Fe-NDC MOG (Fe(III), 2,6-Naphthalenedicarboxylic acid (ndc))	Room temperature reaction	As(V) ions	144 mg/g	/	/	[111]	

(continued on next page)

Table 3 (continued)

Applications	Materials (metal nodes, ligands)	Synthesis Method	Target pollutants	Adsorption Capacity	Selectivity	Regeneration	Ref
	Cu/Cd/Cr-MOG (Cu(II), Cd(II) and Cr(III), ethylene glycol dimethacrylate (EGDMA))	In situ construction	Cu(II), Cd(II), Cr(III) and Sb(V)	/	/	/	[112]
	Fe/Al bimetallic JLUE-MOG (Fe(III) and Al(III), TATB)	Solvothermal reaction	Chlortetracycline hydrochloride	1841.62 mg/g	/	Washing by methanol and distilled water	[113]
	FGO@Al-MOG (Al(III), btc)	Solvothermal reaction	Various oil in water	200 %–500 % of initial mass of the absorbent	Separation of oil from water	/	[114]
	monoMIL-100(Fe)	Room temperature reactions	Typical VOCs (benzene, toluene, p-xylene)	615.0 mg/g benzene, 575 mg/g toluene, 624.0 mg/g p-xylene	/	Heated at 75 °C for regeneration	[115]
	Fe-MOG (Fe(III), btc)	Solvothermal reaction	Organic dyes	182.82 mg/g	/	No regeneration treatment	[116]
	Fe-BTC MOG (Fe(III), btc)	Room temperature reaction	polycyclic aromatic hydrocarbons in water	/	Highest enrichment factor for fluoranthene and pyrene with four rings, followed by phenanthrene and anthracene with three rings and then benzo[b] fluoranthene and benzo[a] fluoranthene with five rings	/	[117]
Applications	Materials	Synthesis Method	Target pollutants	Detection Mechanism	Selectivity	Detection limits & linear range	Ref.
Sensing & detection of environmental contaminants	Al(Hcptpy)-MOG (Al(III), 4-[2,2':6',2'-terpyridine]-4'-ylbenzoic acid (Hcptpy))	Room temperature reaction	Hydroxyl nitro aromatic compounds	Fluorescence quenching	Selective detection of hydroxyl nitro aromatics including 4-NP, 3,5-DNTSA, 2,4-DNP and PA due to the overlap of the light adsorption bands	4.64 μM, 5.0–320.0 μM	[57]
	Cu-MOG (Cu(II), 2,6-Bis(2-benzimidazolyl)pyridine (BBPY))	Reaction under elevated temperature	nitrite	Electrochemical sensing	Selective detection of nitrite from sausage samples	0.86 mM, 2–150 mM	[67]
	BINOL-terpyridine-Cu(II) (Cu(II), BINOL-terpyridine)	Room temperature reaction	(R)- and (S)-phenylglycinol	Fluorescence quenching	Enantioselectivity through reactions between linkers and analytes	/	[118]
	Fe-MOGs (Fe(III), ndc)	Solvothermal reaction	Aromatic compounds	Photoluminescence increase/quenching	Selective detection of toluene and benzene due to electron donor–acceptor interactions	/	[119]
	Tb(III)-MOG (Tb(III), btc)	Metal replacement	Antibiotics, nitroaromatic compounds	Fluorescence quenching	Selective detection of antibiotics due to the overlap of the light adsorption bands	SMZ (sulfamethazine): 0.086 ppm SDZ (sulfadiazine): 0.218 ppm 2,4-DNT (2,4-dinitrophenol): 1.115 ppm 2,6-DNT (2,6-dinitrophenol): 1.589 ppm 0.52 μM, 0–0.016 mM	[43]
	(Fe-Eu) JLUE-MOG (Fe(III) and Eu(III), TATB)	Reaction under elevated temperature	Chlortetracycline hydrochloride	Fluorescence quenching	/	/	[108]
	Cu(II)/ Co(II)-MOG (Cu(II) and Co(II), 2,4,6-tri(4-carboxyphenyl)-1,3,5-triazine)	Room temperature reaction	Hydrogen peroxide and glucose	Fluorescence sensing	Selective detection of H ₂ O ₂ and glucose with high fluorescence intensity under interfering substance	H ₂ O ₂ (81 nM, 1.0 ~ 10 mM) Glucose (0.33 mM)	[120]
	Tb-MOG (Tb(III), Phen and Luminol)	Room temperature reaction	Mercury (Hg ²⁺)	Fluorescence quenching	Selective detection of Hg ²⁺ with interferents (Cu ²⁺ ,	3.6 nM, 0.1–30 mM, negligible fluorescence	[121]

(continued on next page)

Table 3 (continued)

Applications	Materials (metal nodes, ligands)	Synthesis Method	Target pollutants	Adsorption Capacity	Selectivity	Regeneration	Ref
					Co ²⁺ , Ni ²⁺ , Ca ²⁺ , Mg ²⁺ , Zn ²⁺ , Mn ²⁺ , K ⁺ , Na ⁺ , Ag ⁺ , Fe ³⁺ and Al ³⁺) due to the intense chelation of Hg ²⁺ on the amino groups and the photon-induced charge transfer.	changes with interfering substance	
	FGO-Fe-MOG (Fe(III), btc)	Reaction under elevated temperature	Thrombin	Electrochemical sensing	Selective detection of Thrombin from other proteins due to the strong electrostatic attraction between Fe-based MOG and thrombin-binding aptamer	58 pM, 2–14 ng mL ⁻¹ , negligible signal change with interfering substance	[122]
	MOG-Cu-MWCNT (Cu(II), 2,6bis(1H-benzo[d]imidazol-2-yl)pyridine)	Reaction under elevated temperature	Nitrite	Electrochemical sensing	Selective detection of nitrite with interferents (Ca ²⁺ , Mg ²⁺ , K ⁺ , Na ⁺ , Cl ⁻ , CO ₃ ²⁻ , NH ₄ ⁺ , ClO ₃ , formic acid, caffeic acid, glucose and starch) due to effective electrocatalytic oxidation [123] of nitrite	0.086 mM, 0.3 ~ 100 μM, change of signal is smaller than 10 % when the concentration of the interferent is 100-fold.	[124]
	Ag NPs@Ag(I)-AMTD MOG (Ag(I), 2-amino-5-mercapto-1,3,4-thiadiazole)	Room temperature reaction	Hg ²⁺	SERS detection	Selective detection of Hg ²⁺ with interferents (Ca ²⁺ , Co ²⁺ , Na ⁺ , Mn ²⁺ , Ni ²⁺ , Ba ²⁺ , Zn ²⁺ , Fe ³⁺ and Cu ²⁺) results from the interactions between Hg ²⁺ and Ag NPs	1.5*10 ⁻⁷ M, 5.0*10 ⁻⁷ ~ 9.0*10 ⁻⁶ M, interference ions barely produced any SERS signals	[125]
	Eu-Al-MOG (Al (NO ₃) ₃ ·9H ₂ O, Eu (NO ₃) ₃ ·6H ₂ O, H ₃ BTC) N@MOG-C	Reaction under elevated temperature Pyrolysis of polypyrrole Al MOG	doxycycline Cd ions	fluorescence quenching Electrochemical sensing	/	0.77 μM, 2 – 200 μM	[123]
					Selective detection of Cd ²⁺ with interferents (Pb ²⁺ , Co ²⁺ , Mg ²⁺ , Ni ²⁺ , Mn ²⁺ , Zn ²⁺ , Fe ³⁺ and Al ³⁺) due to charge transfer between Cd(II) and N@MOG-C	2.2 nM, 0.025 ~ 5 mM, high concentrations of Cu ²⁺ and Hg ²⁺ (>10 μM) were found to interfere with the sensing of Cd(II); the other metal ions had no influence	[126]
Applications	Materials	Synthesis Method	Target pollutants	Light source (Intensity)	Selectivity	Degradation Efficiency	Ref.
Catalytic purification of environmental contaminants	PMA@MOG-Cr (Cr (III), 2-aminoterephthalic acid)	In-situ solvothermal reaction	Methyl blue (MB), rhodamine B (RhB) and methyl orange (MO)	Visible light	/	99 %, 97 % in 60 min and 91 % in 120 min for MB, RhB and MO	[127]
	MIL-100 (Fe) MOF/MOX (Fe(III), btc)	Solvothermal reaction	BTXS (benzene, toluene, xylenes and styrene)	250 W Xenon light	/	o-xylene (83.15 %), benzene (23 %), toluene (41 %), p-xylene (82 %), m-xylene (79 %), styrene (83 %)	[41]
	MOF-808 metal organic gels (G808)	Reaction at elevated temperature	2-CEES (2-chloroethyl ethyl sulfide)	/	/	Over 95.9 % within 480 min	[128]
	JLUE-MOG (Fe(III), TATB)	Reaction at elevated temperature	Chlortetracycline hydrochloride	300 W Xenon light with 420 nm cut off filter	/	96.92 %	[129]
	Ti-MOG (Ti(IV), pyromellitic acid)	Reaction at elevated temperature	Dye molecules	UV irradiation (365 nm)	/	/	[130]

(continued on next page)

Table 3 (continued)

Applications	Materials (metal nodes, ligands)	Synthesis Method	Target pollutants	Adsorption Capacity	Selectivity	Regeneration	Ref
	Na/Fe-bimetallic MOG (Na(I) and Fe(III), btc)	Solvothermal reaction	o-xylene, acetaldehyde	Xenon light	Fe-rich MOGs are efficient for o-xylene while Na-rich MOGs favored the removal of acetaldehydes. No test was carried out on mixed pollutants.	o-xylene (67.9 %), acetaldehyde (38 %)	[77]
	CQDs@UiO-66 MOG (Zr (IV), btc)	Solvothermal reaction	Aromatic hydrocarbons	250 W Xenon light	/	Toluene (85 %), o-xylene (86 %), styrene (30 %)	[131]
	Ag NPs@m-MIL-100(Fe) (Fe(III), btc)	Solvothermal reaction	o-xylenes	Xenon and visible light	/	97 % (Xenon light), 80.0 % (visible light)	[132]
	CdS/ MOA(Cr) (Cr(III), btc)	Solvothermal reaction	Cr(VI)	Visible light	/	99 %	[133]
	Fe-BDC/TiO ₂	Room temperature reaction	Acetaldehyde	250 W Xenon lamp (light intensity 204 W/m ²)	/	44.6 %	[134]
	Fe-MOG (Fe(III), 5,10,15,20-Tetrakis(4-carboxyphenyl) porphyrin)	Reaction at elevated temperature	RhB	Visible light	/	98.2 %	[135]
	FeCo/C	Pyrolysis of FeCo-MOG	4-nitrophenol (4-NP)	/	/	98 %	[136]

been applied in the adsorptive removal of water contaminants including dyes, trace organics like polycyclic aromatic hydrocarbons (PAHs) and toluene, organic solvents and metal ions. Similar to the circumstance of gas pollutants, large specific surface area, suitable migration channels and abundant open active sites, are the keys to ideal adsorption performances. Mahmood et al. [69] synthesized a gel-state Fe/ Al-bimetallic MOF by solvothermal method followed by supercritical drying and applied it in the fast uptake of dyes. Compared with monometallic MOGs, gel-state Fe/ Al-MOF with high heterogeneity exhibited larger specific surface area (1861 m²/g), pore volume (9.737 cc/g) and increased amount of mesopores, which provided mass-transfer channels for dye molecules (methyl orange (MO) and rhodamine B (RB) with kinetic diameters of ~1.39 nm and ~1.32 nm). Besides, the introduction of Al led to the reduction of Fe(III) to Fe(II) and resulted in open metal sites in bimetallic MOGs. The combined effects of open active sites and hierarchical porous structure enabled a high uptake for dyes (290 mg/g for rhodamine B and 265 mg/g for methyl orange) in both neutral and acid environments with fast adsorption kinetics. Liu et al. [108] built peony-flower-like (Fe-Eu) JLUE-MOGs with ample porous structures for the enrichment and removal of chlortetracycline hydrochloride (CTC). Thanks to the large BET area of JLUE-MOGs (~110.9 m²/g), the hydrogen bonds and π - π interactions between CTC and MOGs, the influences of pH value of the system and the coexistence of inorganic ions are effectively neutralized, suggesting the commercial feasibility of (Fe-Eu) JLUE-MOGs in the removal of CTC (479.05 mg/g). The author also constructed JLUE-MOG @cellulose aerogels and applied them in an adsorption bed. Compared with pure cellulose aerogels, which became useless after 0.42h, the breakthrough point of JLUE-MOG @cellulose emerged at 10h and the adsorption of CTC lasted for 57h.

The hydrophilicity of MOG adsorbents not only determines their performance in gas adsorption, but also interfere with the capture of non-polar organic solvents. Xu et al. [59] modified the surface of micro-meso-macroporous Al-ATA MOG with perfluorooctanoyl chloride, which could react with amino groups of H₂ATA ligand to produce superhydrophobic Al-ATA-F. Compared with the hydrophilic Al-ATA MOG, the water contact angle of which was near zero, the Al-ATA-F MOG showed superhydrophobicity with a water contact angle of 153° (Fig. 11a). Interestingly, increases in the specific surface area (from 391 to 878 m²/g) and volume of micropores happened after the perfluorooctanoyl chloride treatment, which might be related to a possible

structure rearranged in A-ATA-F. Benefited from the superhydrophobicity and increased specific surface area, Al-ATA-F showed improved adsorption capacity for several types of solvents including pentane, hexane, benzene and toluene with high cyclic stability (Fig. 11b-c).

The charge properties of target pollutants is one of the key factors to be considered during the design of MOGs adsorbents [139]. When considering the adsorption of dyes (cationic or anionic) and/or heavy metal ions, the use of MOGs with charge defects on metal nodes and/or linkers, which could provide sites for electrostatic adsorption, are also favorable. Zhang et al. [140] fabricated a Pb-D11 MOG based on lead nitrate and D11 gelator (biscarboxyl-functionalized benzimidazole derivative, 2-(1-(2-carboxyethyl)-2-undecyl-1H-benzo[d]imidazol-3-ium-3-yl)acetate). The MOG was found to be positively charged and showed high affinity towards negatively charged MO molecules at pH>5.

Aside from organic contaminants, gel-state MOFs have also drawn much attention in the removal of heavy metal ions like Pb (II) [107], Hg (II) [109,110], As (V) [61,111,137], Cr (III) [112], Sb (V) [112] etc. from wastewater. Gao et al. [111] developed a "micro-flower" like Fe-NDC MOGs for the adsorptive removal of arsenic ions in water. Removal rates of above 80% were achieved with the initial concentration of As(V) of 2~30 mg/L and the residue concentration of As were lower than 6 mg/L, which could meet the limitation of drinking water, revealing the application potential of MOGs in water purification. Guo et al. [61] further applied gel-state Fe-MOFs (Fe-MOG) based on a series of ligands for the adsorption of As (V) in water. The diffusion of As (V) inside the pores of MOGs was found as the rate-limiting step. Fe-MOG with H₂FA as the ligand was found as an efficient adsorbent for As (V) removal due to its nanosheet micromorphology and abundant open Fe sites. Similarly, Zhang et al. [137] synthesized Ce-MOG for the rapid adsorption of trace As (V) (500 ppb) in water. Ce-MOG could achieve a relatively low residual concentration of As (V) (below 10 ppb) in 1 min, while for the corresponding Ce-MOF, the residual concentration of As (V) was much higher and the equilibrium adsorption takes 60 min. Adsorption kinetics analysis revealed that the hierarchical porous structure and unsaturated coordinated active Ce-OH sites in Ce-MOG was the key to fast and efficient removal of As (V).

In-situ technology, which takes advantages of inherent components in wastewater to fabricate adsorbents like catechol-polyethylenimine deposited membrane, metal oxides, metal sulfide, layered double

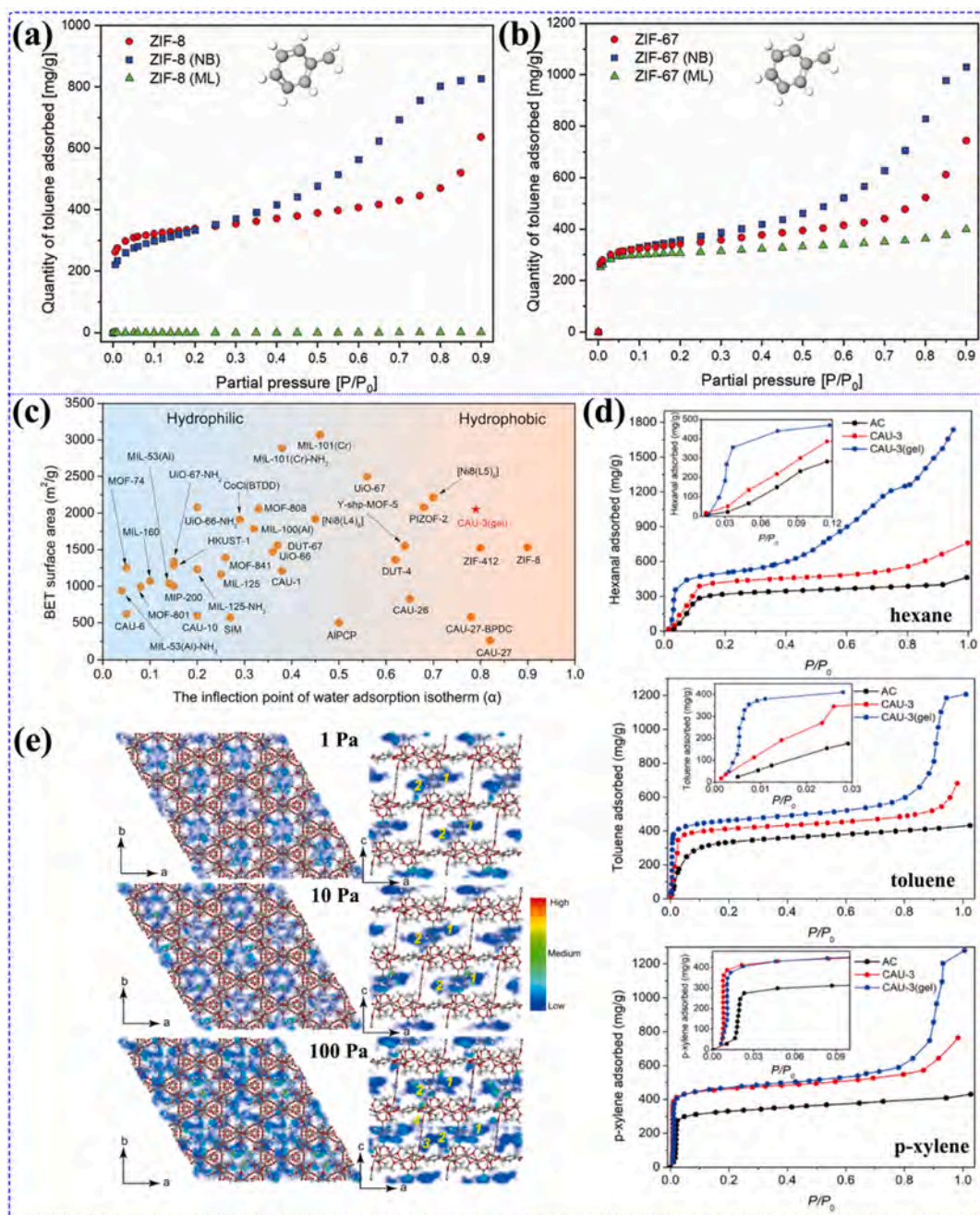


Fig. 9. The toluene vapor adsorption isotherms of (a) ZIF-8 and (b) ZIF-67. NB and ML refers to gel-state ZIF-8 and ZIF-67 based on single (n-butylamine) and multiple modulating ligands (n-butylamine and 1-methylimidazole), respectively [42]; (c) The inflection points of water adsorption isotherms and BET surface areas of different MOFs [40]; (d) Static adsorption isotherms of hexanal (top), toluene (middle), and p-xylene (bottom) on AC, CAU-3, and CAU-3(gel) at 298 K [40]; (e) The density maps of adsorbed hexanal in CAU-3 at 298 K and different pressures: 1.0 Pa (top), 10 Pa (middle), and 100 Pa (bottom) [40]. Reproduced with permission [42]. Copyright 2020 John Wiley & Sons. Reproduced with permission [40]. Copyright 2020 American Chemical Society.

hydroxides and MOFs materials is a newly developed method for wastewater treatment [112]. You et al. proposed an *in-situ* ultrasound-assisted method for synthesizing MOGs and removing heavy metal ions in wastewater. 1,3-dicarboxymethyl-2-methyl benzimidazole (MG) was dissolved into wastewater under ultrasonication to work as the gelator (Fig. 12). MG could coordinate with Cu (II), Cd (II) and Cr (III) ions through the $-\text{COOH}$ groups under ultrasonication with the assistance of cross-linking (EGDMA) and pH-regulation agents (TEA), and therefore achieved the efficient removal of these ions. Considering the HSAB theory, Cu (II) with the highest covalent index (X_{M}^{r}) of 2.60 could strongly coordinate with MG to generate Cu-MG and provide additional bonding sites for Cd (II) and Cr (III) ions to construct MOGs, which

further provided adsorption sites for residue metal ions. The as-prepared MOGs could also be applied as adsorbents for the purification of Sb (V) ions-containing water. The *in-situ* method provides a novel way for the efficient purification of heavy metal ions from actual wastewater.

4.2. Sensing and detection of pollutants in air and water

Aside from adsorptive removal, the detection of both water and air contaminants those are associate with environmental and health issues, e.g., heavy metal ions, organic compounds and toxic gas pollutants, is also an important section of environmental protection. The promising performance of gel-state MOFs in the selective capturing target

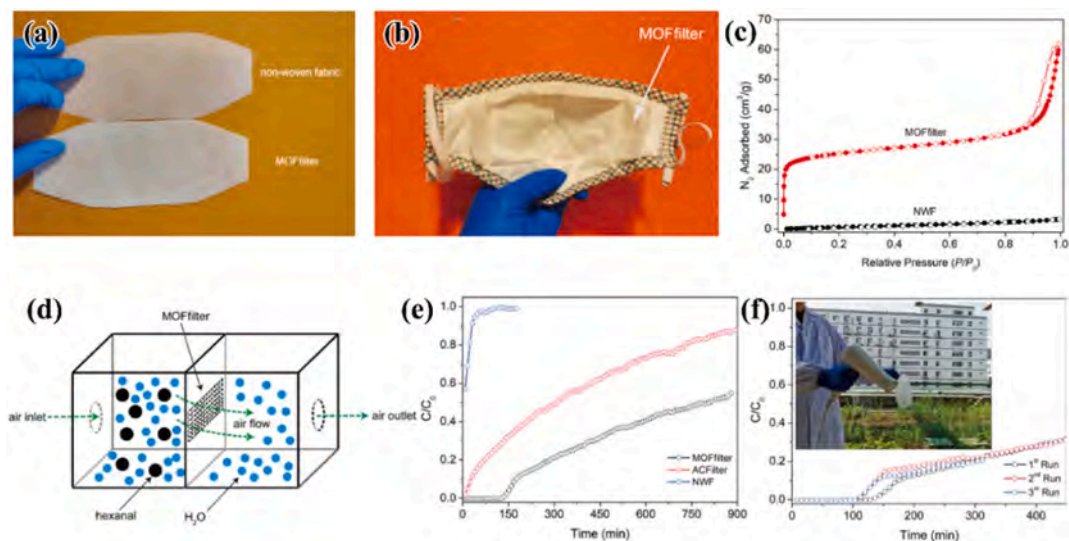


Fig. 10. (a, b) Photographs of filters based on CAU-3 MOG and the mask embedded with the filter. (c) N_2 adsorption–desorption isotherms of NMF and CAU-3 MOG filter at 77 K. (d) Schematic illustration of the home-made setup for breakthrough experiments. (e) Breakthrough curves of hexanal on NWF, AC filter and CAU-3 MOG filter at 298 K under 50 % RH. (f) Breakthrough curves of hexanal on CAU-3 MOG filter in three regeneration cycles. Reproduced with permission [40]. Copyright 2020 American Chemical Society.

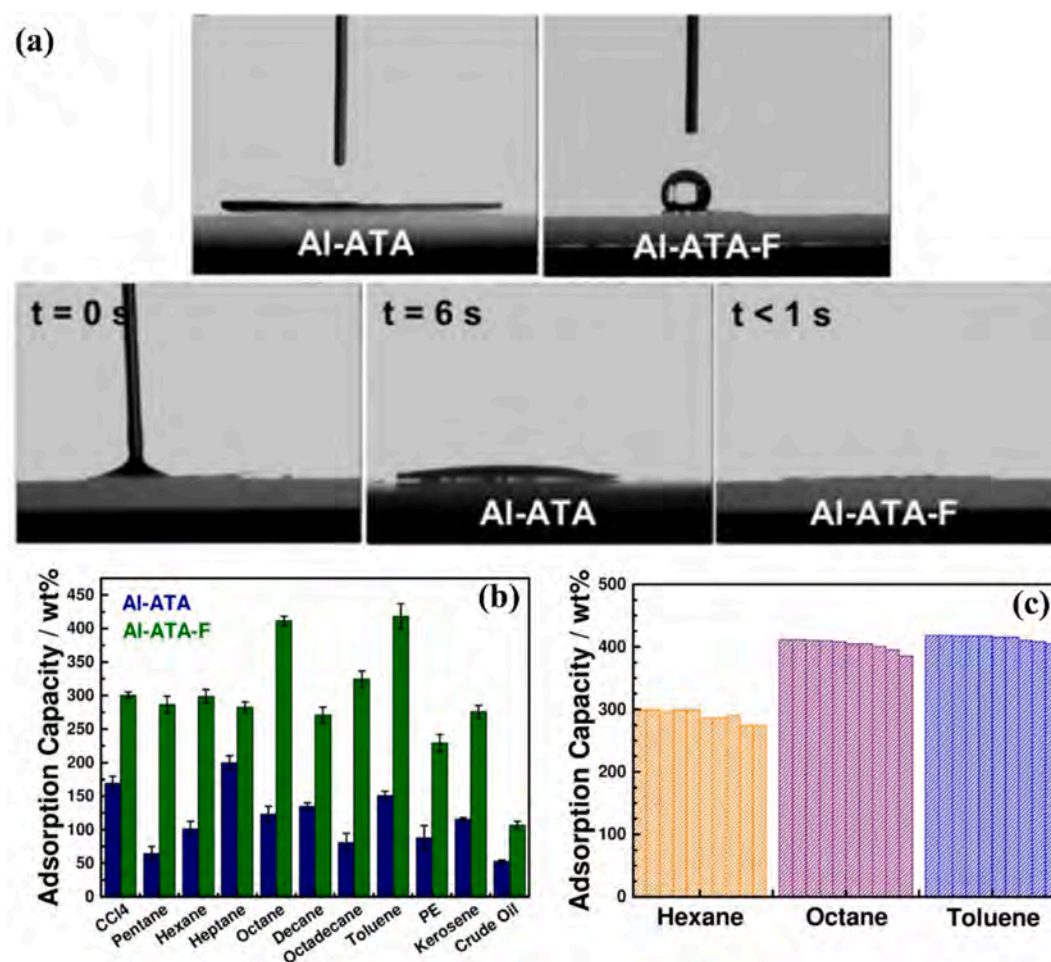


Fig. 11. (a) Water contact angles for Al-ATA and Al-ATA-F (top) and time-dependent decane contact angles on Al-ATA and Al-ATA-F (bottom). (b) Adsorption capacity of Al-ATA and Al-ATA-F for various liquids at 298 K. (c) Cyclic adsorption tests of Al-ATA-F for hexane, octane and toluene. Reproduced with permission [59]. Copyright 2021 John Wiley & Sons.

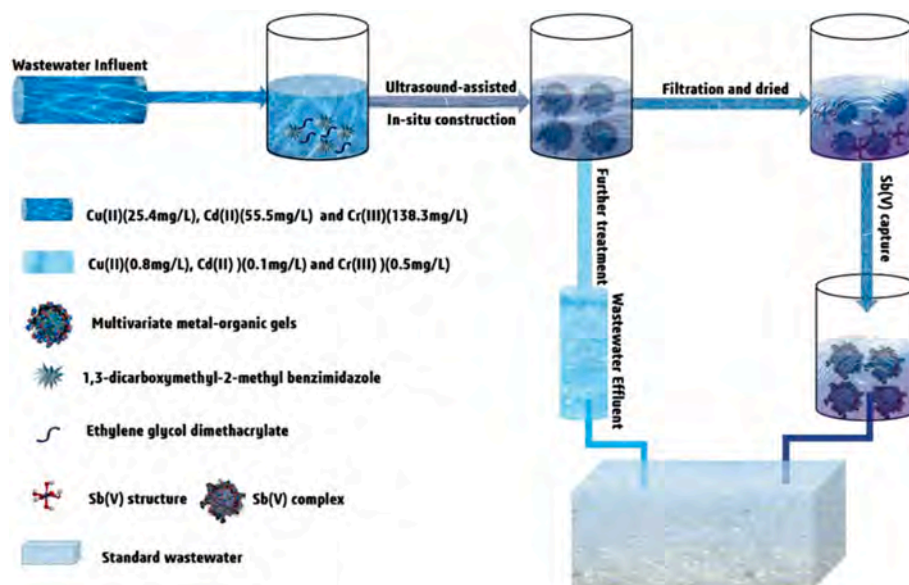


Fig. 12. Illustration of the in-situ construction of multivariate metal–organic gels for capturing metal ions in wastewater. Reproduced with permission [112]. Copyright 2020 Elsevier.

molecules in both gas phase and aqueous solutions make them sensitive sensors or effective analyte enrichment hosts for the detection of air/water pollutants in complex situations [117,141].

As effective adsorbents for target pollutants, MOGs have shown great potential as enrichment hosts for high performance liquid chromatography (HPLC) applications. Hu et al. [117] reported the first MOG-based column for online enrichment of trace analytes. Methacrylic acid (MAA) and ethylene glycol dimethacrylate (EGDMA) were added to strengthen the obtained Fe-BTC MOG, which showed high affinity and relatively excellent enrichment effect (17.2 to 55.6 folds) for amphetamines and PAHs. π - π interaction was found as the main reason for the adsorption of PAHs and the highest enrichment factor was obtained for PAHs with the most aromatic rings (fluoranthene and pyrene with four rings). The adsorption of amphetamines, which mainly relies on the interaction between the electron-rich molecules and Lewis acid sites in the pores of MOGs, was easily influenced by the pH value of the solution.

Other than working as the adsorbent to enrich target molecules, gel-state MOFs have also shown sensing abilities themselves and sensors have been fabricated on the basis of luminescence, electrochemical changes, colorimetry or other signal detection mechanisms. [20,142].

For photoluminescence sensors, fluorescence quenching, fluorescence enhancement and quencher detachment are the mostly invoked categories. Dynamic quenching effect (DQE, the non-radiative deactivation of excited fluorophore upon collision with the quencher) [143], static quenching effect (SQE, formation of nonfluorescent complex by fluorophore with the quencher) [143], fluorescence resonant energy transfer (FRET, the energy transfer between excited fluorescent 'donor' molecules and 'acceptor' molecules through long-range dipole-dipole interactions) [144], electron transfer (ET, the charge transfer between gel-state MOFs and analytes) and inner filter effect (IFE, the competitive light absorption between gel-state MOFs and analytes) are the possible mechanisms for fluorescence changes [57,145]. Structure transformation is a useful way for achieving the quencher detachment approach. In 2010, Chen et al. [118] reported a BINOL-terpyridine-Cu (II) gel for visual chiral sensing. With the addition of target molecules (chiral amino alcohols, (R)- and (S)-phenylglycinol), the coordination between the ligand (conjugation of 1,1'-bi-2-naphthol (BINOL) and terpyridine) and Cu (II) was interrupted, together with the structural collapse of BINOL-terpyridine-Cu (II) gel. Further experiments confirmed that the amino alcohol could displace Cu (II) in BINOL-terpyridine-Cu (II) in an enantio-selective way with (S)-phenylglycinol

more favorable in replacing Cu(II). The fluorescence quenching effect of Cu (II) on the ligand was weakened, therefore achieving the enantio-selective detection of (R)- and (S)- amino alcohols.

In addition to structural transformation, interactions and charge transfer between guest molecules and gel-state MOFs could also cause fluorescence quenching/enhancement effects, which enabled the detection of molecules with different electron donating or accepting properties [119]. Aliev et al. [119] reported the synthesis of two gel-state Fe-MOFs gas sensors by using iron nitrate nonahydrate ($\text{Fe}(\text{NO}_3)_3 \cdot 9\text{H}_2\text{O}$) as the metal source, 2,6-naphthalenedicarboxylic acid (H_2ndc) and 1,2,4,5-benzenetetracarboxylic acid (H_4btc) as the ligands. Compared with pristine gel-state Fe-ndc, variations in the photoluminescence intensities were observed after the adsorption of pollutant molecules including toluene (TN), benzene (BN), nitrobenzene (NB), *meta*-dinitrobenzene (MDNB). For Fe-ndc MOG, $\pi^*-\pi$ transition in the dianion of 2,6-naphthalenedicarboxylic acid was found as the dominant reason for the changes in the photoluminescence intensities. After absorbing excitation light, the adsorbed electron-rich molecules transferred electrons to the framework of Fe-ndc, which inhibited the ndc dianion motions at the excited state and caused an increase in the luminescence intensity. After immersion in toluene and benzene solvents (electron-rich molecules), the maximum luminescence intensities of Fe-ndc MOG were enhanced by 862% and 42%, respectively. On the contrary, the adsorption of electron acceptor molecules of nitrobenzene and *meta*-dinitrobenzene quench its maximum luminescence intensities by 67% and 46%, respectively. On the basis of the electron rich/deficient properties of gas molecules, they achieved the selective detection of various benzyl compounds. Guo et al. [57] synthesized gel-state Al-MOFs for the selective detection of hydroxyl nitro aromatics including 4-Nitrophenol (4-NP), 3,5-Dinitrosalicylic (3,5-DNTSA), 2,4-Dinitrophenol, (2,4-DNP) and picric acid (PA), both are primary constitute of chemical explosives (Fig. 13a). By comparing the fluorescence decay curves, UV absorption spectra and cyclic voltammograms of gel-state Al-MOFs in the absence and presence of PA, inner filter effect (IFE, the competitive light absorption between gel-state Al-MOFs and PA) and electron transfer (ET, the migration of excited-state electron from gel-state Al-MOFs to the lowest unoccupied molecular orbital of PA) [141] were found as the main fluorescent quenching mechanisms.

When combining with specific ligands, rare earth ions like Tb^{3+} and Eu^{3+} could emit strong luminescence due to energy transfer, a phenomenon often known as the antenna effect [146,147]. Qin et al. [43]

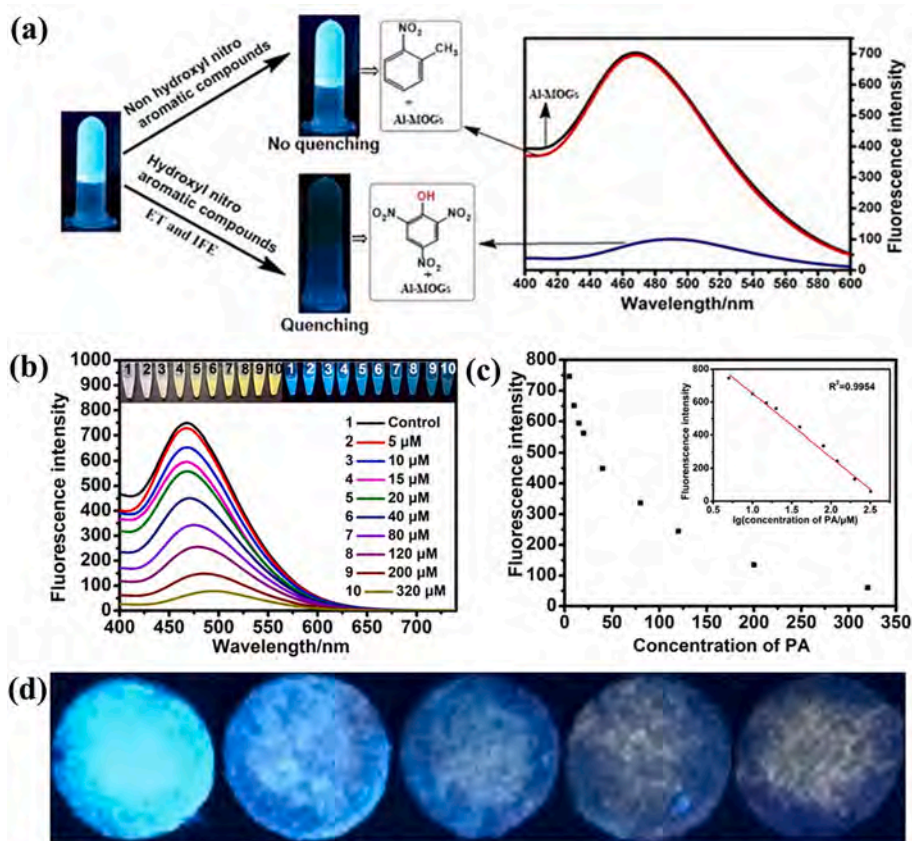


Fig. 13. (a) Schematic illustration of gel-state Al-MOFs for the detection of chemical explosives. (b) The fluorescence emission spectra of gel-state Al-MOFs quenched by picric acid with different concentrations. (c) Calibration curve of the fluorescence intensity versus the concentrations of picric acid; (d) gel-state Al-MOFs based paper sensors for PA recognition. Reproduced with permission [57]. Copyright 2017 Elsevier.

constructed MOG(Tb) xerogel by immersing Al-MOF gel into an ethanol solution of $\text{Tb}(\text{NO}_3)_3 \cdot 6\text{H}_2\text{O}$ for several days. The obtained MOG(Tb) displayed a strong green luminescence under UV light due to the f-f transition of Tb^{3+} ($^5\text{D}_4 \rightarrow ^7\text{F}_j$, $J=3-6$). Benefited from its water stability and luminescence property, the obtained MOG(Tb) was applied in the selective detection of sulfonamides antibiotics (sulfamethazine and sulfadiazine) and nitroaromatics (2,4-DNT and 2,6-DNT) with low detection limits. UV-vis analysis revealed that the overlapping of the absorption bands of analytes with the excitation band of MOG(Tb) was the main reason for the quenching of fluorescence. The adsorbed sulfonamides antibiotics, 2,4-DNT and 2,6-DNT competed with MOG(Tb) for excitation energy and decreased the light absorption by ligand. As a consequence, the energy transfer from ligand to Tb^{3+} decreased, which quenched the characteristic luminescence of Tb^{3+} . Similar mechanism was also proposed for MOG(Eu) in the selective detection of 4-nitrophenol (4-NP) [148].

Aside from fluorescence detection, electrochemical sensing is also widely applied in the detection of environmental contaminants with high accuracy, fast response and simple experimental procedures [149,150]. The numerous open metal sites of gel-state MOFs, which enables the capture of target molecules, made them potential electrode modifiers for electrochemical detection. Peng et al. [67] constructed Cu-MOF xerogel with excellent dispersibility as the electrode modifier for detecting nitrite. The electrocatalytic activity of MOG xerogel/ glassy carbon electrode (GCE) towards nitrite resulted in electrochemical responses upon the concentration of nitrite in solvent.

4.3. Catalytic elimination of environmental pollutants

Due to the advantages of low cost, energy efficient, and direct use of

sunlight, photocatalytic technology has shown great potentiality in the elimination and mineralization of low concentration air/water pollutants. In recent years, MOF photocatalysts like Fe-MOFs [31,151], Cu-MOFs [152,153], Ti-MOFs [154] and Zr-MOFs [155,156] have been developed [157,158]. Similar to the crystalline counterparts, gel-state MOFs could be excited under light irradiation through ligand-to-metal charge transfer (LMCT)[159,160] or metal-to-ligand charge transfer (MLCT)[161] to generate excited charge carrier (electrons and holes), which could then react with absorbed O_2 and H_2O to generate reactive oxidative radicals (ROs) or directly oxidize pollutant molecules.

Chen et al. [41] synthesized MIL-100(Fe) xerogel and characterized its performance in the photocatalytic degradation of typical VOCs. Open Fe-O sites as Lewis acid sites enabled the efficient capture of xylene. The hierarchical porous structure of Fe-MOG and the existence of open channels further lowered the mass-transfer resistance and made the active sites more accessible to VOCs molecules. MIL-100(Fe) MOG showed improved photocatalytic degradation rate towards o-xylene under visible light, about 1.73 times the degradation rate of crystalline MIL-100(Fe) (apparent first-order reaction rate constants of 0.00267 vs 0.00154 min^{-1}). The reversible transition between Fe (III) and Fe (II) under visible light promoted the generation of highly oxidative radicals for the efficient degradation of xylenes. Liu et al. [129] synthesized two novel triazine-based frameworks (JLUE-MOG-1 and JLUE-MOG-2) with Fe and Al as the metal nodes and applied them in the adsorption and photocatalytic degradation of CTC. Benefited from the large specific surface area and suitable HOMO-LUMO gap, Fe-based JLUE-MOG-1 exhibited high catalytic reaction rate and removal ratio towards CTC ($0.23 \times 10^{-2} \text{ mg} \cdot \text{L}^{-1} \cdot \text{min}^{-1}$, 96.92%, Fig. 14b and 14c). Synergistic effect of Fenton-like reaction and photocatalytic process was observed and the PCO degradation of CTC was further promoted in the JLUE-MOG-1/

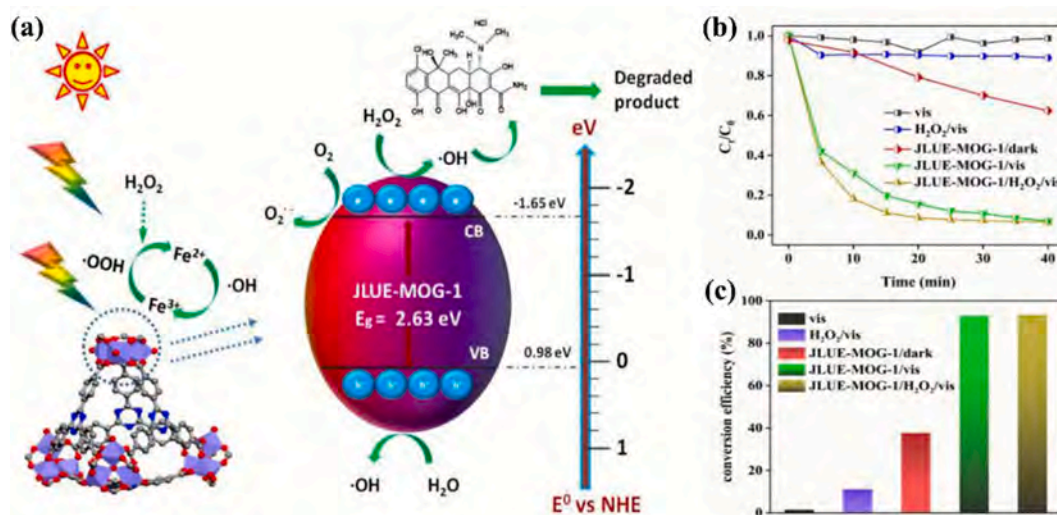


Fig. 14. (a) Schematic illustration of photocatalytic degradation of CTC in JLUE-MOG-1/H₂O₂/vis; (b) Photocatalytic degradation of CTC and (c) the corresponding removal efficiencies in various reaction systems. Reproduced with permission [129]. Copyright 2019 The Royal Society of Chemistry.

H₂O₂/vis system, in which the photocatalytic rate was almost 1.6 times the JLUE-MOG-1/vis system (Fig. 14a). The reversible conversion between Fe(II) and Fe(III) and their interaction with H₂O₂ accounts for the generation of highly oxidative •OH, which is essential for the highly effective degradation of CTC.

In addition to Fe-MOGs, other MOGs have also been applied as effective photocatalysts. Zhou et al. [162] applied UiO-66-NH₂ (Zr-MOF) xerogels in the catalytic decomposition of chemical warfare agents (CWAs). Compared to its crystalline counterparts, UiO-66-NH₂ xerogels exhibited faster reaction rates during the degradation of 2-chloroethyl ethyl sulfide (2-CEES, a sulfur mustard simulant), sulfur mustard (HD) and nerve agent O-ethyl S[2-(diisopropylamino)ethyl] methylphosphonothioate (VX). The higher specific surface area and larger pore size of UiO-66-NH₂ xerogels allowed for the fast migration of CWAs molecules and increased the accessibility of active sites. Kim et al. [130] synthesized Ti-MOGs with Ti-oxo clusters and H₄PA as the ligand. The obtained Ti-MOG showed high stability in water for at least 14 days, indicating its great potential in water decontamination. To characterize the performance of Ti-MOGs as photocatalyst, dye molecules with different charges and sizes including methylene blue (cationic, MB), rhodamine B (cationic, RhB) et al. were chosen as the target molecules. The hierarchical porous structure and carboxylic acid groups of Ti-MOG enabled the fast adsorption of target dye molecules, while the Ti⁴⁺/Ti³⁺ circulation under light irradiation participated in the efficiently decomposition of dyes in water.

The fast and effective adsorption of pollutant molecules onto the active sites is the prerequisite for photocatalytic degradation. As discussed in section 5.1, the adsorption of pollutants may happen on different sites (OMSS, linkers, voids, etc.) through different interactions (Lewis acid-basic interactions, π - π interactions, hydrogen bonds, van der Waals interaction, etc.). The host-guest interaction and charge transfer would significantly influence the degradation paths and efficiency of pollutants. The adjustable active sites of gel-state MOGs provide possibilities for revealing the relationship between adsorption modes and degradation mechanisms and performance optimization. In addition, the light absorption ability, the excitation and migration of excited electron-holes, as well as the ability to generate ROSS, should all be taken into consideration during the design and optimization of MOGs photocatalysts for the catalytic degradation of target molecules.

4.4. Adsorption and catalytic reduction of CO₂

As one of the major greenhouse gases, the capture and catalytic

conversion of low concentration CO₂ in air and industrial emissions is of utmost importance in response to the worsening climate change [163,164]. In 2010, Thallapally et al. [49] firstly applied gel-state MOFs for the capture of CO₂. By using Fe-MOG as the adsorbent, the CO₂ uptake at low (1 bar) and high pressure (30 bar) could reach 6 and 33 wt %, in line with crystalline MOFs reported previously, making gel-state MOFs great candidates for CO₂ capture. Diaz et al. [53] studied the differences of CO₂ uptake performance between crystalline and gel-state MOFs. Compared with Ca-5TIA-MOF, Ca-5TIA-xerogel showed a 20% increased adsorption capacity towards CO₂. The author did not give a specific reason for the increased CO₂ adsorption behavior. Herein, we suspect that the exposure of unsaturated coordinated Ca sites and the open channels inside Ca-5TIA-xerogel might contribute to the improved CO₂ adsorption performance. Fan et al [165], have found that the closely packed structure of γ -cyclodextrin MOG led to a much higher water stability than its crystalline counterparts, which made it a better adsorbent for CO₂. The obtained γ -CD MOG exhibited a CO₂ adsorption capacity of 44.04 cm³/cm³ at 273K and a CO₂/N₂ selectivity of 36.5, which could remain stable after being exposed to humid air for 14 days.

Aside from the uptake of CO₂, some gel-state MOFs also show catalytic activity towards the conversion of CO₂. Liu et al. [45] synthesized ZrBDC-NH₂-MOG for the adsorption and conversion of CO₂. Benefited from the open metal sites, high specific surface area and amino moieties, excellent CO₂ uptake capacity of 18.5 wt% at 0.1 MPa and high selectivity of CO₂ over N₂ were achieved. In addition to the high uptake capacity, the Zr clusters in ZrBDC-NH₂-MOG could activate epoxide and CO₂, which therefore facilitated the catalytic cycloaddition of CO₂. With n-Bu₄NBr acting as the co-catalyst, over 90% yields were performed for the cycloaddition of a wide variety of terminal epoxide substrates. They further compared the catalytic performance with crystalline UiO-66-NH₂ and revealed that the fast transportation of reactants and products through the mesopores and the exposure of open metal sites enabled the remarkably high performance of ZrBDC-NH₂-MOG.

The types of metal nodes and ligands have been found as key factors in determining the adsorption and conversion of CO₂ for they may not only act as active sites, but also participate in the excitation of CO₂ and migration of charge carriers [166]. Albo et al. [167] compared the performance of gel-state Cu-DTA and CuZn-DTA in the electrocatalytic reduction of CO₂. Synergistic effect between Cu and Zn made CuZn-DTA MOG a more effective catalyst for the conversion of CO₂ than Cu-DTA MOGs. The exposure of unsaturated coordinated sites in CuZn-DTA MOG favored the formation of alcohols. Porphyrin (POR) has been regarded as an attractive photosensitizer for it could strongly absorb

visible light and generate long-lived triplet excited states for catalyzing CO₂ conversion [168,169]. Verma et al. [44] functionalized porphyrin with terpyridine (TPY) to produce a TPY-POR linker, on the basis of which Ru-TPY-POR was synthesized (Fig. 15). Due to the coordinative interaction, electrons generated by POR under the irradiation of visible light migrated to [Ru(TPY)₂]²⁺, the catalytic active center for CO₂ reduction. In the presence of TEA as sacrificial electron donor, CO₂ were effectively reduced to CO with >99% selectivity by Ru-TPY-POR coordination gel under visible light. The corresponding turnover number was 92.7 in 12h, the best known visible-light photocatalytic performance. Replacing the sacrificial electron donor with 1-Benzyl-1,4-dihydropyridinamide (BNAH), which was more easily to be oxidized, the charge transfer was accelerated and CH₄ with a selectivity of >95% was detected as the dominant product for CO₂ reduction. The covalent colocalization of both photo-sensitizer and catalysts by purposely constructing gel-state MOFs was proven to be an effective way for visible-light-driven CO₂ reduction.

4.5. Comparison between gel-state MOFs and other environmental materials

In order to evaluate the potential of MOGs in environmental decontamination, we compared them with some commonly applied environmental materials including MOFs, nanosized metal oxides (NMOs), carbon nanostructures, MXene, activated carbon, polymers and g-C₃N₄ from the aspects of efficiency, selectivity and scalability. Table 4 gives the detailed comparison between the above-mentioned materials.

The relatively high pore volume and specific surface area, as well as the abundant active sites (OMSs) both on the surface and inside the pores of MOFs and MOGs enabled the effective adsorption of various environmental pollutants like metal ions [170], hazardous gases and vapors [171] and dye molecules [172]. MOGs have shown superior adsorption capacities (up to 700 mg/g) towards various metal ions, much higher than those of commonly applied adsorbents, such as activated carbon (AC, only a few dozen mg/g), carbonaceous materials (125 mg/g), metal oxides (100 mg/g), LDHs (26–330 mg/g), GOs (100–299 mg/g) and CNTs (19–212 mg/g) [173]. In addition to adsorption capacity, the adsorption kinetics, which give the contact time required for adsorption completion, is also an important criterion for adsorbents. Despite the outstanding adsorption capacity of MOFs, its adsorption kinetics for pollutants, especially the ones with large molecular dynamic diameters, is limited. Audu et al. [174] studied the adsorption of As (V) by UiO-66 and found that after occupying all the active sites on the surface of UiO-66, the migration of As (V) into the nanopores of MOFs became the rate-limit step. Similar problems also happen for layered double hydroxides (LDHs), NMOs, clays and some carbon

nanostructures. The hierarchical porous structure of MOGs provides an effective solution for improving adsorption kinetics by providing mesopores and open channels for the migration of pollutants, while abundant OMSs could work as active sites for target molecules/atoms.

In terms of selectivity, MOFs has been proven to be promising due to its adjustable pore size and surface properties. Both chemical selectivity (OMSs, functional groups or exposed linkers) and size-exclusive selectivity (micropores with adjustable sizes) could be achieved during the selective removal of target molecules. For example, MOFs have been widely used for the separation of U (VI) from nuclear waste water among various interfering metal cations (Cs⁺, Zn²⁺, Pb²⁺, Co²⁺, Ni²⁺, Sr²⁺ and Cr³⁺) through the selective coordination between carboxyl oxygen and U (VI) ions [175–177]. Compared with MOFs, MOGs exhibit more active sites with chemical selectivity due to the higher exposure degree of OMSs and linkers, making them promising adsorbents with high and easily tuned selectivity for target pollutants. Chen et al. [80] utilized the differences in the electron-affinity between Fe (III) and Na (I) to adjust the Lewis acid/basic sites in MIL-100(Fe) MOGs and achieve the selective capture and photocatalytic degradation of electron-rich xylene and electron-deficient acetaldehydes. As for other commonly applied environmental materials, such as nanosized metal oxides, activated carbon and MXene, the selectivity for target molecules is quite limited, which cannot meet the demands for practical application.

Despite the surpassing performance of MOGs adsorbents, the weak interaction between colloid particles, as well as the amorphous phase and fixed solvent molecules around them, severely limited the excitation and spacial separation of charge carriers during the sensing or catalytic degradation of pollutants. MOGs are sometimes poorer than some commonly applied catalysts like TiO₂, MXene, carbon nanostructures and MOFs in generating highly oxidative radicals (ROs). Building heterojunctions with metal nanoparticles, semiconductors or carbon nanostructures, as will be discussed in the next section, has shown potential to address the above issues.

The possibility and cost of scaling-up synthesis, as well as the long-term stability, are also key criteria when evaluating the usefulness of environmental materials. The commercial fabrication and application have been achieved for MOFs by chemical companies like BASF, Framery and Nuada due to their game-changer properties in gas capturing [178]. Compared to MOFs, MOGs could be synthesized under a much more moderate condition, which gives the possibility of scaling-up synthesis and utilization. However, the work on the scaling-up of MOGs is still in its infancy and more future work are needed before the real application of MOGs in environmental decontamination.

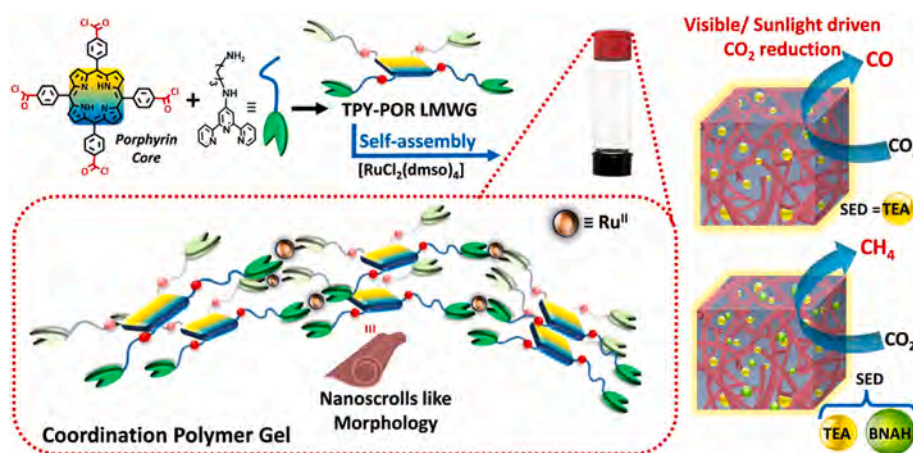


Fig. 15. Schematic illustration of the synthesis of Ru-TPY-POR gel and its application in photocatalytic CO₂ reduction. Reproduced with permission [44]. Copyright 2022 John Wiley & Sons.

Table 4

The comparison between gel-state MOFs and other common environmental materials.

	Applications	Efficiency	Selectivity	Fabrication Methods	Scaling-up
MOFs	Adsorbents	High adsorption capacity; Limited adsorption kinetics for pollutants with large molecular dynamic diameters	High selectivity towards target molecules/ions through chemical selectivity or size-exclusive selectivity	Hydro-/solve-thermal reactions, Room-temperature reactions, Mechanical grinding, Micro-assisted reactions, Electrochemical synthesis, Ultrasonic reaction.	The commercialized synthesis of some MOFs like ZIF-8, MIL-53(Al), HKUST-1, MIL-100 (Fe), PCN-250, etc. have been achieved by companies like BASF, Framergy and Nuada.
	Catalysts	Visible light activity; Unsatisfied conductivity; Adjustable catalytic degradation efficiency for both inorganic and organic pollutants.			
	Sensors	Low detection limit and high resolution			
COFs	Adsorbents, catalysts, sensors	High adsorption capacity; Electro- and photo-catalytic activity; Ultralow limits of detections for gases like NO _x , H ₂ S and SO ₂	High selectivity towards target molecules/ions through chemical selectivity (surface functional groups) or size-exclusive selectivity	Solvothermal synthesis, Ionothermal synthesis, Microwave synthesis, Synthesis in ambient condition, Sonochemical synthesis, microfluidic synthesis, Mechanochemical synthesis, Devitrification Biomimetic synthesis, Stepwise synthesis (from low dimension to high dimension)	Harsh synthesis conditions and high synthesis costs.
Nanosized metal oxides (TiO ₂ , ZnO, MnO, Fe ₂ O ₃ , etc.)	Catalysts	High photo-/thermo-catalytic efficiency; Poor adsorption capacity and slow adsorption kinetics, especially for gas molecules; Easy deactivation; Poor visible light activity	Poor selectivity	Hydro-/solve-thermal synthesis, Vapor deposition, Spray granulation, Electrochemical synthesis, sol-gel combustion synthesis.	Low cost and easily scaling-up
Carbon nanostructures (GO, graphene, carbon quantum dots, carbon nanotube, etc.)	Adsorbents, catalysts, sensors	High adsorption capacity and kinetics; Catalytic activity when combined with noble metal nanoparticles	High chemical selectivity (adjustable surface functional groups)	Chemical derivation, CVD growth, arc discharge, laser ablation, mechanical exfoliation, electro-chemical synthesis.	Complicated preparation processes, high energy demands and small production scale
MXene	Adsorbents, catalysts	Photo catalytic activity; Limited adsorption capacity which depends strongly on the type of MXene and the synthesis approach	Chemical selectivity through surface functionalization	HF-etching, molten salt etching, alkali etching.	High cost, low yield, complex synthesis processes and poor chemical stability
Activated carbon	Adsorbents	High adsorption capacity and kinetics	Chemical selectivity after purposive surface functionalization	Pyrolysis, gasification, hydrothermal carbonization	Low-cost and easily produced on a large scale from coal, wood, agricultural wastes and other biomass sources.
polymers	Adsorbents, sensors	High adsorption capacity and a large amount of active sites Low detection limits and rapid response	Chemical selectivity through functionalization	Solution reactions, electropolymerization, hydrolysis, sonication/ultrasonication, mechanical processes	Scaling-up possibility from underutilized biomass feedstock
MOGs	Adsorbents, catalysts, sensors	High adsorption capacity and kinetics; Visible light activity; Unsatisfied conductivity; Adjustable catalytic degradation efficiency for both inorganic and organic pollutants; Low detection limit and high resolution.	Chemical selectivity (OMSs, exposed linkers and functional groups)	Hydro-/solve-thermal reactions; Room-temperature reactions; Mechanical grinding; Micro-assisted reactions; Electrochemical synthesis; Ultrasonic reaction.	Scaling-up possibility due to moderate reaction conditions and high mechanical stability. Future work is needed on choosing environmental benign and low-cost agents and solvents.

5. Optimization of gel-state MOFs for environmental decontamination

As discussed above, despite the many advantages of gel-state MOFs-like hierarchical porous structure, open active sites and easy formability, their applications in environmental decontamination still face several obstacles. Further optimization of textural properties, type and distribution of active sites, conductivity of charge carriers, as well as chemical stability, are necessary for the efficient and selective adsorption, sensing and degradation of various pollutants.

5.1. The modification of metal/ligand in gel-state MOFs

The synthesis of mixed metal-MOGs is not only an effective way for

utilizing the synergistic effect between different metals and constructing high performance catalysts [179], but also a promising method for adjusting the pore structure of MOGs [69]. As reported by Mahmood et al., [69] the co-existence of mixed metals in FeAl-MOGs caused the mismatch growth and formed bridges between colloid particles, as the result of which the binary FeAl-MOA/ MOX exhibited not only improved surface area, but also higher pore size (Fig. 16a). The high surface area and large mesopores made the active sites more accessible for both small (H₂) and large molecules (Dyes, MO and rhodamine B (RB) with diameters of ~1.39 nm and ~1.32 nm, respectively). In addition, the introduction of Al as the second metal also caused the partial reduction of Fe (III) to Fe (II), which could capture the dye molecules by chemisorption at low pH conditions. Due to the synergistic effects of high surface area, open active sites and mixed valance metals, the obtained

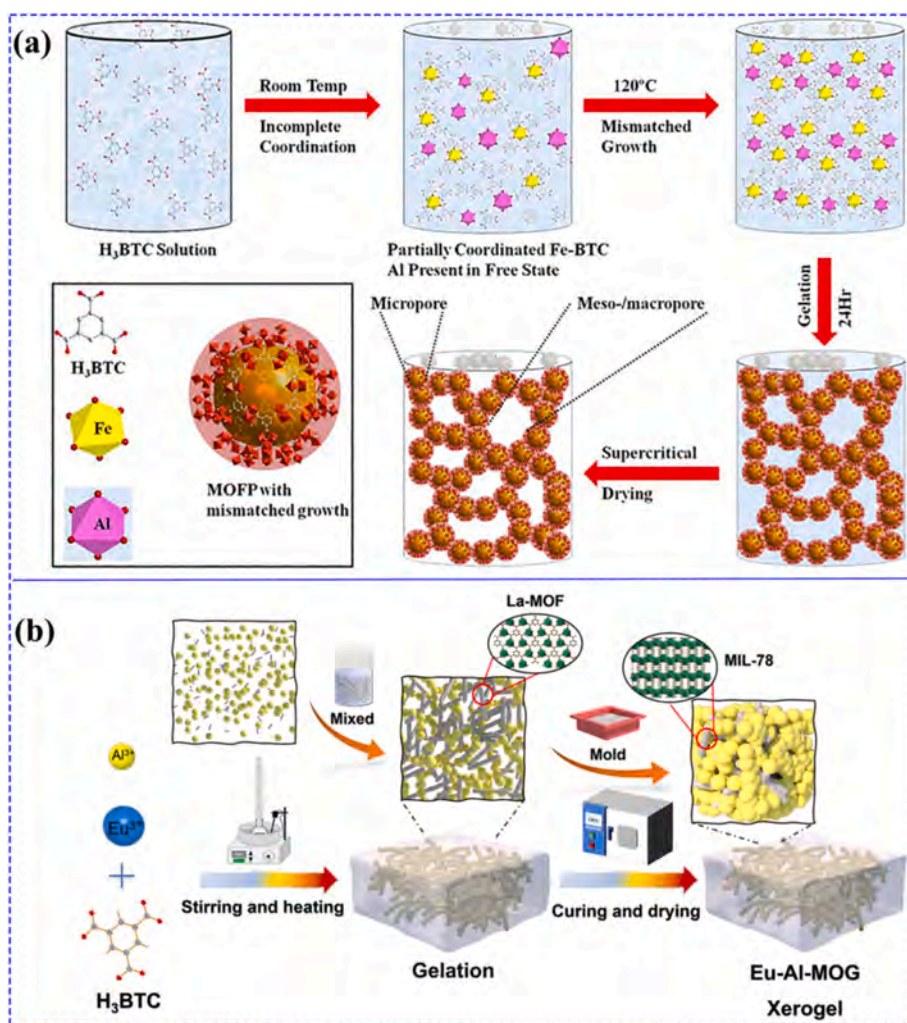


Fig. 16. Schematic illustration of (a) the formation of homogeneous FeAl-MOGs with micro- and mesopores and (b) the synthesis of Eu-Al-MOG heterojunctions. Reproduced with permission [69]. Copyright 2015 Nature. Reproduced with permission [123]. Copyright 2023 American Chemical Society.

FeAl MOA/ MOX displays high adsorption capacity for dyes (290 mg/g of RB and 265 mg/g of MO). Liu et al. [113] constructed several bimetallic FeAl-MOGs by altering the ratio between Fe and Al and analyzed the adsorptive removal of CTC under various conditions. Electrostatic interaction, hydrogen bonding and π - π interaction were found as the dominant forces between CTC and FeAl-MOGs. When containing the same concentration of Fe and Al, the bimetallic MOG with the highest heterogeneity and surface area exhibited the best performance towards CTC removal, reaching a relatively high adsorption capacity of 1600 mg/g. They further combine the MOGs with cellulose for usage in an adsorption bed, the excellent thermal- and mechanical stability make FeAl-MOG a great candidate for removing CTC from pollutant water and a removal efficiency of 95% could be obtained after undisturbed 24h operation. The differences in the reaction rates of different metals during the synthesis of bimetallic MOFs could also lead heterojunctions with metal I-MOFs coated on the surface of metal II-MOGs. Pang et al. [123] fabricated a Eu-Al-MOG with Al-MOG as the substrate and Eu-MOF as the decorator (Fig. 16b). Al-MOG could promote the adsorption of doxycycline (DOX) and Eu-MOF enabled the effective DOX detection through fluorescence quenching. The lowest limit of detection reached $0.77 \mu M$.

Aside from adjusting the micro-morphology, introducing alien metal into MOGs was also found as an effective way for modulating the type of active sites. By using sodium benzoate as the modulator, Chen et al. [77] synthesized bimetallic FeNa-MOG with tunable Lewis acid/basic sites

for the controllable adsorption and catalytic degradation of both electron rich (o-xylene) and deficient (acetaldehyde) VOCs. Na with relatively lower electron affinity was found to replace Fe centers, which induced local charge imbalance in the carboxyl groups and created Lewis basic sites. The successive regulation of Lewis acid/basic sites, which was confirmed by NH_3 -TPD, CO_2 -TPD and in-situ FTIR tests, not only altered the adsorption behavior of o-xylene and acetaldehyde molecules, but also promoted the generation of highly oxidative radicals. As a consequence of the controllable adsorption of VOCs and the increased concentration of $\cdot OH$ radicals, the effective mineralization of both electron rich o-xylene and electron deficient acetaldehyde was achieved.

As an importance section of the LMCT and MLCT processes, the type of metal nodes and the introduction of alien metal centers may also alter the charge transfer and influence the performance of gel-state MOFs as sensors or catalysts. Zhao et al. [120] synthesized gel-state Co/Cu-MOFs with various Co/Cu ratios as enzyme mimic catalysts for the fluorometric detection of H_2O_2 and glucose. Non-fluorescent terephthalic acid (TPA) was applied as the probe molecule for it could be oxidized by H_2O_2 into fluorescent 2-hydroxyterephthalic acid (TAOH) with the assistance of gel-state Co/Cu-MOFs, which showed promoted peroxidase-like activity than gel-state Cu-MOF and Co-MOF. By analyzing the valence state of Cu and Co through Cu LMM Auger spectra and XPS, electron transfer between Cu and Co was confirmed, which accelerated the redox cycles of Cu(II)/Cu(I) and Co(III)/Co(II) pairs and

enhanced the catalytic activity of bimetallic organic gels. As a consequence of the improved enzyme mimic catalyst activity, low detection limits were obtained for both H_2O_2 (~ 81 nM) and glucose (~ 0.33 μM). Similarly, Liu et al. [108] utilized the abnormal charge transfer in gel-state FeEu-MOFs to promote the effective detection of CTC in water. Due to the 4–4f transitions of Eu^{3+} -system, FeEu-MOGs showed high CTC sensibility with low detection limit (0.52 μM), quick response time (0.5 min) and large linear region through the abnormal energy transfer of bimetallic FeEu-MOGs.

In addition to metal centers, the modification of linkers has also been proven to be effective in optimizing the performance of MOGs. As discussed in Section 4.3 and 4.4, the functionalization of linkers with groups like $-\text{NH}_2$, $-\text{CH}_3$ would alter the light absorption behavior of MOGs or improve their affinity towards target molecules. Wang et al. [121] proposed a dual-ligand method for the fabrication of 2-dimensional Tb-MOG nanosheet. The luminol ligand could generate strong fluorescence intensity at 424 nm, while 1,10-phenanthroline-2, 9-dicarboxylic acid (PDA), the second ligand, enabled the formation of MOG nanosheets by replacing the coordination of water to promote the exposure of active sites. Besides, the introduction of PDA could also sensitize the luminescence of Tb^{3+} at 544 nm, which provided a reference fluorescence for the ratiometric detection of Hg^+ in pollutant water.

5.2. Heterojunctions based on gel-state MOFs

Building heterojunctions has been proven to be an efficient way in constructing high performance materials for it could not only take advantages from both sides, but also create synergistic effects. For example, combining gel-state MOFs with conductive materials would be an effective way for accelerating the separation of electron-hole pairs, adjusting the energy of excited charges and improve their catalytic performance. Besides, some components could alter the growth of gel-state MOFs by providing specific functional groups, and therefore

optimizing their porous structure and mechanical stability for the detection and removal of environmental contaminants.

5.2.1. Mogs-carbon material heterojunctions

Typical carbon nanomaterials, including carbon quantum dots (CQDs), carbon nanotubes (CNTs), graphene oxide (GO) and reduced graphene oxide (rGO), were proven to have well-defined microstructure and high stability, which made them ideal template for the controllable growth of MOGs with well-defined porous structures [180]. Besides, some of the carbon materials have specific properties like up-conversion effect (CQDs) and high conductivity (CQDs, CNTs, rGO). With the purposely implantation of these components, MOG-carbon material with organized porous structure, extended light absorption range and improved charge separation ability were obtained, which significantly improved their performance as sensors, adsorbents or catalysts.

Jayaramulu et al. [114] synthesized hierarchically porous fluorinated graphene oxide (FGO)@gel-state MOF composites through a facile solvothermal process for the quick and stable adsorptive removal of oil from polluted water. The plentiful oxygen functional groups (carboxylate, hydroxyl, and epoxy) of FGO enabled the selective and controllable growth of gel-state MOFs (Fig. 17a). The composite exhibited a complex 3D fibrillary micro-/ meso-network structure with mesopores ranging from 2 to 70 nm (Fig. 17b). The synergistic effect between FGO and gel-state Al-MOG created a surface much more hydrophobic (water contact angle of 125°) and oleophilic (oil contact angle of 0°) (Fig. 17 c-h) than any of the single components, which is beneficial for improving the chemical stability of the composites. In addition, the combination of FGO as skeletons improved the mechanical stability of the composites. Benefited from the large pore volume, strong hydrophobicity and superoleophilic nature, the FGO@ gel-state MOFs showed greatly enhanced performance in adsorbing various organic solvents and oil including decane, heptane, crude oil and veg oil, suggesting its proof-of-concept commercial value in oil spill clean-up (Fig. 17i). Urbanova et al. [122] synthesized FGO@gel-state Fe MOF composites through a

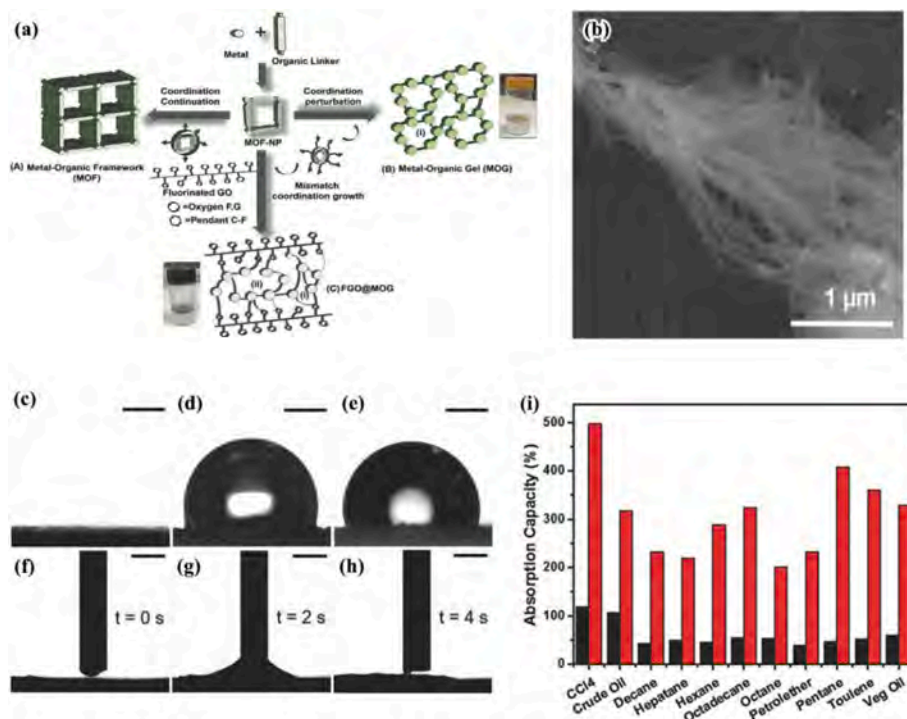


Fig. 17. (a) Schematic illustration of the formation of FGO@MOG composites; (b) The SEM image of FGO@gel-state MOF with fibrous networks; Photographs of water drops on (c) pristine gel-state MOF; (d) pristine FGO and (e) FGO@gel-state MOF; (f-h) The time dependent hexadecane contact angles on FGO@gel-state MOF. (i) Adsorption capacity of gel-state MOF (black bars) and FGO@gel-state MOF (red bars) towards various organic solvents and oil. Reproduced with permission [114], Copyright 2017 John Wiley & Sons.

similar method and applied them in the electrochemical detection of unlabeled thrombin. Compared with pristine Fe-MOG, more mesopores were detected in the FGO@ gel-state Fe MOF composites, which provided abundant binding sites for the analyte. When interacting with thrombin, the charge-transfer resistance of Fe-MOG (the redox probe) increased due to electrostatic repulsion and steric hindrance effects of TBA (5'-GGTTGGTGTGGTTGG-3', the thrombin binding aptamer)-thrombin complex, thus achieving the detection of thrombin. The composites also showed adequate detection results in complex matrix like human serum, which provided with the possibility of clinical practice applications. In addition to surface modified GO, the controllable synthesis of Fe-MOGs could also be achieved by using modified graphene as the template [180].

Multiwall carbon nanotubes (MWCNTs) are tubules of multiple walls with outstanding electronic conductivity, high length-to-diameter ratio and good electrocatalytic activity. The doping of MOGs with MWCNTs could efficiently improve its electrochemical sensing performances. Ding et al. [124] synthesized a MOG-Cu-MWCNTs composite for the electrochemical detection of nitrite. Compared with bare glass carbon electrode (GCE), MWCNTs/ GCE and MOG-Cu/ GCE, the synthesized MOG-Cu-MWCNTs/ GCE gave a much higher peak current density of

nitrite oxidation, which could be attributed to the synergistic effect between MOG-Cu and MWCNTs. The large electrochemical active surface area and high conductivity of MWCNTs enabled the fast charge transfer to nitrite, while the abundant active Cu sites and positive zeta potential of MOG-Cu facilitated the effective adsorption and electrochemical reaction of nitrite. Owing to these favorable properties, MOG-Cu-MWCNTs was proven to be an effective electrochemical sensor for nitrite with a detection limit is 0.086 μM .

Aside from better conductivity, the introduction of specific carbon nanomaterials like carbon quantum dots (CQDs) would also alter the light absorption ability and photocatalytic activity of gel-state MOFs. Yu et al. [131] reported a visible-light active CQDs@ gel-state UiO-66 MOF composite for the photocatalytic oxidation of toluene (Fig. 18e). CQDs were imbedded into the MOG matrix through a 'quasi-in-situ' method, in which CQDs were added to the colloid formed by re-dispersing gel-state UiO-66 MOF in water. CQDs was found to introduce new active sites for the adsorption of toluene molecules. Besides, the up-conversion effect and conductivity of CQDs promoted the light adsorption and charge separation gel-state UiO-66 MOF, thus resulting in the formation of more oxidative active radicals by CQDs@ gel-state UiO-66 MOF composite under visible light. A degradation efficiency of 35% towards toluene was

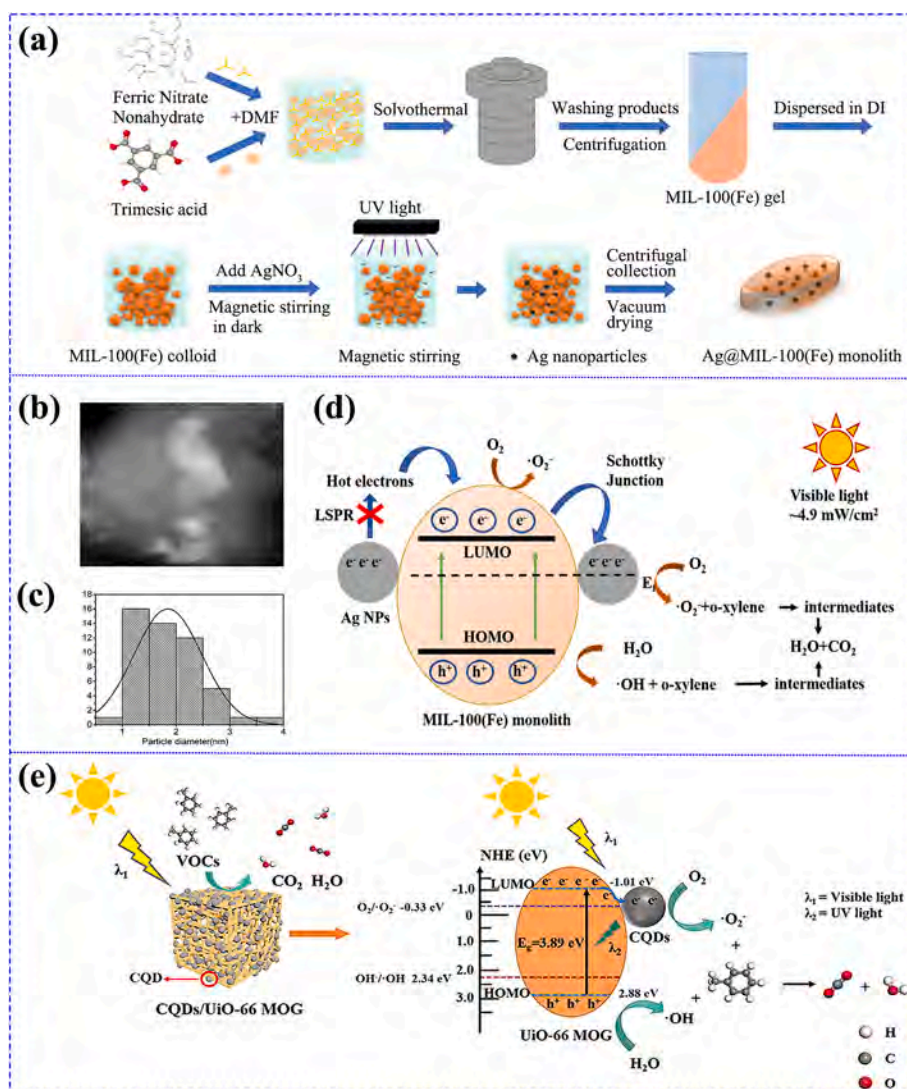


Fig. 18. (a) Schematic illustration of the 'quasi-in-situ' synthesis of Ag@ gel-state MIL-100(Fe) [132]; (b) HAADF-SEM image of Ag NPs@MIL-100(Fe) MOG and (c) The size distribution of Ag NPs [132]. Schematic illustration of the structure and separation of excited electron-holes during photocatalytic reactions in (d) Ag NPs@MIL-100(Fe) MOG [132] and (e) CQDs@ gel-state UiO-66 MOF [131]. Reproduced with permission [131]. Copyright 2022 Elsevier. Reproduced with permission [132]. Copyright 2022 American Chemical Society.

obtained, 4 times the performance of pristine UiO-66, together with a relatively high mineralization ratio of ~85% and long-term stability (no performance attenuation in 120 min).

5.2.2. Gel-state MOFs-metal nanoparticle heterojunctions

The combination of metal nanoparticles (NPs) and porous MOFs has long been regarded as an effective way in constructing effective catalysts for environmental decontamination [181–186]. The highly versatile and tunable porous structure of gel-state MOFs could provide confined spaces for the stabilization of metal NPs with various shapes and sizes, while the implantation of metal NPs would promote the separation of excited electron-holes pairs in MOGs or work as new active sites for catalytic reactions.

The self-assembly of small MOF colloids during the sol–gel transition of gel-state MOFs enables the in-situ implantation of guest nanoparticles [78] Alkordi et al. [181] incorporated Au NPs into HKUST-1 monoliths by adsorbing pre-formed Au NPs on the surface of nanocolloids. During the assembly of HKUST-1 colloids, the adsorbed Au NPs are uniformly included in the matrix with no appreciable aggregation of Au NPs being observed. However, citrate shell around Au NPs is still needed to stabilize the Au NPs and facilitate the adsorption of Au NPs, which may impede the charge transfer between Au NPs and the MOGs matrix and influence the gelation of MOFs. Tang et al. [132] proposed a ‘quasi-in-situ’ method for the construction of Ag NPs@ gel-state MIL-100(Fe) based on the reversible conversion between MIL-100(Fe) sol and gel with the addition or removal of solvents (Fig. 18a). Ag precursors were firstly dissolved in MIL-100(Fe) sol and then photo-reduced to form Ag NPs. Thanks to the adsorption of Ag⁺ on colloids and the Van der Waals interaction between adjacent MIL-100(Fe) particles, the reduction of Ag⁺ could be well-controlled and uniform Ag NPs with diameters of 2–3 nm were obtained. When extracting solvent from the MIL-100(Fe) sol, the aggregation of MIL-100(Fe) colloids happened and Ag NPs were consequently embedded in the gel matrix (Fig. 18b, c). The direct contact between Ag NPs and gel-state MIL-100(Fe) matrix enabled the separation of electron-hole pairs in Fe-MOG and significantly improved the photocatalytic performance and stability of Ag NPs@ gel-state MIL-100(Fe) (Fig. 18d) in the elimination of o-xylene (degradation efficiency increases from 55% to 85%, with no deactivation in 180 min), an important aromatic hydrocarbon in air. The efficient generation of ROSS and the complete mineralization was found as the main reason for the long-term stability. Similar methods have also been applied in the encapsulation of large molecules like organometallic compounds, biomolecules and enzymes [75].

In-situ synthesis is another commonly applied method for constructing metal NPs@ MOGs composites. Cheng et al. fabricated Ag

NPs@Ag(I)-AMTD by directly mixing Ag precursor with 2-amino-5-mercapto-1,3,4-thiadiazole (AMTD) in a DMF/ H₂O mixed solvents and applied the composites in the catalytic reduction of 4-nitrophenol (4-NP) [187] and the detection of Hg⁺ [125]. The N and S atoms from the amine and thiol groups of AMTD could coordinate to Ag ions to form 1D linear polymers (Fig. 19a). These 1D coordination polymers then linked with each other through hydrogen-bonding interactions in a random way to form gel-state MOFs. Ag NPs were deposited on the surface of 1D polymers under suitable temperature and reaction time and immobilized in the gel matrix (Fig. 19b-c). Ag(I)-AMTD exhibited strong Raman peak at 1408 cm⁻¹ (C=N stretching mode of AMTD), which decreased with the addition of Ag NPs due to the shielding effect. Upon the addition of Hg⁺ ions, the formation of Ag amalgam happened and the 1408 cm⁻¹ peak increased linearly with the concentration of Hg⁺, achieving the detection of Hg⁺ from aqueous solution.

5.2.3. Mogs-semiconductor heterojunctions

The construction of semiconductors/MOGs composites, was found as another possible means for improving the performance of MOGs catalysts. Heterojunctions formed between the two components could help with the migration/separation of photo excited charges and adjusting the band structure for efficient light-absorption and utilization.

Banerjee et al. [188] proposed a one-pot method for the implantation of CdS quantum dots into a Zn (II) based gel-state MOF by adding the precursor of CdS (cadmium chloride monohydrate and sodium sulfide) into the colloidal solution of Zn-MOF. Due to the H-bond acceptor and donor nature of VA ligand (an L-Valine based molecule, with an amine functionality to act as H bond donor and a pyridine functionality to act as H bond acceptor) and the participation of water solvent, gelation happened at room temperature within 30 s. Pyridine nitrogen from VA ligand bonded to Cd of CdS quantum dots of less than 10 nm and stabilized them inside the gel matrix. Similarly, Wang et al. [133] built CdS/MOA(Cr) (MOF aerogel) composites by directly mixing the precursors of CdS (Cd(Ac)₂·2H₂O and dimethyl sulfoxide) and MOA (1,3,5-benzene tricarboxylic acid and Cr(NO₃)₃·9H₂O) in a solvothermal process.

Polyoxometalates (POMs), as a subset of metal oxides with controllable shape and size, has drawn much attention in catalysis for they could undergo reversible multielectron redox transformation under mild conditions. However, the inherent metastability of POMs restricted their practical application. The implantation of polyoxometalates (POMs) into gel-state MOF matrix is found as a promising way for resolving the problems. By mixing phosphomolybdic acid hydrate with the precursors for gel-state Cr-MOF, Zhou et al. [127] fabricated PMA@NH₂-MIL-101-Cr composite photocatalyst through a facile solvothermal process for the

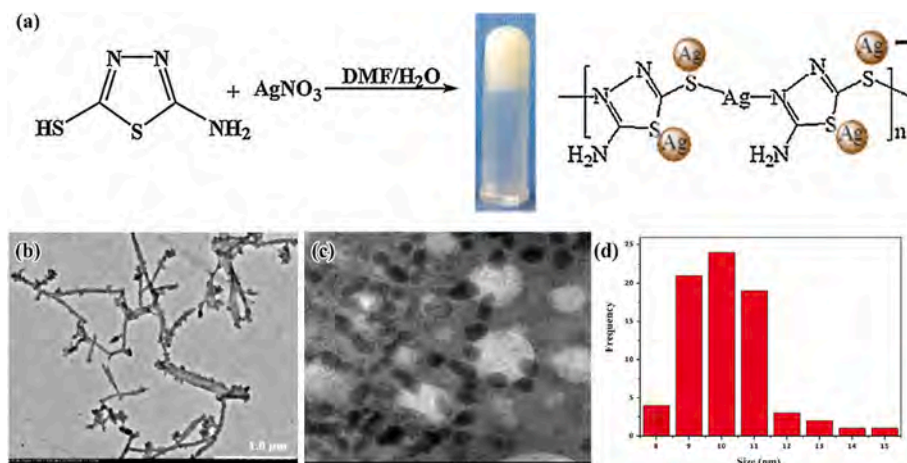


Fig. 19. (a) The synthesis of Ag NPs@Ag(I)-AMTD and its proposed coordination structure. (b,c) TEM images of Ag NPs@Ag(I)-AMTD. (c) Size distribution of Ag NPs in Ag NPs@Ag(I)-AMTD. Reproduced with permission [187]. Copyright 2019 Elsevier.

degradation of dye pollutants. Nearly 97% MB dye and 99% RhB were degraded in 60 min and almost negligible performance decay was observed in 4 cycles. The charge transfer between PMA and Cr-MOG promoted the separation of photo-induced electron-hole pairs and the generation of highly oxidative $\bullet\text{O}_2^-$, h^+ and $\bullet\text{OH}$ radicals, which was found as the main reason for improving the performance and stability of PMA@NH₂-MIL-101-Cr catalysts.

Aside from promoting the generation of radicals, the implantation of metal oxide can also induce new properties to gel-state MOFs or trigger specific catalytic reactions. Fe₃O₄ is a typical metal oxide which not only exhibit magnetic behavior, but also show photo-Fenton behavior. Gu et al. [135] proposed an in-situ solvothermal method for the fabrication of reusable Fe₃O₄/Fe-MOG composites for water purification (Fig. 20). With the assistance of H₂O₂ and light, Fenton-like catalytic reactions could not only effectively remove ~98.8% and 94.5% of RhB in water by Fe-MOG and Fe₃O₄/Fe-MOG (Fig. 20a, c), respectively, but also kill bacteria (*E. coli* and *S. aureus*) in water. In virtue of the magnetic property of Fe₃O₄, the composites showed high reusability and could be easily recovered from water (Fig. 20c), which provided possibilities for practical water purification and targeted photodynamic therapy.

5.3. Gel-state MOFs derivatives

As a hierarchically porous structure with high specific surface area, composition diversity and uniform dispersion of metal nodes, gel-state MOFs have shown great potential in constructing derivatives like metal-based compounds (oxides, carbides, sulfides, et al.), carbon materials and their combinations [136,189,190]. The most commonly applied derivation methods applied today are pyrolysis and solution infiltration, which used heat or solution to remove the unwanted parts from gel-state MOFs. The micromorphology, porosity and composition of the derivatives could be rational tailored by designing MOGs precursors or adjusting the parameters of derivation reactions [191,192]. Efforts have been devoted to the construction of various derivatives for environmental remediation.

5.3.1. Gel-state MOFs derived porous carbon materials

Porous carbon materials with high conductivity, excellent chemical stability and adjustable porosity are attractive candidates of catalysts, sensors and adsorbents. In the past few years, the preparation of porous carbon materials from the derivation of crystalline or gel-state MOF precursors has drawn much attention. In 2013, Zou et al. [190] firstly reported the use of gel-state MOFs (both xerogels and aerogels) as precursors for fabricating porous carbon materials (Fig. 21a). They discovered an inheritance of the porous structure of parenting MOGs by the carbon derivatives (Fig. 21b, c). Due to the high porosity and loose structure of MOF aerogels (MOA), macropores were only found in MOA derived C, while MOF xerogels (MOX) derived C showed high concentration of micro- and mesopores. Relatively high BET surface areas of 3770 cm²/g and 1820 cm²/g was detected for MOX and MOA derived porous carbon materials, respectively, confirming their high potentiality in gas adsorption, storage and separation. Zheng et al. [39] synthesized N-doped granular carbons from gel-state CAU-3-NH₂ and used them in the adsorptive removal of toluene, a common VOC in air (Fig. 21d). Compared with the mother material, the carbonized products showed higher affinity towards toluene. KOH activation was applied after the pyrolysis to partially turn graphitization carbon into amorphous state carbon and improve the uniformity of pores due to its etching effect (Fig. 21e). Compared with pristine CAU-3-NH₂, the derived carbons C700K (carbon materials synthesized by a 700 °C treatment of gel-state CAU-3-NH₂, activated by KOH) showed increased hydrophobicity and relatively high toluene uptake capacity (9.0 mmol/g) under both dry and humid conditions, higher than several widely used adsorbents, including BPL activated carbon, coconut shell activated carbon and representative water stable MOFs (Fig. 21f). Besides, the highly connected channels inside C700K reduced the diffusion length of toluene, and therefore led to a lower regeneration temperature and faster desorption kinetics (Fig. 21g-i).

Due to the inheritance relationship between gel-state MOFs and their carbon derivatives, the composition and microstructures of carbon materials could be well tuned. The addition of N precursors into MOF monoliths is a commonly applied way for synthesizing N-doped carbon materials. Cui et al. [126] synthesized N@MOG-C (nitrogen doped gel-

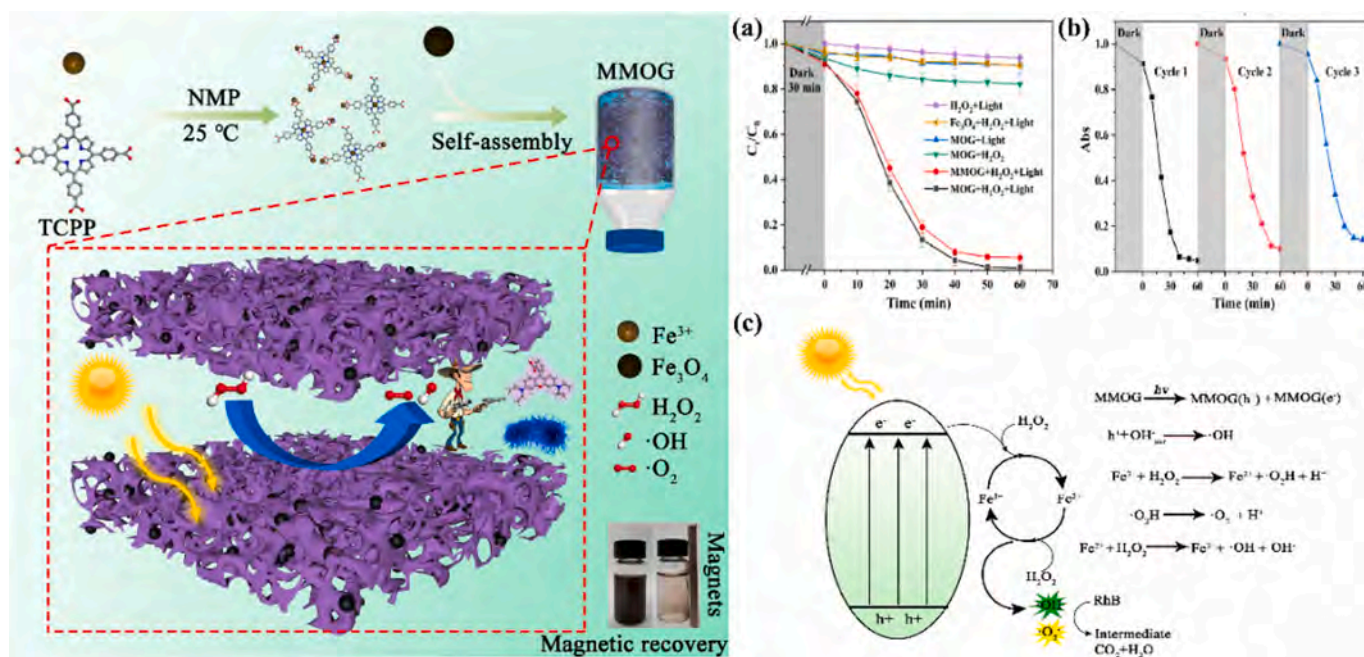


Fig. 20. Schematic illustration of the formation of Fe₃O₄/Fe-MOG (left). (a) The performance of different catalysts in RhB removal in visible light-H₂O₂ systems. (b) Magnetic recovery reusability of Fe₃O₄/Fe-MOG in removing RhB. (c) Proposed reaction mechanism of Fe₃O₄/Fe-MOG co-catalytic photo-Fenton reaction. Reproduced with permission [135]. Copyright 2022 Elsevier.

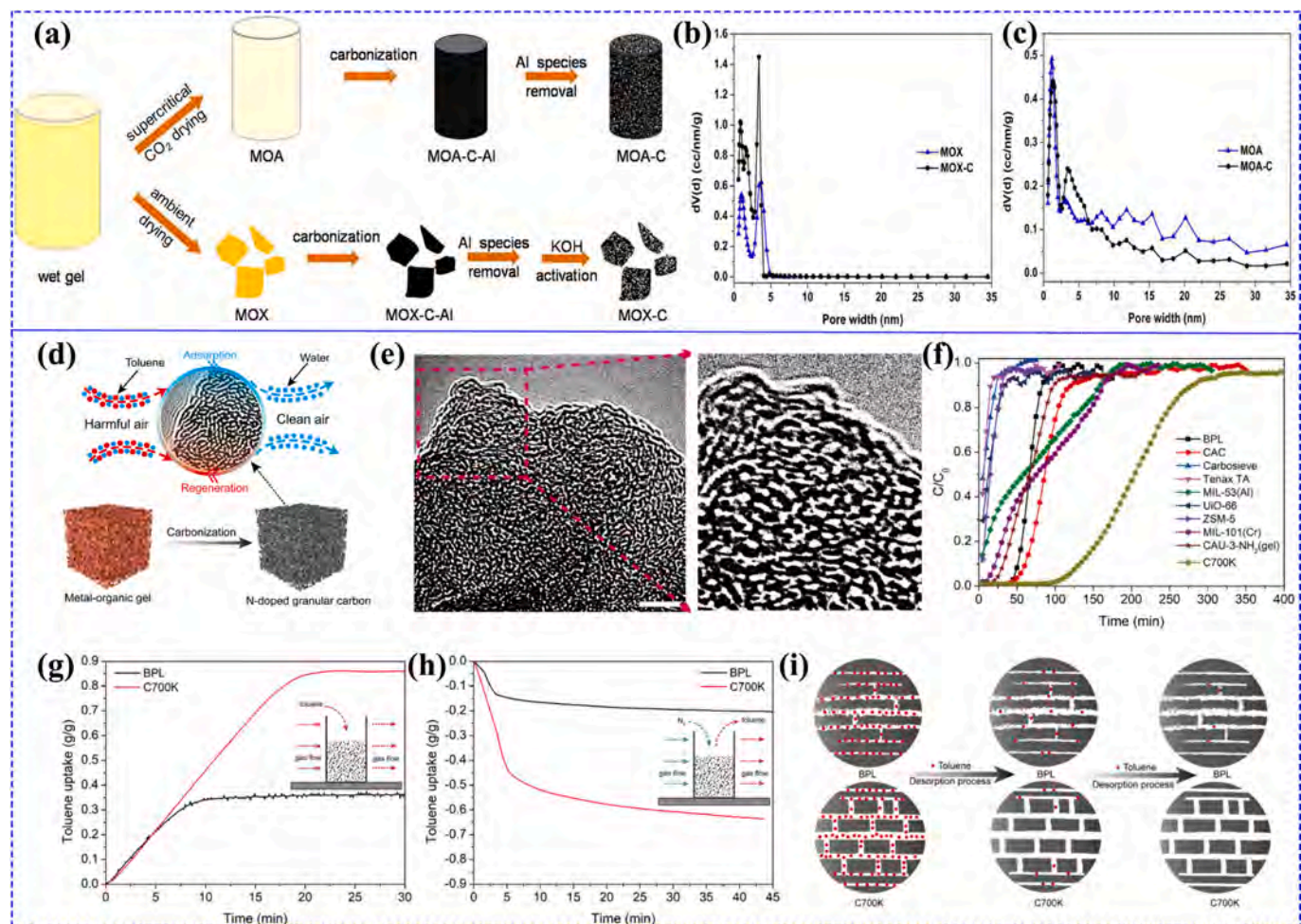


Fig. 21. (a) Typical synthesis procedures of the MOA and MOC derived porous carbon products; The pore size distribution of (b) MOX, MOX-C and (c) MOA, MOA-C [190]; (d) Schematic illustration for the removal of toluene by N-doped granular carbon derived from CAU-3-NH₂; (e) HRTEM images of C700K; (f) Breakthrough curves of toluene on C700K and common adsorbents at 298 K and 60 % RH; The dynamic toluene vapor (g) adsorption and (h) desorption curves of BPL and C700K in loose packed bed; (i) Schematic illustration for the desorption of toluene in BPL and C700K [39]. Reproduced with permission [190]. Copyright 2013 Nature. Reproduced with permission [39]. Copyright 2021 American Chemical Society.

state MOF derived carbon materials) with 3-D interconnected mesoporous by the pyrolysis and HF etching of polypyrrole-doped gel-state Al MOF for the detection of heavy-metal ions in water. The porous structure of gel-state Al MOF could be well maintained during polypyrrole doping and pyrolysis. The relatively high specific surface area ($\sim 1542.6 \text{ m}^2/\text{g}$) of N@MOG-C, which enabled much faster electron transfer kinetics than MOG-C and other commercial carbon materials, made it highly sensitive electrochemical detector of heavy metal ions. Good linearity in the range of $0.025\text{--}5 \mu\text{M}$ was obtained during the detection of Cd(II) and the detection limit was calculated as low as 2.2 nM , much lower than the permitted value in drinking water.

Interestingly, some of the N precursors would also participate in the coordination or gelation of MOF monoliths, which therefore modifies the microstructure of both MOF monoliths and carbon derivatives. By altering the addition sequence of chitosan (precursor for N doping) and the ligand of gel-state Fe-MOF, Shijina et al. [193] proposed Fe entrenched graphitic nanocapsule (CHI-TMA-Fe-CW) and Fe distributed carbon sheets (CHI-TMA-Fe-CW-M1). Unlike the fabrication of CHI-TMA-Fe-CW-M1, during which chitosan was added to preformed Fe-MOG as the intercalation agent, chitosan was firstly coordinated with Fe ions and ligand (trimesic acid) was then added to enable the gelation and the formation of CHI-TMA-Fe-CW (Fig. 22a, b). The strong electrostatic interaction between cationic N in chitosan and Fe(III) established new cross-linking in Fe-MOG and facilitated improved surface

area, more mesopores and higher N dosage in CHI-TMA-Fe-CW-M1 (Fig. 22c-e).

As MOGs are combinations of organic linkers and metal nodes, porous carbon materials modified with metal species of a high dosage is also an important kind of MOGs derivatives. [194] Ke et al. [136] fabricated a porous carbons nanostructure modified with FeCo alloy particles through the pyrolysis derivation of FeCo bimetallic gel-state MOFs. With the molar ratio of Fe:Co reaching 2:1 and 1:1, Co atoms incorporated into the Fe lattice and FeCo alloy nanoparticles were found to uniformly dispersed on carbon nanosheets, with no Fe₂O₃ detected in the composites. The relatively high specific surface area and superparamagnetic property made FeCo/ C composite an important recyclable catalyst for the reduction of 4-nitrophenol (4-NP), a common chemical contaminant in waste water. The high adsorption capacity of porous carbon towards 4-NP and the highly dispersed active Co sites led to 33 times increase in the 4-NP to 4-aminophenol (4-AP) conversion kinetics compared with Fe-MOG, which was comparable to some noble metal-based catalysts. Similarly, by using MIL-100(Fe) MOG as both the parent material and the template, Zhu et al. [116] synthesized magnetic Fe-doped carbon. The high adsorptive removal efficiency of methyl orange and the easy separation of adsorbents provided a novel porous material for eliminating water contaminants.

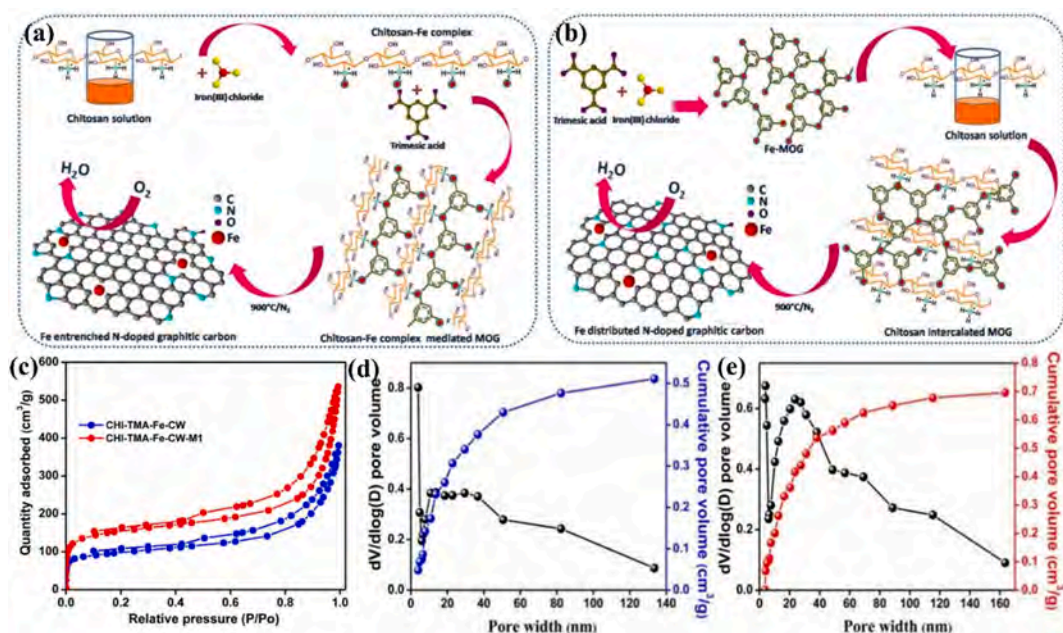


Fig. 22. Schematic illustration of the formation of (a) CHI-TMA-Fe-CW and (b) CHI-TMA-Fe-CW-M1. (c) N₂ adsorption–desorption isotherms of CHI-TMA-Fe-CW and CHI-TMA-Fe-CW-M1. Pore size distribution of (d) CHI-TMA-Fe-CW and (e) CHI-TMA-Fe-CW-M1. Reproduced with permission [193]. Copyright 2017 John Wiley & Sons.

5.3.2. MOG derived metal-based materials

Depending on the atmosphere under which the pyrolysis was carried out, metal-based materials, including metal oxides, phosphides, sulfides etc., as well as their carbon supported composites could be synthesized. Unlike common methods including hydrothermal crystallization, liquid–liquid two-phase method and electrostatic attracting methods, etc., which are usually time consumable and labor intensive, MOG pyrolysis provides a much facile method for the fabrication of metal-based materials or carbon–metal/metal oxides hybrids. Besides, the existence of organic linkers in MOGs prohibits the agglomeration of metal/metal-oxide nanoparticles, which guarantees a relatively higher surface area and larger porosity for the acting as adsorbents, sensors [195] and catalysts [196–198]. Huang et al. [199] proposed a simple pyrolysis approach for synthesizing metastable ZrO₂ supported by nano-porous carbons (ZrO₂-NPC). UiO-66(Zr) MOG was used as the precursor and its organic ligands served as the carbon source. Metastable ZrO₂ (a mixture of monoclinic and tetragonal ZrO₂) was obtained at a pyrolysis temperature of 900 °C, much lower than the commonly applied

temperature for metastable ZrO₂ (usually at 1200 °C to 1400 °C). Microstructure analysis revealed that ZrO₂ nanoparticles were uniformly distributed on NPCs with micro- and mesopores. The existence of Lewis acidic Zr⁴⁺ sites and carboxylic acid groups in NPCs assisted the adsorption of the analyte while ZrO₂ promoted the ionization of neurotransmitters, together making the composite great candidate for laser desorption/ionization tandem mass spectrometry (LDI-MS) applications.

To further prohibit the aggregation of metal oxide NPs during pyrolysis, Wang et al. [197] mixed CNT dispersion with the precursors for Fe-MOG to construct Fe-MOG/CNT composites. The introduction of CNT improved the dispersity of Fe-Fe₂O₃ particles and reduced their particle size during pyrolysis (Fig. 23). The derivative of Fe-MOG/CNTs showed 2.5 times the surface area and 5 times the pore volume of the product obtained by pristine Fe-MOG. Tang et al. [198] applied a similar method for the construction of rodlike FeSe₂-C. GO, as the precursor for rGO, could attract Fe³⁺ through electrostatic adsorption and enable the uniform growth of Fe-MOG on the GO sheets. By annealing the mixture of Fe-MOG/GO composite and Se powders, FeSe₂-C nanorods with width

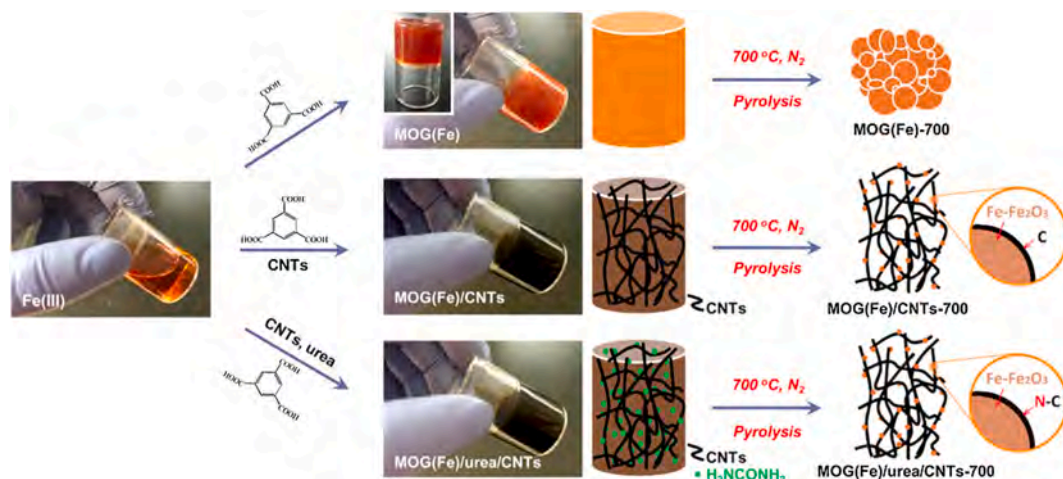


Fig. 23. Fabrication of Fe-MOG, Fe-MOG /CNTs, Fe-MOG /urea/CNTs and their derivatives. Reproduced with permission [197]. Copyright 2017 Elsevier.

of ~200 nm and various lengths were wrapped by rGO nanosheets. These results shed light on the fabrication of effective environmental materials.

6. Scaling-up synthesis of gel-state MOFs and their industrial applications in environmental decontamination

As a great candidate for environmental purification, the scaling-up synthesis and industrial application of gel-state MOFs materials have also attracted attention from both the scientific and industrial communities. Efforts have been devoted to bridge the gap between laboratory research and practical applications from the following aspects.

6.1. The total cost and space–time yields (STY) of gel-state MOFs

Cost and energy demand during the synthesis processes are important criteria when evaluating the scaling-up synthesis of MOGs products. As discussed in Table 1 and 3 of the manuscript, most of the sol–gel synthesis of MOGs are carried out under elevated temperatures (~80 to 180 °C), long aging time (hours to days) and/or increased pressure, which requires high energy inputs and is a great obstacle for scaling-up fabrication. In addition, high pressure reactors and Teflon liners are usually required, which further increase the capital costs. The need for a large quantity of solvent during both reaction and product washing processes, further increases the capital need for synthesizing gel-state MOFs [200]. Advanced methods which could be operate under room temperature, atmospheric vessels and short aging time are necessary for future scaling-up synthesis.

Microwave-assisted and mechanochemical routes processes, which apply microwave and mechanical energy for synthesizing MOFs materials [178,201–204], respectively, have emerged as energy/ time-save and sustainable means for scaling-up synthesis. However, despite the many efforts devoted to the synthesis of MOFs, the work on gel-state MOFs is rare. The fact that microwave may generate hot-spots and create heterogeneous phases and the small scope of application of mechanochemical routes severely limit their use in the scaling-up synthesis of gel-state MOFs. Future efforts like parameter adjustment and reactor design are in need.

Despite the advances in novel scaling-up synthesis methods, the STY of synthesis in batch are still limited and cannot meet the needs for industrial application. Continuous flow processes, which involves flow reactors with enhanced heat and mass transport efficiencies and low residence time, provides opportunities for high STY of MOGs products. Lim et al. [205] firstly developed a direct ink writing method (3-D extrusion continuous flow process) by using colloidal gel of HKUST-1

nanoparticles dispersed in ethanol as ink for the fabrication of densely packed and self-standing MOF monoliths. Pre-synthesized HKUST-1 gel was aged in ambient conditions for a month before 3-D printing through a 10 mL syringe (Fig. 24a). 10 layers of gel with the thickness of each layer set as 0.41 mm were printed in stacks to form square or circle monoliths of 5 mm in height (Fig. 24d–f). The 3-D printing gel-state HKUST-1 show a slightly lower BET surface area (1134 m²/g) than the crystalline powders (1850 m²/g), which could be related to its lower crystallinity. Liu et al. [206] developed a meniscus-guided 3-D printing method for the fabrication of HKUST-1 monolith by using the DMSO solution of copper (II) nitrate trihydrate and trimeric acid (H₃BTC) (the precursors of HKUST-1) as the ink. The evaporation of solvent at the edge of the meniscus formed at the pipette–substrate gap allows for the nucleation of HKUST-1 by increasing the concentration of precursors. In addition to HKUST-1, 3-D printing also has the potential for preparing other gel-state MOFs like MOF-5 [207], zeolitic imidazolate frameworks (ZIFs) [208] and other porous materials like covalent organic frameworks (COFs) [209] as long as the fundamental crystallization kinetics in a confined solution meniscus are understood. Similar to mechanochemical processes, extrusive 3-D printing needs only a small amount of solvent for reaction and product washing, and therefore is a sustainable means for the scaling-up synthesis and application of gel-state MOFs. Expanding the scope of application of extrusive 3-D printing as a continuous flow scaling-up synthesis process without scarifying the surface area and gas adsorption performance of gel-state MOFs, is an important section for future research.

6.2. Stability of MOGs during industrial applications

Stability, including mechanical, thermal and chemical stability, are key factors determining the recyclability and reusability of environmental materials. MOGs have shown improved mechanical stability and easy formability due to the close packing of small colloid particles, which is beneficial for applications like water or air purification. Zhang et al. [210] synthesized a series of MOGs based on phytic acid and metal ions (Fe³⁺, Zr⁴⁺, Al³⁺, Ce³⁺, Y³⁺, Co²⁺, Ni²⁺, Mn²⁺, Cu²⁺, Zn²⁺, Mg²⁺). PA-Fe MOGs exhibited high moldability and could bear up to 200 times its own weight. Castillo et al. [211] synthesized MOGs by using dithiooxamidato (DTA) as the linker with metals ions (Ni, Cu, Pd) and characterized their mechanical stability. According to their compression test results, the Ni-DTA-MOGs could hold up to 2 kg of dumbbell weights. The obtained Ni-MOA also behaved as a plastic material, which allowed processing into films by simply pressing. In addition to excellent mechanical stability, the DTA-MOGs also show high chemical stability in both acid, basic and oxidative solutions, and stand up to temperatures

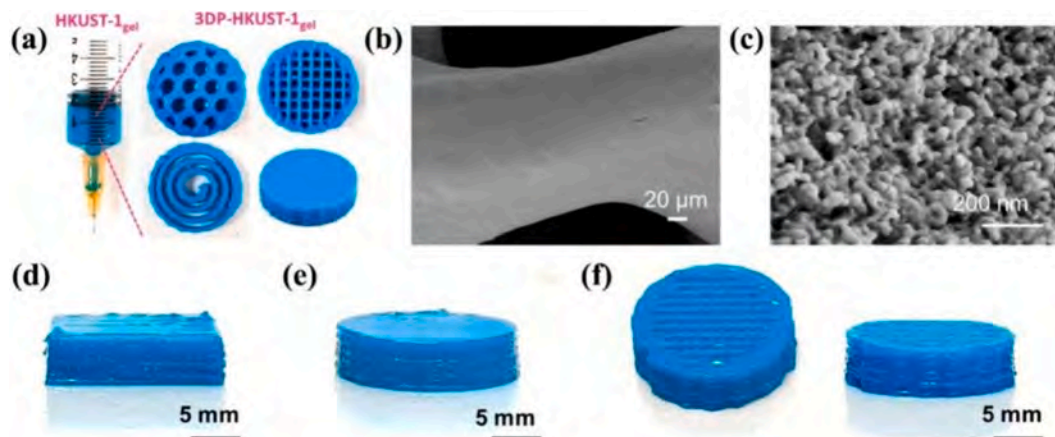


Fig. 24. Syringe loaded with HKUST-1gel and different 3-D printed structures; (b,c) SEM images of dried 3-D printed HKUST-1gel monoliths; Side view of 3-D printed (d) square-shaped and (e) circular shaped monoliths with 10 layers; (f) Top and side view of a high-profile mesh-like monolith. Reproduced with permission [205]. Copyright 2019 American Chemical Society.

as high as 648 K. Qiao et al. [113] combined JLUE-MOG with cellulose to construct composite aerogels with improved mechanical stability. The shape of JLUE-MOG@ cellulose aerogels was maintained after being immersed in water for 24h, indicating its potentiality for practical application in removing CTC from waste water. In addition to cellulose, carbon materials including GO and carbon nanotubes have also been applied as skeletons to improve the formability and mechanical stability of MOGs. Most of the MOGs developed could stand heating to 200 °C or even 300 °C, which could satisfy the demands for water/air purification in most occasions.

Chemical stability, especially water stability, of MOGs, strongly affect their performance in removing water or air contaminants. According to the hard and soft acid and basis (HSAB) theory, high-valent metals (hard acid), like Zr^{4+} , Fe^{3+} , Al^{3+} , Cr^{3+} , etc., tend to form strong interaction with O donor ligands (hard base), therefore leading to MOGs with high chemical stability. These materials could not only remain stable in water, but also stand acidic or basic conditions. Low-valent metals (soft acid), on the other hand, could combine with suitable N-containing linkers (soft base) and form MOGs with reliable performance in water but vulnerable to acidic conditions. Surface fictionalization is another effective means for improving chemical stability. Despite the many methods (post-synthetic treatment, hydrophobic surface treatment, and composite fabrication) reported to improve the chemical stability of MOFs, the efforts on MOGs and their composites are rare. Future research should be done to verify the effectiveness of the existing means for MOG materials.

In addition to the mechanical and chemical stability, the performance stability and regeneration of gel-state MOFs, is another key factor to be considered during the industrial applications. The accumulation of pollutants on the surface of gel-state MOFs may cover the active sites for adsorption, sensing and catalytic degradation and deactivate the material. Therefore, revealing the changes of MOG materials through online methods like in-situ FTIR/ Raman/ XRD during the deactivation and regeneration processes, and material optimization accordingly, are the prerequisite for practical application. In addition, long-term (several weeks or even months) or cyclic (hundreds to thousands of cycles) stability of MOG materials must be evaluated in ahead, especially in harsh conditions with high humidity, improved temperature or even acid/base solutions.

6.3. Life-cycle assessments of MOGs for environmental decontamination

Life-cycle assessment, including both economical (the costs and market prospects) and environmental assessments over all stages of the life cycle of MOGs, is the prerequisite for industrial application in environmental decontamination.

The cost of ingredients (metal precursors, linkers, solvents and modulators, etc.) are important economic factors to be considered. Earth-abundant metals, like Fe, Al, Ca, Mg, Zn, Ti, and Zr are not only low-cost, but also environmentally safe choices. Similarly, low cost and commercially available linkers like terephthalic acid, trimeric acid, fumaric acid, and isophthalic acid are favorable choices while auxiliary linkers should be avoided. In addition, linkers that could be transformed from PET wastes, bio-sourced and biomass materials are also ideals alternatives. Solvent, which not only participates in the synthesis processes, but also plays a key role in washing products, is another important component for cost evaluation. Despite the ideal hydrogen bond donor and acceptor ability of DMF, DMSO and DMA, their high cost would be an obstacle for large-scale fabrication. One solution is to replace these solvents with low-cost solvents like ethanol, methanol or even water, especially during the washing processes. Recently, Zhang et al. [115] achieved the synthesis of monolithic MIL-100(Fe) in aqueous solution at room temperature by using NaOH as the modulator. Their work confirmed the possibility of water as solvents for scaling-up synthesis of MOGs. Another option is to apply novel synthesis methods which are solvent-free or only need a small amount of solvent like

mechanicochemical or micro- or millifluidic processes.

The eco-safety of reagents applied, the by-products of MOGs synthesis, as well as possible wastes generated during the disposal of MOGs, should all be taken into consideration during safety evaluation. Toxic solvents and modulators like HF and TEA are not favorable for large-scale fabrication. Besides, the risk that solvents like DMF may decompose and release toxic substance, should also be aware. As for metal precursor, toxic or even radioactive elements like Cd, Co, In, Cr, U and Th should be avoided. In addition, metal nitrates and chlorides are commonly applied due to their high reactivity and easy soluble in the most applied solvents. However, the high corrosiveness of these metal salts put forward higher safety requirements for production and handling processes. As alternatives, metal precursors with higher safety like acetates, carbonates and oxides have been applied during the large-scale fabrication of MOFs by BASF and other companies [69].

As far as we concerned, most of the research published today are still remain in the laboratory for small batch/pilot preparation and performance testing and the life-cycle assessments of MOGs in industrial practitioners are rare. Future work is necessary before the large-scale synthesis and industrial application of gel-state MOFs.

7. Conclusion and outlooks

As a newly emerging porous material, gel-state MOFs have drawn tremendous attention in the past decades. By adjusting the synthesis parameters like solvents applied, type of precursors, aging temperature/time, modulators and solvent extraction methods, countless types of MOGs have been constructed for the adsorption, detection and catalytic removal/ conversion of air/ water contaminants. Advanced characterization means have been developed for revealing the composition, pore structure and micro-morphology of gel-state MOFs. Modifications have been conducted through surface functionalization, metal/ ligand modification, constructing heterojunctions, derivation, etc. to optimize the performance of MOGs and meet the enquirers of practical applications. Despite all those efforts, numerous challenges and opportunities still exist in the development of high-performance MOGs and their industrial applications.

7.1. Controllable synthesis of gel-state MOFs

Building bridges between the reaction parameters, the interactions between solvents, metal ions, ligands and modulators, and the microstructures (the sizes/alignment colloid particles, the shape and distribution of pores, etc.) of gel-state MOFs, is necessary for the controllable synthesis. Despite the many efforts discussed in Section 2, only case-by-case discussions over the controllable synthesis were found in previous literature. The multiple combinations of metal centers and ligands provide tremendous possibilities for the assembly of MOGs. As the gelation of MOGs strongly rely on the coordination between metal ions and ligands/solvents, the suitable reaction parameters for gelation vary for different MOGs, which brought difficulties in the development of new materials. Systematic investigation is needed to establish universal laws or build libraries for the controllable synthesis of MOGs and avoid repeated verification of experimental parameters. The application of machine learning, combined with artificial intelligence (AI) and intelligent experimental robots, may greatly decrease the time, labor and cost needed for the systematic investigations and help with the controllable synthesis of gel-state MOFs.

7.2. The precisely characterization of gel-state MOFs

The lack of long-range ordering and poor conductivity of gel-state MOFs hindered their fine characterization through XRD and electronic microscopy (SEM and TEM). The formation of gel-state MOFs was usually confirmed by simple 'test-tube reversion' tests or N_2 adsorption-desorption isotherms. Precisely characterizations over the

microstructure of MOGs, including the crystallinity, alignment of colloid particles, size and distribution of pores, are sometimes ignored in previous work, which not only hindered the in-depth understanding of the formation mechanisms, but also limited the scaling-up synthesis and industrial applications of gel-state MOF. In recent years, PDF analysis based on total scattering patterns has shown great potential in revealing the microstructure on different length scales of gel-state MOFs. However, PDF analysis usually has high demand for funding and technology, which impeded its wide application, especially in the industrial scale. The seeking for simple and easily accessible test methods is still needed in future work.

7.3. Interactions of gel-state MOFs with complex environmental factors

Unlike lab conditions, the actual working conditions of environmental purification are extremely complex, which places higher demands on material design. The co-existence of multiple pollutants, for example, usually happen in actual conditions. Selectivity for target pollutants is such a complex environment, is an important criterion when evaluating the usability of environmental materials. Clarifying the interactions between gas pollutants and MOGs, as well as the design and optimization of active sites on this basis to achieve high selectivity for target pollutants, are among the important directions in material design. Aside from interfering atoms/ ions/ molecules, other environmental factors like pH value, temperature, light intensity, air/ water velocity should also be taken into consideration. Environmental simulation chamber reactions would be necessary before practical applications.

7.4. The removal of newly emerging pollutants by gel-state MOFs

Micro-/nano-plastics (MP/NPs), persistent organic pollutants (POPs), environmental endocrine (EDCs) and antibiotics, as newly emerging pollutants (EPs), have drawn increasing attention due to their harmful effects to human health and ecological environment. Unlike traditional water pollutants like metal ions or dye molecules, these new contaminants usually show larger sizes (several nanometers to micrometers), which brings higher demands for large migration channels and abundant open active sites. The resistance of adsorbents to water flow during pollutant removal, is another issue to be concerned. Gel-state MOFs, with hierarchical porous structures, unparalleled accessible active sites with adjustable chemical properties (Lewis acid/ basic sites, hydrogen bonding, π - π interactions, etc.), suitable band structures, easy formability and high mechanical stability, show great potential in the removal of these newly emerged contaminants. However, work in this area is still in its infancy and future efforts are needed. Water stability under both acidic and basic conditions, is the first and primary factor to be considered. In addition, understanding the interactions between gel-state MOFs and EPs, revealing the influences of pH, temperature and co-existing ions and/ or organic pollutants, are also necessary before practical application.

Despite the unique hierarchical porous structure, high formability and promising performance, the research on the design, synthesis and application of MOGs for environmental decontamination is still in its infancy. We hope that this review could inspire new ideas of researchers and stimulate the design of novel gel-state MOFs for solving environmental problems. Cooperative research between the fields of MOGs design/ synthesis, environmental purification, computer science (machine learning, artificial intelligence and modeling) and engineering are expected for further advancing the practical application of gel-state MOFs.

CRedit authorship contribution statement

Xiao Wang: Writing – review & editing, Writing – original draft, Project administration, Investigation, Conceptualization. **Yan Wang:** Project administration, Investigation. **Lu Chen:** Project administration,

Formal analysis. **Xiaofeng Xie:** Writing – review & editing, Project administration, Data curation. **Jing Sun:** Writing – review & editing, Supervision, Project administration, Conceptualization.

Declaration of competing interest

The authors declare that they have no known competing financial interests or personal relationships that could have appeared to influence the work reported in this paper.

Data availability

No data was used for the research described in the article.

Acknowledgements

This study was financially supported by the National Natural Science Foundation of China (52072387), the Key Collaborative Research Program of the Alliance of International Science Organization (ANSO-CR-KP-2020-13), the Natural Science Foundation of Shanghai (22ZR1471800), the China Postdoctoral Science Foundation (2023M740514).

References

- [1] M. Anpo, P.V. Kamat, Environmentally Benign Photocatalysts (2010).
- [2] Y. He, Y. Wang, J. Shi, X. Lu, Q. Liu, Y. Liu, T. Zhu, D. Wang, Q. Yang, Incorporating metal-organic frameworks into substrates for environmental applications, *Chem. Engin. J.* 446 (2022) 136866.
- [3] X. Wang, A. Mahmood, G. Lu, X. Xie, J. Sun, Synergistic photocatalytic treatment of aromatic hydrocarbons/ NO_x mixtures over TiO_2 : the activation and replenishment of lattice oxygen, *Chem. Engin. J.* 450 (2022) 138168.
- [4] Z. Rao, G. Lu, L. Chen, A. Mahmood, G. Shi, Z. Tang, X. Xie, J. Sun, Photocatalytic oxidation mechanism of gas-phase VOCs: unveiling the role of holes, $\cdot\text{OH}$ and $\cdot\text{O}_2$, *Chem. Engin. J.* 430 (2022) 132766.
- [5] Z. Rao, G. Lu, A. Mahmood, G. Shi, X. Xie, J. Sun, Deactivation and activation mechanism of TiO_2 and $\text{rGO/Er}^{3+}\text{-TiO}_2$ during flowing gaseous VOCs photodegradation, *Appl. Catal. B-Environ.* 284 (2021) 119813.
- [6] Z. Wang, Y. Huang, M. Chen, X. Shi, Y. Zhang, J. Cao, W. Ho, S.C. Lee, Roles of N-vacancies over porous $\text{g-C}_3\text{N}_4$ microtubes during photocatalytic NO_x removal, *ACS Appl. Mater. Interfaces* 11 (2019) 10651.
- [7] B. Chu, Y. Wang, W. Yang, J. Ma, Q. Ma, P. Zhang, Y. Liu, H. He, Effects of NO_2 and C_3H_6 on the heterogeneous oxidation of SO_2 on TiO_2 in the presence or absence of UV irradiation, *Atmos. Chem. Phys.* 19 (2019) 14777.
- [8] R.M. Rego, G. Kuriya, M.D. Kurkuri, M. Kigga, MOF based engineered materials in water remediation: recent trends, *J. Hazard. Mater.* 403 (2021) 123605.
- [9] S. Yu, H. Pang, S. Huang, H. Tang, S. Wang, M. Qiu, Z. Chen, H. Yang, G. Song, D. Fu, B. Hu, X. Wang, Recent advances in metal-organic framework membranes for water treatment: a review, *Sci. Total Environ.* 800 (2021) 149662.
- [10] K.A. Hofmann, F. Kuspert, Verbindungen von Kohlenwasserstoffen mit Metallsalzen, *Z. Anorg. Chem.* 15 (1897) 204.
- [11] S.-L. Li, Q. Xu, Metal-organic frameworks as platforms for clean energy, *Energ. Environ. Sci.* 6 (2013) 1656.
- [12] H. Wang, J. Li, Microporous metal-organic frameworks for adsorptive separation of C5–C6 alkane isomers, *Acc. Chem. Res.* 52 (2019) 1968.
- [13] X.W. Gu, J. Pei, K. Shao, H.M. Wen, B. Li, G. Qian, Chemically stable hafnium-based metal-organic framework for highly efficient $\text{C}_2\text{H}_6/\text{C}_2\text{H}_4$ separation under humid conditions, *ACS Appl. Mater. Interfaces* 13 (2021) 18792–18799.
- [14] X. Jiang, W. Han, J. Liu, J. Mao, M.J. Lee, M. Rodriguez, Y. Li, T. Luo, Z. Xu, K. Yang, M. Bissonnette, R.R. Weichselbaum, W. Lin, Tumor-Activatable nanoparticles target low-density lipoprotein receptor to enhance drug delivery and antitumor efficacy, *Adv. Sci. (weinh)* (2022) e2201614.
- [15] K. Ni, T. Luo, G.T. Nash, W. Lin, Nanoscale Metal-Organic Frameworks for Cancer Immunotherapy, *Acc. Chem. Res.* 53 (2020) 1739–1748.
- [16] Y. Zhu, Y. Huang, T.H. Yan, J. Li, Y. Li, H.F. Drake, H. Zhong, Y. Jin, R. Zhao, H. C. Zhou, Metal-organic framework-based nanoheater with photo-triggered cascade effects for on-demand suppression of cellular thermoresistance and synergistic cancer therapy, *Adv. Healthc. Mater.* 11 (2022) e2200004.
- [17] T.N. Ang, S. Baroutian, B.R. Young, M.M. Hyland, M. Taylor, R. Burrell, Adsorptive separation of volatile anaesthetics: a review of current developments, *Sep. Purif. Technol.* 211 (2019) 491–503.
- [18] X. Ma, Y. Chai, P. Li, B. Wang, Metal-organic framework films and their potential applications in environmental pollution control, *Acc. Chem. Res.* 52 (2019) 1461–1470.
- [19] B.M. Connolly, J.P. Mehta, P.Z. Moghadam, A.E.H. Wheatley, D. Fairen-Jimenez, From synthesis to applications: metal-organic frameworks for an environmentally sustainable future, *Curr. Opin. Green Sustainable Chem.* 12 (2018) 47–56.

- [20] X. Fang, B. Zong, S. Mao, Metal-organic framework-based sensors for environmental contaminant sensing, *NanoMicro Lett.* 10 (2018) 64.
- [21] R.B. Lin, S.Y. Liu, J.W. Ye, X.Y. Li, J.P. Zhang, Photoluminescent metal-organic frameworks for gas sensing, *Adv. Sci. (weinh)* 3 (2016) 1500434.
- [22] G. Yilmaz, S.B. Peh, D. Zhao, G.W. Ho, Atomic- and molecular-level design of functional metal-organic frameworks (MOFs) and derivatives for energy and environmental applications, *Adv. Sci.* 1901129 (2019).
- [23] F. Xu, W. Shang, G. Ma, Y. Zhu, M. Wu, Metal organic framework wrapped gold nanourchin assembled on filter membrane for fast and sensitive SERS analysis, *Sensor. Actuat. B-Chem.* 326 (2021) 128968.
- [24] Z. Chen, X. Wang, R. Cao, K.B. Idrees, X. Liu, M.C. Wasson, O.K. Farha, Water-based synthesis of a stable iron-based metal-organic framework for capturing toxic gases, *ACS Mater. Lett.* 2 (2020) 1129–1134.
- [25] R.K. Motkuri, H.V. Annareddy, M. Vijaykumar, H.T. Schaefer, P.F. Martin, B. P. McGrail, L.X. Dang, R. Krishna, P.K. Thallapally, Fluorocarbon adsorption in hierarchical porous frameworks, *Nat. Commun.* 5 (2014) 4368.
- [26] R. El Osta, A. Carlin-Sinclair, N. Guillou, R.I. Walton, F. Vermoortele, M. Maes, D. de Vos, F. Millange, Liquid-phase adsorption and separation of xylene isomers by the flexible porous metal-organic framework MIL-53(Fe), *Chem. Mater.* 24 (2012) 2781–2791.
- [27] D.M. Polyukhov, A.S. Poryvaev, S.A. Gromilov, M.V. Fedin, Precise measurement and controlled tuning of effective window sizes in ZIF-8 framework for efficient separation of xylenes, *Nano Lett.* 19 (2019) 6506–6510.
- [28] H.F. Barton, J.D. Jamir, A.K. Davis, G.W. Peterson, G.N. Parsons, Doubly protective MOF-photo-fabrics: facile template-free synthesis of PCN-222-textiles enables rapid hydrolysis, photo-hydrolysis and selective oxidation of multiple chemical warfare agents and simulants, *Chem.* 27 (2021) 1465–1472.
- [29] Y. Liu, S.Y. Moon, J.T. Hupp, O.K. Farha, Dual-function metal-organic framework as a versatile catalyst for detoxifying chemical warfare agent simulants, *ACS Nano* 9 (2015) 12358–12364.
- [30] L. Chen, X. Wang, Z. Rao, Z. Tang, J.J.C.E.J. Sun, In-situ synthesis of Z-scheme MIL-100(Fe)/ α -Fe₂O₃ heterojunction for enhanced adsorption and visible-light photocatalytic oxidation of O-xylene, *Chem. Engin. J.* 416 (2021) 129112.
- [31] K.G. Laurier, F. Vermoortele, R. Ameloot, D.E. De Vos, J. Hofkens, M.B. Roeffaers, Iron(III)-based metal-organic frameworks as visible light photocatalysts, *J. Am. Chem. Soc.* 135 (2013) 14488–14491.
- [32] T. Islamoglu, Z. Chen, M.C. Wasson, C.T. Buru, K.O. Kirlikovali, U. Afrin, M. R. Mian, O.K. Farha, Metal-organic frameworks against toxic chemicals, *Chem. Rev.* 120 (2020) 8310.
- [33] A.M. Plonka, T.G. Grissom, D.G. Musaev, A. Balboa, W.O. Gordon, D.L. Collins-Wildman, S.K. Ghose, Y. Tian, A.M. Ebrahim, M.B. Mitchell, C.L. Hill, J.R. Morris, A.I. Frenkel, Effect of carbon dioxide on the degradation of chemical warfare agent simulant in the presence of Zr metal organic framework MOF-808, *Chem. Mater.* 31 (2019) 9904.
- [34] J. Jover, C.K. Brozek, M. Dincă, N. López, Computational exploration of NO single-site disproportionation on Fe-MOF-5, *Chem. Mater.* 31 (2019) 8875.
- [35] N. Stock, S. Biswas, Synthesis of metal-organic frameworks (MOFs): routes to various MOF topologies, morphologies, and composites, *Chem. Rev.* 112 (2012) 933–969.
- [36] J.P. Zhang, X.C. Huang, X.M. Chen, Supramolecular isomerism in coordination polymers, *Chem. Soc. Rev.* 38 (2009) 2385–2396.
- [37] Y.-K. Seo, J.W. Yoon, J.S. Lee, U.H. Lee, Y.K. Hwang, C.-H. Jun, P. Horcajada, C. Serre, J.-S. Chang, Large scale fluorine-free synthesis of hierarchically porous iron(III) trimesate MIL-100(Fe) with a zeolite MTN topology, *Microporous Mesoporous Mater.* 157 (2012) 137–145.
- [38] K. Yang, Q. Sun, F. Xue, D. Lin, Adsorption of volatile organic compounds by metal-organic frameworks MIL-101: influence of molecular size and shape, *J. Hazardous Mater.* 195 (2011) 124–131.
- [39] X. Zheng, Z. Wu, J. Yang, S. Rehman, R. Cao, P. Zhang, Metal-organic gel derived N-doped granular carbon: remarkable toluene uptake and rapid regeneration, *ACS Appl. Mater. Interfaces* 13 (2021) 17543–17553.
- [40] X. Zheng, W. He, S. Rehman, P. Zhang, Facile synthesis of hydrophobic metal-organic gels for volatile organic compound capture, *ACS Appl. Mater. Interfaces* 12 (2020) 41359–41367.
- [41] L. Chen, X. Wang, Z. Rao, Z. Tang, G. Shi, Y. Wang, G. Lu, X. Xie, D. Chen, J. Sun, One-pot synthesis of the MIL-100 (Fe) MOF/MOX homojunctions with tunable hierarchical pores for the photocatalytic removal of BTXS, *Appl. Catal. B-Environ.* 303 (2022) 120885.
- [42] E. Hunter-Sellars, P.A. Saenz-Cavazos, A.R. Houghton, S.R. McIntyre, I.P. Parkin, D.R. Williams, Sol-gel synthesis of high-density zeolitic imidazolate framework monoliths via ligand assisted methods: exceptional porosity, hydrophobicity, and applications in vapor adsorption, *Adv. Funct. Mater.* 31 (2020) e2008357.
- [43] Z.-S. Qin, W.-W. Dong, J. Zhao, Y.-P. Wu, Q. Zhang, D.-S. Li, A Water-stable Tb(III)-based metal-organic gel (MOG) for detection of antibiotics and explosives, *Inorg. Chem. Front.* 5 (2018) 120–126.
- [44] P. Verma, F.A. Rahimi, D. Samanta, A. Kundu, J. Dasgupta, T.K. Maji, Visible-light-driven photocatalytic CO₂ reduction to CO/CH₄ using a metal-organic “soft” coordination polymer gel, *Angew. Chem. Int. Ed. Engl.* 61 (2022) e202116094.
- [45] L. Liu, J. Zhang, H. Fang, L. Chen, C.Y. Su, Metal-organic gel material based on UiO-66-NH₂ nanoparticles for improved adsorption and conversion of carbon dioxide, *Chem. Asian J.* 11 (2016) 2278–2283.
- [46] M.R. Lohe, M. Rose, S. Kaskel, Metal-organic framework (MOF) aerogels with high micro- and macroporosity, *Chem. Commun. (Camb)* (2009) 6056–6058.
- [47] J. Hou, A.F. Sapnik, T.D. Bennett, Metal-organic framework gels and monoliths, *Chem. Sci.* 11 (2020) 310–323.
- [48] Z. Liu, W. He, Z. Guo, Metal coordination in photoluminescent sensing, *Chem. Soc. Rev.* 42 (2013) 1568–1600.
- [49] S.K. Nune, P.K. Thallapally, B.P. McGrail, Metal organic gels (MOGs): a new class of sorbents for CO₂ separation applications, *J. Mater. Chem.* 20 (2010) 7623.
- [50] C. Duan, Y. Yu, J. Xiao, X. Zhang, L. Li, P. Yang, J. Wu, H. Xi, Water-based routes for synthesis of metal-organic frameworks: a review, *Sci. China Mater.* 63 (2020) 667–685.
- [51] A.K. Chaudhari, I. Han, J.C. Tan, Multifunctional supramolecular hybrid materials constructed from hierarchical self-ordering of in situ generated metal-organic framework (MOF) nanoparticles, *Adv. Mater.* 27 (2015) 4438–4446.
- [52] Y. Qi, C.-T. He, J. Lin, S. Lin, J. Liu, J. Huang, W. Xue, G. Yu, H.-Y. Chao, Y. Tong, Z. Qiao, Mild metal-organic-gel route for synthesis of stable sub-5-nm metal-organic framework nanocrystals, *Nano Res.* 10 (2017) 3621–3628.
- [53] A. Mallick, E.-M. Schön, T. Panda, K. Sreenivas, D.D. Díaz, R. Banerjee, Fine-Tuning the balance between crystallization and gelation and enhancement of CO₂ uptake on functionalized calcium based MOFs and metalogels, *J. Mater. Chem.* 22 (2012) 14951.
- [54] S.C. Wei, M. Pan, K. Li, S. Wang, J. Zhang, C.Y. Su, A multistimuli-responsive photochromic metal-organic gel, *Adv. Mater.* 26 (2014) 2072–2077.
- [55] B. Bueken, N. Van Velthoven, T. Willhammar, T. Stassin, I. Stassen, D.A. Keen, G. V. Baron, J.F.M. Denayer, R. Ameloot, S. Bals, D. De Vos, T.D. Bennett, Gel-based morphological design of zirconium metal-organic frameworks, *Chem. Sci.* 8 (2017) 3939–3948.
- [56] S. Xiang, L. Li, J. Zhang, X. Tan, H. Cui, J. Shi, Y. Hu, L. Chen, C.-Y. Su, S. L. James, Porous organic-inorganic hybrid aerogels based on Cr³⁺/Fe³⁺ and rigid bridging carboxylates, *J. Mater. Chem.* 22 (2012) 1862–1867.
- [57] M.X. Guo, L. Yang, Z.W. Jiang, Z.W. Peng, Y.F. Li, Al-based Metal-organic gels for selective fluorescence recognition of hydroxyl nitro aromatic compounds, *Spectrochim Acta A Mol. Biomol Spectrosc.* 187 (2017) 43–48.
- [58] B. Zhu, G. Liu, L. Chen, L. Qiu, L. Chen, J. Zhang, L. Zhang, M. Barboiu, R. Si, C.-Y. Su, Metal-organic aerogels based on dinuclear rhodium paddle-wheel units: design, synthesis and catalysis, *Inorg. Chem. Front.* 3 (2016) 702–710.
- [59] M.Y. Xu, T.X. Wang, Postsynthetic modification of mixed-ligand metal-organic gels for adsorbing nonpolar organic solvents, *ChemistrySelect* 6 (2021) 12351–12357.
- [60] S. Banerjee, N.N. Adarsh, P. Dastidar, A crystal engineering rationale in designing a CdII coordination polymer based metalogel derived from a C3 symmetric trisamide-tris-carboxylate ligand, *Soft Matter* 8 (2012) 7623.
- [61] Z. Gao, J. Sui, X. Xie, X. Li, S. Song, H. Zhang, Y. Hu, Y. Hong, X. Wang, J. Cui, J. Hao, Metal-organic gels of simple chemicals and their high efficacy in removing arsenic(V) in water, *AIChE J* 64 (2018) 3719–3727.
- [62] A.K. Chaudhari, H.J. Kim, I. Han, J.C. Tan, Optochemically responsive 2D nanosheets of a 3D metal-organic framework material, *Adv. Mater.* 29 (2017) e1701463.
- [63] M. Tricarico, J.-C. Tan, Mechanical properties and nanostructure of monolithic zeolitic imidazolate frameworks: a nanoindentation, nanospectroscopy, and finite element study, *Mater. Today Nano* 17 (2022) 100166.
- [64] B. Li, D. Xiao, D. Deng, H. Ye, Q. Zhou, L. Tang, A Metal-organic gel based on Fe(III) and Bi-pyridine ligand for template synthesis of core/shell composite polymer nanowires, *Soft Matter* 14 (2018) 8764–8770.
- [65] H. Zhao, Q. Shi, H. Xiao, X. Li, Supramolecular approach to metal-organic gels using excess organic ligand as building units, *J. Porous Mater.* 21 (2014) 691–697.
- [66] S. Samai, K. Biradha, Chemical and mechano responsive metal-organic gels of bis (benzimidazole)-based ligands with Cd(II) and Cu(II) halide salts: self sustainability and gas and dye sorptions, *Chem. Mater.* 24 (2012) 1165–1173.
- [67] Z.W. Peng, D. Yuan, Z.W. Jiang, Y.F. Li, Novel metal-organic gels of bis (benzimidazole)-based ligands with copper(II) for electrochromically selective sensing of nitrite, *Electrochim. Acta* 238 (2017) 1–8.
- [68] L. Li, S. Xiang, S. Cao, J. Zhang, G. Ouyang, L. Chen, C.Y. Su, A Synthetic route to ultralight hierarchically micro/mesoporous Al(III)-carboxylate metal-organic aerogels, *Nat. Commun.* 4 (2013) 1774.
- [69] A. Mahmood, W. Xia, N. Mahmood, Q. Wang, R. Zou, Hierarchical heteroaggregation of binary metal-organic gels with tunable porosity and mixed valence metal sites for removal of dyes in water, *Sci. Rep.* 5 (2015) 10556.
- [70] M.J. Kamlet, J.L.M. Abboud, M.H. Abraham, R.W. Taft, Linear solvation energy relationships. 23. A comprehensive collection of the solvatochromic parameters, π^* , α , and β , and some methods for simplifying the generalized solvatochromic equation, *J. Org. Chem.* 48 (2002) 2877–2887.
- [71] C.T. Dziobkowski, J.T. Wroblewski, D.B. Brown, Magnetic properties and mossbauer spectra of several iron(III)-dicarboxylic acid complexes, *Inorg. Chem.* 20 (2002) 671–678.
- [72] F. Al-dolaimy, M.H. Kzar, S.A. Hussein, A.H. Dakheel, M.F. Ramadan, A. S. Abdulwahid, F.A. Rasen, M.L. Shaghnaab, A.H. Alawadi, A. Alsalamy, H. Bahir, Advancements in exploring metal-organic gels: structure, synthesis, and characterization with a focus on preparation conditions, *J. Clust. Sci.* 741–763 (2023).
- [73] A. Bernet, R.Q. Albuquerque, M. Behr, S.T. Hoffmann, H.-W. Schmidt, Formation of a supramolecular chromophore: a spectroscopic and theoretical study, *Soft Matter* 8 (2012) 66–69.
- [74] J. Wang, R.S. Andriamitantoa, D.G. Atinafu, H. Gao, W. Dong, G. Wang, A one-step in-situ assembly strategy to construct PEG@MOG-100-Fe shape-stabilized composite phase change material with enhanced storage capacity for thermal energy storage, *Chem. Phys. Lett.* 695 (2018) 99–106.

- [75] T.N. Tu, S.A. Khalate, K. Chang, J. Kim, "Ship-in-a-Bottle" entrapment of biomolecules in MOF-based xerogel monoliths for high-performance electrochemical hydrogen evolution, *J. Mater. Chem. A* (2024) 7622.
- [76] C.R. Marshall, J.P. Dvorak, L.P. Twright, L. Chen, K. Kadota, A.B. Andreeva, A. E. Overland, T. Ericson, A.F. Cozzolino, C.K. Brozek, Size-dependent properties of solution-processable conductive MOF nanocrystals, *J. Am. Chem. Soc.* 144 (2022) 5784–5794.
- [77] L. Chen, X. Wang, G. Shi, G. Lu, Y. Wang, X. Xie, D. Chen, J. Sun, The regulation of Lewis acid/basic sites in NaFe bimetal MOFs for the controllable photocatalytic degradation of electron-rich/deficient VOCs, *Appl. Catal. B-Environ.* 334 (2023) 122850.
- [78] T.N. Tu, S.A. Khalate, K. Chang, J. Kim, "Ship-in-a-bottle" entrapment of biomolecules in MOF-based xerogel monoliths for high-performance electrochemical hydrogen evolution, *J. Mater. Chem. A* 12 (2024) 7622–7630.
- [79] S. Hermes, T. Witte, T. Hikov, D. Zacher, S. Bahnmüller, G. Langstein, K. Huber, R.A. Fischer, Trapping metal-organic framework nanocrystals: an in-situ time-resolved light scattering study on the crystal growth of MOF-5 in solution, *J. Am. Chem. Soc.* 129 (2007) 5324–5325.
- [80] Z. Wang, C. Villa Santos, A. Legrand, F. Haase, Y. Hara, K. Kanamori, T. Aoyama, K. Urayama, C.M. Doherty, G.J. Smiles, B.R. Pauw, Y.J. Colon, S. Furukawa, Multiscale structural control of linked metal-organic polyhedra gel by aging-induced linkage-reorganization, *Chem. Sci.* 12 (2021) 12556–12563.
- [81] X. de Hatten, N. Bell, N. Yufa, G. Christmann, J.R. Nitschke, A Dynamic covalent, luminescent metallopolymer that undergoes sol-to-gel transition on temperature rise, *J. Am. Chem. Soc.* 133 (2011) 3158–3164.
- [82] G. Cravotto, P. Cintas, Molecular self-assembly and patterning induced by sound waves. The case of gelation, *Chem. Soc. Rev.* 38 (2009) 2684–2697.
- [83] S.M. Moosavi, A. Chidambaram, L. Talirz, M. Haranczyk, K.C. Stylianou, B. Smit, Capturing chemical intuition in synthesis of metal-organic frameworks, *Nat. Commun.* 10 (2019) 539.
- [84] Z. Li, X. Shan, P. Yang, Z. Gao, Q. Fang, M. Xue, S. Qiu, Preparation, characterization and gas adsorption properties of metal-organic aerogels, *Chem. J. Chinese Universities* 40 (2019) 1116.
- [85] I. Miyazaki, Y. Masuoka, K. Oh-Ishii, N. Setoyama, M. Umehara, High-throughput screening and characterization of novel zeolitic imidazolate framework gels, *J. Mater. Chem. A* (2024) 9102.
- [86] H.Y. Mansoor Al-Jarsha, M.M. Ghareeb, Application of Taguchi orthogonal array in optimization of the synthesis and crystallinity of metal-organic framework 5 (MOF-5), *Trop. J. Pharm. Res.* 22 (2024) 2473.
- [87] I. Sahin, Y. Ozbakir, Z. Inonu, Z. Ulker, C. Erkey, Kinetics of supercritical drying of gels, *Gels* 4 (2017) 3.
- [88] S.M.F. Vilela, P. Salcedo-Abraira, L. Micheron, E.L. Solla, P.G. Yot, P. Horcajada, A robust monolithic metal-organic framework with hierarchical porosity, *Chem. Commun. (Camb)* 54 (2018) 13088–13091.
- [89] B.M. Connolly, M. Aragones-Anglada, J. Gandara-Loe, N.A. Danaf, D.C. Lamb, J. P. Mehta, D. Vulpe, S. Wuttke, J. Silvestre-Albergo, P.Z. Moghadam, A.E. H. Wheatley, D. Fairen-Jimenez, Tuning porosity in macroscopic monolithic metal-organic frameworks for exceptional natural gas storage, *Nat. Commun.* 10 (2019) 2345.
- [90] A. Ahmed, T. Hasell, R. Clowes, P. Myers, A.I. Cooper, H. Zhang, Aligned macroporous monoliths with intrinsic microporosity via a frozen-solvent-templating approach, *Chem. Commun. (Camb)* 51 (2015) 1717–1720.
- [91] J. Santos-Lorenzo, R. San José-Velado, J. Albo, G. Beobide, P. Castaño, O. Castillo, A. Luque, S. Pérez-Yáñez, A straightforward route to obtain zirconium based metal-organic gels, *Microporous Mesoporous Mater.* 284 (2019) 128–132.
- [92] D. Sanli, S.E. Bozbag, C. Erkey, Synthesis of nanostructured materials using supercritical CO₂: Part I. Physical transformations, *J. Mater. Sci.* 47 (2011) 2995–3025.
- [93] A.S. Shalygin, A.L. Nuzhdin, G.A. Bukhtiyarova, O.N. Martynov, Preparation of HKUST-1@Silica Aerogel composite for continuous flow catalysis, *J. Sol-Gel Sci. Technol.* 84 (2017) 446–452.
- [94] H. Liu, J. Chen, W. Yuan, C. Jiang, H. Li, J. Li, Y. Li, B. Zhang, Z. Chen, Structure engineering of Fe-based MOF aerogel by halloysite nanotubes for efficient methylene blue adsorption, *J. Sol-Gel Sci. Technol.* 99 (2021) 55–62.
- [95] W. Abdelwahed, G. Degobert, S. Stainmesse, H. Fessi, Freeze-drying of nanoparticles: formulation, process and storage considerations, *Adv. Drug Deliv. Rev.* 58 (2006) 1688–1713.
- [96] T. Tian, J. Velazquez-García, T.D. Bennett, D. Fairen-Jimenez, Mechanically and chemically robust ZIF-8 monoliths with high volumetric adsorption capacity, *J. Mater. Chem. A* 3 (2015) 2999–3005.
- [97] J. Sunil, C. Narayana, G. Kumari, K. Jayaramulu, Raman spectroscopy, an ideal tool for studying the physical properties and applications of metal-organic frameworks (MOFs), *Chem. Soc. Rev.* 52 (2023) 3397–3437.
- [98] A.F. Sapnik, I. Bechis, S.M. Collins, D.N. Johnstone, G. Divitini, A.J. Smith, P. A. Chater, M.A. Addicoat, T. Johnson, D.A. Keen, K.E. Jelfs, T.D. Bennett, Mixed hierarchical local structure in a disordered metal-organic framework, *Nat. Commun.* 12 (2021) 2062.
- [99] A.F. Sapnik, I. Bechis, A.M. Bumstead, T. Johnson, P.A. Chater, D.A. Keen, K. E. Jelfs, T.D. Bennett, Multivariate analysis of disorder in metal-organic frameworks, *Nat. Commun.* 13 (2022) 2173.
- [100] I. Bechis, A.F. Sapnik, A. Tarzia, E.H. Wolpert, M.A. Addicoat, D.A. Keen, T. D. Bennett, K.E. Jelfs, Modeling the effect of defects and disorder in amorphous metal-organic frameworks, *Chem. Mater.* 34 (2022) 9042–9054.
- [101] J.E.M. Laulainen, D.N. Johnstone, I. Bogachev, L. Longley, C. Calahoo, L. Wondraczek, D.A. Keen, T.D. Bennett, S.M. Collins, P.A. Midgley, Mapping short-range order at the nanoscale in metal-organic framework and inorganic glass composites, *Nanoscale* 14 (2022) 16524–16535.
- [102] D.A. Keen, T.D. Bennett, Structural investigations of amorphous metal-organic frameworks formed via different routes, *Phys. Chem. Chem. Phys.* 20 (2018) 7857–7861.
- [103] A.F. Sapnik, C. Sun, J.E.M. Laulainen, D.N. Johnstone, R. Brydson, T. Johnson, P. A. Midgley, T.D. Bennett, S.M. Collins, Mapping nanocrystalline disorder within an amorphous metal-organic framework, *Commun. Chem.* 6 (2023) 92.
- [104] X. Zheng, H. Zhang, S. Rehman, P. Zhang, Energy-efficient capture of volatile organic compounds from humid air by granular metal-organic gel, *J. Hazard. Mater.* 411 (2021) 125057.
- [105] B. Li, X. Zhou, B. Yan, Y. Li, H. Ye, G. Huang, Q. Zhou, In₂S₃-polymer hybrid gels derived from In(III) metal-organic gels for dye adsorption, photodegradation, and bacteria removal, *Macromol. Mater. Eng.* 306 (2021) e2100290.
- [106] A. Wang, M. Jin, N. Li, Y. Ma, L. Chen, D. Ma, B.-X. Chen, F. Gao, Y.-Q. Tian, Y.-K. Shi, Zeolitic imidazolate framework monoliths with high mesoporosity and effective adsorption of toluene from aqueous solution, *New J. Chem.* 41 (2017) 8031–8035.
- [107] Q. Liu, S. Li, H. Yu, F. Zeng, X. Li, Z. Su, Covalently crosslinked zirconium-based metal-organic framework aerogel monolith with ultralow-density and highly efficient Pb(II) removal, *J. Colloid Interface Sci.* 561 (2020) 211–219.
- [108] M. Liu, Z. Liu, T. Ma, Z. Liu, Y. Li, D. Zou, Luminescent cellulose-based porous binary metal-organic gels in an adsorption bed for effective adsorption and sensitive detection of chlortetracycline hydrochloride, *J. Hazard. Mater.* 414 (2021) 125473.
- [109] F. Liu, W. Xiong, X. Feng, L. Shi, D. Chen, Y. Zhang, A novel monolith ZnS-ZIF-8 adsorption material for ultraeffective Hg(II) capture from wastewater, *J. Hazard. Mater.* 367 (2019) 381–389.
- [110] J.F. Chen, X. Liu, J.F. Ma, B.B. Han, J.D. Ding, Q. Lin, H. Yao, Y.M. Zhang, T. B. Wei, A pillar[5]arene-based multiple-stimuli responsive metal-organic gel was constructed for facile removal of mercury ions, *Soft Matter* 13 (2017) 5214–5218.
- [111] J. Sui, L. Wang, W. Zhao, J. Hao, Iron-naphthalenedicarboxylic acid gels and their high efficiency in removing arsenic(V), *Chem. Commun. (Camb)* 52 (2016) 6993–6996.
- [112] D. You, H. Shi, Y. Xi, P. Shao, L. Yang, K. Yu, K. Han, X. Luo, Simultaneous heavy metals removal via in situ construction of multivariate metal-organic gels in actual wastewater and the reutilization for Sb(V) capture, *Chem. Engin. J.* 400 (2020) 125359.
- [113] M. Liu, D. Zou, T. Ma, Z. Liu, H. Yu, Y. Li, Z.-A. Qiao, Stable cellulose-based porous binary metal-organic gels as highly efficient adsorbents and their application in an adsorption bed for chlortetracycline hydrochloride decontamination, *J. Mater. Chem. A* 8 (2020) 6670–6681.
- [114] K. Jayaramulu, F. Geyer, M. Petr, R. Zboril, D. Vollmer, R.A. Fischer, Shape controlled hierarchical porous hydrophobic/oleophilic metal-organic nanofibrous gel composites for oil adsorption, *Adv. Mater.* 29 (2017) e1605307.
- [115] X. Zheng, S. Rehman, P. Zhang, Room temperature synthesis of monolithic MIL-100(Fe) in aqueous solution for energy-efficient removal and recovery of aromatic volatile organic compounds, *J. Hazard. Mater.* 442 (2023) 129998.
- [116] L. Wang, F. Ke, J. Zhu, Metal-organic gel templated synthesis of magnetic porous carbon for highly efficient removal of organic dyes, *Dalton Trans.* 45 (2016) 4541–4547.
- [117] Y. Hu, Y. Fan, Z. Huang, C. Song, G. Li, In situ fabrication of metal-organic hybrid gels in a capillary for online enrichment of trace analytes in aqueous samples, *Chem. Commun. (Camb)* 48 (2012) 3966–3968.
- [118] X. Chen, Z. Huang, S.Y. Chen, K. Li, X.Q. Yu, L. Pu, Enantioselective gel collapsing: a new means of visual chiral sensing, *J. Am. Chem. Soc.* 132 (2010) 7297–7299.
- [119] S.B. Aliev, S.I. Gurskiy, V.N. Zakharov, L.M. Kustov, Synthesis of novel nanoporous metal-organic gels with tunable porosity and sensing of aromatic compounds, *Microporous Mesoporous Mater.* 264 (2018) 112–117.
- [120] T.T. Zhao, Z.W. Jiang, S.J. Zhen, C.Z. Huang, Y.F. Li, A Copper(II)/Cobalt(II) organic gel with enhanced peroxidase-like activity for fluorometric determination of hydrogen peroxide and glucose, *Mikrochim. Acta* 186 (2019) 168.
- [121] X. Wang, C. Hu, X. Wang, Z. Luo, S. Zhen, L. Zhan, C. Huang, Y. Li, Facile synthesis of dual-ligand terbium-organic gels as ratiometric fluorescence probes for efficient mercury detection, *J. Hazard. Mater.* 436 (2022) 129080.
- [122] V. Urbanova, K. Jayaramulu, A. Schneemann, S. Kment, R.A. Fischer, R. Zboril, Hierarchical porous fluorinated graphene oxide@metal-organic gel composite: label-free electrochemical aptasensor for selective detection of thrombin, *ACS Appl. Mater. Interfaces* 10 (2018) 41089–41097.
- [123] L. Pang, H. Zhou, Z. Qian, H.A. Munir, J. Li, H. Liu, Water-Stable luminescent Eu-Al-nanoscale metal-organic gels for the detection of doxycycline, *ACS Appl. Nano Mater.* 6 (2023) 20220–20230.
- [124] F. Ding, G. Zhang, C. Chen, S. Jiang, H. Tang, L. Tan, M. Ma, A metal-organic gel-carbon nanotube nanocomposite for electrochemical detection of nitrite, *ACS Appl. Electron.* 3 (2021) 761–768.
- [125] Y. Cheng, J. Li, S. Deng, F. Sun, AgNPs@Ag(I)-AMTD metal-organic gel-nanocomposites act as a SERS probe for the detection of Hg²⁺, *Compos. Commun.* 13 (2019) 75–79.
- [126] L. Cui, J. Wu, H. Ju, Nitrogen-doped porous carbon derived from metal-organic gel for electrochemical analysis of heavy-metal ion, *ACS Appl. Mater. Interfaces* 6 (2014) 16210–16216.
- [127] X.J. Zhou, Y.X. Ji, J.F. Cao, Z.F. Xin, Polyoxometalate Encapsulated in Metal-Organic Gel as an Efficient Catalyst for Visible-Light-Driven Dye Degradation Applications, *Appl. Organomet. Chem.*, 32 (2017) e4206.

- [128] C. Zhou, L. Li, H. Qin, Q. Wu, L. Wang, C. Lin, B. Yang, C.A. Tao, S. Zhang, Humidity enhances the solid-phase catalytic ability of a bulk MOF-808 metal-organic gel toward a chemical warfare agent simulant, *ACS Appl. Mater. Interfaces* 15 (2023) 54582–54589.
- [129] M. Liu, D. Zou, T. Ma, Z. Liu, Y. Li, Simultaneous efficient adsorption and accelerated photocatalytic degradation of chlortetracycline hydrochloride over novel Fe-based MOGs under visible light irradiation assisted by hydrogen peroxide, *Inorg. Chem. Front.* 6 (2019) 1388–1397.
- [130] B. Kim, Y. Keum, Y.P. Chen, H.S. Oh, J.Y. Lee, J. Park, Stimuli-responsive Ti-Organic gels and aerogels derived from Ti-oxo clusters: hierarchical porosity and photocatalytic activity, *Inorg. Chem.* 58 (2019) 15936–15941.
- [131] J. Yu, X. Wang, L. Chen, G. Lu, G. Shi, X. Xie, Y. Wang, J. Sun, Enhanced adsorption and visible-light photocatalytic degradation of toluene by CQDs/UiO-66 MOG with hierarchical pores, *Chem. Engin. J.* 435 (2022) 135033.
- [132] Z. Tang, H. Tao, X. Wang, L. Chen, C. Song, G. Lu, X. Xie, J. Sun, Quasi-in situ synthesis of Ag NPs@m-MIL-100(Fe) for the enhanced photocatalytic elimination of flowing xylenes, *ACS Appl. Mater. Interfaces* 14 (2022) 52894–52906.
- [133] H. Yang, L. Jiang, W. Wang, Z. Luo, J. Li, Z. He, Z. Yan, J. Wang, One-pot synthesis of CdS/metal-organic framework aerogel composites for efficient visible photocatalytic reduction of aqueous Cr(VI), *RSC Adv.* 9 (2019) 37594–37597.
- [134] H. Xue, G. Shi, G. Lu, X. Xu, X. Ren, Y. Wang, X. Wang, X. Xie, J. Sun, A novel Z-scheme heterojunction Fe-BDC/TiO₂ for efficient photocatalytic degradation of acetaldehyde, *J. Photoch. Photobiol. A* 447 (2024) 115252.
- [135] D. Gu, Y. Liu, H. Zhu, Y. Gan, B. Zhang, W. Yang, J. Hao, Magnetic porphyrin-based metal organic gel for rapid RhB Removal and enhanced antibacterial activity by heterogeneous photo-fenton reaction under visible light, *Chemosphere* 303 (2022) 135114.
- [136] F. Ke, Y. Li, C. Zhang, J. Zhu, P. Chen, H. Ju, Q. Xu, J. Zhu, MOG-derived porous FeCo/C nanocomposites as a potential platform for enhanced catalytic activity and lithium-ion batteries performance, *J. Colloid Interface Sci.* 522 (2018) 283–290.
- [137] B. Zhang, J. Zhang, Y. Zhang, Q. Zuo, H. Zheng, Ce(IV)-based metal-organic gel for ultrafast removal of trace arsenate from water, *Langmuir* 39 (2023) 10892–10903.
- [138] J. Yu, X. Wang, Y. Wang, X. Xie, H. Xie, N. Vorayos, J. Sun, Heating-induced adsorption promoting the efficient removal of toluene by the metal-organic framework UiO-66 (Zr) under visible light, *J. Colloid Interface Sci.* 653 (2024) 1478–1487.
- [139] Y. Hong, Z. Gao, M. Chen, J. Hao, S. Dong, Metal-organic gels of catechol-based ligands with Ni(II) acetate for dye adsorption, *Langmuir* 34 (2018) 9435–9441.
- [140] H. Yao, X.-M. You, Q. Lin, J.-J. Li, Y. Guo, T.-B. Wei, Y.-M. Zhang, Multi-stimuli responsive metal-organic gel of benzimidazol-based ligands with lead nitrate and their use in removal of dyes from waste-water, *Chin. Chem. Lett.* 24 (2013) 703–706.
- [141] Y. Zhao, H. Zeng, X.W. Zhu, W. Lu, D. Li, Metal-organic frameworks as photoluminescent biosensing platforms: mechanisms and applications, *Chem. Soc. Rev.* 50 (2021) 4484–4513.
- [142] J.K. Wychowanic, H. Saini, B. Scheibe, D.P. Dubal, A. Schneemann, K. Jayaramulu, Hierarchical porous metal-organic gels and derived materials: from fundamentals to potential applications, *Chem. Soc. Rev.* 51 (2022) 9068–9126.
- [143] W. Zhai, C. Wang, P. Yu, Y. Wang, L. Mao, Single-layer MnO₂ nanosheets suppressed fluorescence of 7-hydroxycoumarin: mechanistic study and application for sensitive sensing of ascorbic acid in vivo, *Anal. Chem.* 86 (2014) 12206–12213.
- [144] X. Wang, P. Sheng, L. Zhou, X. Tong, L. Shi, Q. Cai, Fluorescence immunoassay of octachlorostyrene based on forster resonance energy transfer between CdTe quantum dots and rhodamine B, *Biosens. Bioelectron.* 60 (2014) 52–56.
- [145] E.A. Dolgoplova, A.M. Rice, C.R. Martin, N.B. Shustova, Photochemistry and photophysics of MOFs: steps towards MOF-based sensing enhancements, *Chem. Soc. Rev.* 47 (2018) 4710.
- [146] B.B. Chen, M.L. Liu, L. Zhan, C.M. Li, C.Z. Huang, Terbium(III) modified fluorescent carbon dots for highly selective and sensitive ratiometry of stringent, *Anal. Chem.* 90 (2018) 4003–4009.
- [147] Y. Li, Z.W. Jiang, S.Y. Xiao, C.Z. Huang, Y.F. Li, Terbium(III) organic gels: novel antenna effect-induced enhanced electrochemiluminescence emitters, *Anal. Chem.* 90 (2018) 12191–12197.
- [148] Z.S. Qin, W.W. Dong, J. Zhao, Y.P. Wu, Z.F. Tian, Q. Zhang, D.S. Li, Metathesis in metal-organic gels (MOGs): a facile strategy to construct robust fluorescent Ln-MOG sensors for antibiotics and explosives, *Eur. J. Inorg. Chem.* 2018 (2018) 186–193.
- [149] K. Dagci, M. Alanyalioglu, Preparation of free-standing and flexible graphene/Ag nanoparticles/poly(pyronin Y) hybrid paper electrode for amperometric determination of nitrite, *ACS Appl. Mater. Interfaces* 8 (2016) 2713–2722.
- [150] P.K. Rastogi, V. Ganesan, S. Krishnamoorthi, A promising electrochemical sensing platform based on a silver nanoparticles decorated copolymer for sensitive nitrite determination, *J. Mater. Chem. A* 2 (2014) 933–943.
- [151] M. Wang, L. Yang, C. Guo, X. Liu, L. He, Y. Song, Q. Zhang, X. Qu, H. Zhang, Z. Zhang, S. Fang, Bimetallic Fe/Ti-based metal-organic framework for persulfate-assisted visible light photocatalytic degradation of orange II, *ChemistrySelect* 3 (2018) 3664–3674.
- [152] D.M. Chen, C.X. Sun, C.S. Liu, M. Du, Stable Layered semiconductive Cu(I)-organic framework for efficient visible-light-driven Cr(VI) reduction and H₂ evolution, *Inorg. Chem.* 57 (2018) 7975–7981.
- [153] S. Mangal, S.S. Priya, N.L. Lewis, S. Jonnalagadda, Synthesis and characterization of metal organic framework-based photocatalyst and membrane for carbon dioxide conversion, *Mater. Today* 5 (2018) 16378–16389.
- [154] S. Chen, F. Yang, H. Gao, J. Wang, X. Chen, X. Zhang, J. Li, A. Li, Construction of dual ligand Ti-based MOFs with enhanced photocatalytic CO₂ reduction performance, *J. CO₂ Util.* 48 (2021) 101528.
- [155] T. Toyao, M. Saito, Y. Horiuchi, M. Matsuoka, Development of a novel one-pot reaction system utilizing a bifunctional Zr-based metal-organic framework, *Cat. Sci. Technol.* 4 (2014) 625.
- [156] J. Long, S. Wang, Z. Ding, S. Wang, Y. Zhou, L. Huang, X. Wang, Amine-functionalized zirconium metal-organic framework as efficient visible-light photocatalyst for aerobic organic transformations, *Chem. Commun. (Camb)* 48 (2012) 11656–11658.
- [157] C. Lu, D. Xiong, C. Chen, J. Wang, Y. Kong, T. Liu, S. Ying, F.Y. Yi, Indium-based metal-organic framework for efficient photocatalytic hydrogen evolution, *Inorg. Chem.* 61 (2022) 2587–2594.
- [158] N. Abdollahi, A. Ostovan, K. Rahimi, M. Zahedi, A.Z. Moshfegh, Magnetically recyclable Fe₃O₄@TMU-32 metal-organic framework photocatalyst for tetracycline degradation under visible light, *Inorg. Chem.* 60 (2021) 17997–18005.
- [159] N. Kolobov, M.G. Goesten, J. Gascon, Metal-organic frameworks: molecules or semiconductors in photocatalysis? *Angew. Chem. Int. Ed.* 26038 (2021).
- [160] A. Bavykina, N. Kolobov, I.S. Khan, J.A. Bau, A. Ramirez, J. Gascon, Metal-organic frameworks in heterogeneous catalysis: recent progress, new trends, and future perspectives, *Chem. Rev.* 120 (2020) 8468.
- [161] T. Zhang, W. Lin, Metal-organic frameworks for artificial photosynthesis and photocatalysis, *Chem. Soc. Rev.* 43 (2014) 5982–5993.
- [162] C. Zhou, S. Zhang, H. Pan, G. Yang, L. Wang, C.-A. Tao, H. Li, Synthesis of macroscopic monolithic metal-organic gels for ultra-fast destruction of chemical warfare agents, *RSC Adv.* 11 (2021) 22125–22130.
- [163] F. Wang, J.D. Harindintwali, Z. Yuan, M. Wang, F. Wang, S. Li, Z. Yin, L. Huang, Y. Fu, L. Li, S.X. Chang, L. Zhang, J. Rinklebe, Z. Yuan, Q. Zhu, L. Xiang, D.C. W. Tsang, L. Xu, X. Jiang, J. Liu, N. Wei, M. Kästner, Y. Zou, Y.S. Ok, J. Shen, D. Peng, W. Zhang, D. Barcelo, Y. Zhou, Z. Bai, B. Li, B. Zhang, K. Wei, H. Cao, Z. Tan, L.-B. Zhao, X. He, J. Zheng, N. Bolan, X. Liu, C. Huang, S. Dietmann, M. Luo, N. Sun, J. Gong, Y. Gong, F. Brahmshu, T. Zhang, C. Xiao, X. Li, W. Chen, N. Jiao, J. Lehmann, Y.-G. Zhu, H. Jin, A. Schaeffer, J.M. Tiedje, J.M. Chen, Technologies and perspectives for achieving carbon neutrality, *The Innovation* 2 (2021) 100180.
- [164] M. Ding, R.W. Flaig, H.L. Jiang, O.M. Yaghi, Carbon capture and conversion using metal-organic frameworks and MOF-based materials, *Chem. Soc. Rev.* 48 (2019) 2783–2828.
- [165] S.T. Fan, Z.H. Chen, Z. Yang, J.F. Feng, L.P. Yu, Z.J. Qiu, W.T. Liu, B.J. Li, S. Zhang, Facile preparation of humidity stable green γ -cyclodextrin metal-organic framework monolith for CO₂ capture, *AIChE J.* 68 (2022) 17872.
- [166] X. Zhao, Y. Wang, D.S. Li, X. Bu, P. Feng, Metal-organic frameworks for separation, *Adv. Mater.* 30 (2018) e1705189.
- [167] J. Albo, D. Vallejo, G. Beobide, O. Castillo, P. Castano, A. Irbien, Copper-based metal-organic porous materials for CO₂ electrocatalytic reduction to alcohols, *ChemSusChem* 10 (2017) 1100–1109.
- [168] H.J. Son, S. Jin, S. Patwardhan, J.J. Wezenberg, N.C. Jeong, M. So, C.E. Wilmer, A.A. Sarjeant, G.C. Schatz, R.Q. Snurr, O.K. Farha, G.P. Wiederrecht, J.T. Hupp, Light-harvesting and ultrafast energy migration in porphyrin-based metal-organic frameworks, *J. Am. Chem. Soc.* 135 (2013) 862–869.
- [169] A. Fateeva, P.A. Chater, C.P. Ireland, A.A. Tahir, Y.Z. Khimyak, P.V. Wiper, J. R. Darwent, M.J. Rosseinsky, A water-stable porphyrin-based metal-organic framework active for visible-light photocatalysis, *Angew. Chem. Int. Ed. Engl.* 51 (2012) 7440–7444.
- [170] J. Li, X. Wang, G. Zhao, C. Chen, Z. Chai, A. Alsaedi, T. Hayat, X. Wang, Metal-organic framework-based materials: superior adsorbents for the capture of toxic and radioactive metal ions, *Chem. Soc. Rev.* 47 (2018) 2322–2356.
- [171] E. Barea, C. Montoro, J.A.R. Navarro, Toxic gas removal – metal-organic frameworks for the capture and degradation of toxic gases and vapours, *Chem. Soc. Rev.* 43 (2014) 5419–5430.
- [172] Y. Qian, F. Zhang, D.J. Kang, H. Pang, A review of metal-organic framework-based compounds for environmental applications, *Energy Environ. Mater.* 6 (2023) e12414.
- [173] Y. Feng, H. Jiang, S. Li, J. Wang, X. Jing, Y. Wang, M. Chen, Metal-organic frameworks HKUST-1 for liquid-phase adsorption of uranium, *Colloids Surf.* 431 (2013) 87–92.
- [174] C.O. Audu, H.G.T. Nguyen, C.Y. Chang, M.J. Katz, L. Mao, O.K. Farha, J.T. Hupp, S.T. Nguyen, The dual capture of As(V) and As(III) by UiO-66 and analogues, *Chem. Sci.* 7 (2016) 6492–6498.
- [175] L. Li, W. Ma, S. Shen, H. Huang, Y. Bai, H. Liu, A combined experimental and theoretical study on the extraction of uranium by amino-derived metal-organic frameworks through post-synthetic strategy, *ACS Appl. Mater. Interfaces* 8 (2016) 31032–31041.
- [176] J.Q. Li, L.L. Gong, X.F. Feng, L. Zhang, H.Q. Wu, C.S. Yan, Y.Y. Xiong, H.Y. Gao, F. Luo, Direct extraction of U(VI) from alkaline solution and seawater via anion exchange by metal-organic framework, *Chem. Engin. J.* 316 (2017) 154–159.
- [177] W. Yang, Z.Q. Bai, W.Q. Shi, L.Y. Yuan, T. Tian, Z.F. Chai, H. Wang, Z.M. Sun, MOF-76: from a luminescent probe to highly efficient U(VI) sorption material, *Chem. Commun. (Camb)* 49 (2013) 10415–10417.
- [178] D. Chakraborty, A. Yurdusen, G. Mouchaham, F. Nouar, C. Serre, Large-scale production of metal-organic frameworks, *Adv. Funct. Mater.* (2023) e2309089.

- [179] Y.J. Wang, J.-H. Wei, S. Li, J.-Y. Luo, X.-W. Chang, Y.-Y. Sun, Q. Pi, Y.-P. Wu, D.-S. Li, Convenient synthesis of polymetallic metal-organic gels for efficient methanol electro-oxidation, *Inorg. Chem. Front.* 8 (2021) 927–933.
- [180] E.C. Vermisoglou, P. Jakubec, O. Malina, V. Kupka, A. Schneemann, R.A. Fischer, R. Zboril, K. Jayaramulu, M. Otyepka, Hierarchical porous graphene-iron carbide hybrid derived from functionalized graphene-based metal-organic gel as efficient electrochemical dopamine sensor, *Front. Chem.* 8 (2020) 544.
- [181] M.H. Hassan, O. El-Basha, R.R. Haikal, A.H. Ibrahim, M.H. Alkordi, Metallic nanoparticles assimilation within metal-organic framework monolith, *ACS Appl. Mater. Interfaces* 10 (2018) 32942–32945.
- [182] M.L. Mendonca, R.Q. Snurr, Computational screening of metal-organic framework-supported single-atom transition-metal catalysts for the gas-phase hydrolysis of nerve agents, *ACS Catal.* (2019) 1310–1323.
- [183] Y.L. Wu, G.P. Yang, S. Cheng, J. Qian, D. Fan, Y.Y. Wang, Facile incorporation of au nanoparticles into an unusual twofold entangled Zn(II)-MOF with nanocages for highly efficient CO₂ fixation under mild conditions, *ACS Appl. Mater. Interfaces* 11 (2019) 17437.
- [184] E.S. Gutterod, A. Lazzarini, T. Fjermestad, G. Kaur, M. Manzoli, S. Bordiga, S. Svelle, K.P. Lillerud, E. Skulason, S. Oien-Odegaard, A. Nova, U. Olsbye, Hydrogenation of CO₂ to methanol by pt nanoparticles encapsulated in UiO-67: deciphering the role of the metal-organic framework, *J. Am. Chem. Soc.* 142 (2020) 999.
- [185] J.D. Xiao, L. Han, J. Luo, S.H. Yu, H.L. Jiang, Integration of plasmonic effects and schottky junctions into metal-organic framework composites: steering charge flow for enhanced visible-light photocatalysis, *Angew. Chem. Int. Ed.* 57 (2018) 1103–1107.
- [186] Q. Yang, Q. Xu, H.-L. Jiang, Metal-organic frameworks meet metal nanoparticles: synergistic effect for enhanced catalysis, *Chem. Soc. Rev.* 46 (2017) 4774–4808.
- [187] Y. Cheng, F. Sun, Q. Feng, Q. Zhao, Y. Zhou, In situ synthesis of AgNPs@Ag(I)-AMTD metal-organic gel composite and its catalytic properties, *Colloids Surf.* 522 (2017) 43–50.
- [188] S. Saha, G. Das, J. Thote, R. Banerjee, Photocatalytic metal-organic framework from CdS quantum dot incubated luminescent metallohydrogel, *J. Am. Chem. Soc.* 136 (2014) 14845–14851.
- [189] Y.-Z. Chen, R. Zhang, L. Jiao, H.-L. Jiang, Metal-organic framework-derived porous materials for catalysis, *Coord. Chem. Rev.* 362 (2018) 1–23.
- [190] W. Xia, B. Qiu, D. Xia, R. Zou, Facile preparation of hierarchically porous carbons from metal-organic gels and their application in energy storage, *Sci. Rep.* 3 (2013) 1935.
- [191] S. Dang, Q.-L. Zhu, Q. Xu, nanomaterials derived from metal-organic frameworks, *Nat. Rev. Mater.* 3 (2017) 17075.
- [192] W. Zhan, L. Sun, X. Han, Recent progress on engineering highly efficient porous semiconductor photocatalysts derived from metal-organic frameworks, *Nano-Micro Lett.* 11 (2019) 1.
- [193] K. Shijina, R. Illathvalappil, S. Kurungot, B.N. Nair, A.P. Mohamed, T. Yamaguchi, G.M. Anilkumar, U.S. Hareesh, G.S. Sailaja, Chitosan intercalated metal organic gel as a green precursor of Fe entrenched and Fe distributed N-doped mesoporous graphitic carbon for oxygen reduction reaction, *ChemistrySelect* 2 (2017) 8762–8770.
- [194] P. Yan, W. Guo, Z. Liang, W. Meng, Z. Yin, S. Li, M. Li, M. Zhang, J. Yan, D. Xiao, R. Zou, D. Ma, Highly efficient K-Fe/C catalysts derived from metal-organic frameworks towards ammonia synthesis, *Nano Res.* 12 (2019) 2341–2347.
- [195] Z. Cao, Z. Jiang, L. Cao, Y. Wang, C. Feng, C. Huang, Y. Li, Lattice expansion and oxygen vacancy of alpha-Fe₂O₃ during gas sensing, *Talanta* 221 (2021) 121616.
- [196] H. Jiang, C. Li, H. Shen, Y. Liu, W. Li, J. Li, Supramolecular gel-assisted synthesis Co₂P particles anchored in multielement co-doped graphene as efficient bifunctional electrocatalysts for oxygen reduction and evolution, *Electrochim. Acta* 231 (2017) 344–353.
- [197] H. Wang, X. Cheng, F. Yin, B. Chen, T. Fan, X. He, Metal-organic gel-derived Fe-Fe₂O₃@nitrogen-doped-carbon nanoparticles anchored on nitrogen-doped carbon nanotubes as a highly effective catalyst for oxygen reduction reaction, *Electrochim. Acta* 232 (2017) 114–122.
- [198] M. Tian, X. Cui, M. Yuan, J. Yang, J. Ma, Z. Dong, Efficient chemoselective hydrogenation of halogenated nitrobenzenes over an easily prepared γ -Fe₂O₃-modified mesoporous carbon catalyst, *Green Chem.* 19 (2017) 1548–1554.
- [199] J.C. Huang, Y.H. Shih, S. Lirio, S.Y. Wu, H.T. Chen, W.L. Liu, C.H. Lin, H. Y. Huang, A simple approach to achieve a metastable metal oxide derived from carbonized metal-organic gels, *Chem. Commun. (Camb)* 55 (2019) 4475–4478.
- [200] C. Camur, R. Babu, J.A. Suarez Del Pino, N. Rampal, J. Perez-Carvajal, P. Hugenell, S.J. Ernst, J. Silvestre-Albero, I. Imaz, D.G. Madden, D. Maspoch, D. Fairen-Jimenez, Monolithic zirconium-based metal-organic frameworks for energy-efficient water adsorption applications, *Adv. Mater.* 35 (2023) e2209104.
- [201] W.L. Teo, W. Zhou, C. Qian, Y. Zhao, Industrializing metal-organic frameworks: Scalable synthetic means and their transformation into functional materials, *Mater. Today* 47 (2021) 170–186.
- [202] M. Rubio-Martinez, C. Avci-Camur, A.W. Thornton, I. Imaz, D. Maspoch, M. R. Hill, New synthetic routes towards MOF production at scale, *Chem. Soc. Rev.* 46 (2017) 3453–3480.
- [203] T. Paul, A. Juma, R. Alqerem, G. Karanikolos, H.A. Arafat, L.F. Dumée, Scale-up of metal-organic frameworks production: engineering strategies and prospects towards sustainable manufacturing, *J. Environ. Chem. Eng.* 11 (2023) 111112.
- [204] P.A. Julien, C. Mottillo, T. Friščić, Metal-organic frameworks meet scalable and sustainable synthesis, *Green Chem.* 19 (2017) 2729–2747.
- [205] G.J.H. Lim, Y. Wu, B.B. Shah, J.J. Koh, C.K. Liu, D. Zhao, A.K. Cheetham, J. Wang, J. Ding, 3D-Printing of pure metal-organic framework monoliths, *ACS Mater. Lett.* 1 (2019) 147–153.
- [206] Y. Liu, J. Yang, C. Tao, H. Lee, M. Chen, Z. Xu, H. Peng, X. Huan, J. Li, X. Cheng, J. T. Kim, Meniscus-guided 3D microprinting of pure metal-organic frameworks with high gas-uptake performance, *ACS Appl. Mater. Interfaces* 14 (2022) 7184–7191.
- [207] A.I. Cherevko, G.L. Denisov, I.A. Nikovskii, A.V. Polezhaev, A.A. Korlyukov, V. V. Novikov, Composite materials manufactured by photopolymer 3D printing with metal-organic frameworks, *Russ. J. Coord. Chem.* 47 (2021) 319–325.
- [208] J. Lefevre, B. Claessens, S. Mullens, G. Baron, J. Cousin-Saint-Remi, J.F. M. Denayer, 3D-printed zeolitic imidazolate framework structures for adsorptive separations, *ACS Appl. Nano Mater.* 2 (2019) 4991–4999.
- [209] M. Zhang, L. Li, Q. Lin, M. Tang, Y. Wu, C. Ke, Hierarchical-coassembly-enabled 3D-printing of homogeneous and heterogeneous covalent organic frameworks, *J. Am. Chem. Soc.* 141 (2019) 5154–5158.
- [210] Y. Xiao, X. Gong, J. Zhang, Self-foaming metal-organic gels based on phytic acid and their mechanical, moldable, and load-bearing properties, *Chemistry* 27 (2021) 8791–8798.
- [211] D. Vallejo-Sánchez, P. Amo-Ochoa, G. Beobide, O. Castillo, M. Fröba, F. Hoffmann, A. Luque, P. Ocón, S. Pérez-Yáñez, Chemically resistant, shapeable, and conducting metal-organic gels and aerogels built from dithiooxamidato ligand, *Adv. Funct. Mater.* 27 (2017) 1605448.